ND ISOTOPES:
INVESTIGATION OF CRETACEOUS OCEAN ANOXIC EVENT 2 AND A SYSTEMATIC STUDY OF FE-MN OXIDE COATINGS

By

SUSANNA WHITMAN BLAIR

A THESIS PRESENTED TO THE GRADUATE SCHOOL
OF THE UNIVERSITY OF FLORIDA IN PARTIAL FULFILLMENT
OF THE REQUIREMENTS FOR THE DEGREE OF
MASTER OF SCIENCE

UNIVERSITY OF FLORIDA

2006

This document is dedicated to Dr. Mary K. Blair and Dr. Blair Plimpton.

ACKNOWLEDGMENTS

I would first like to sincerely thank Dr. Ellen Martin for her continued help and guidance on this project. Though there were a number of challenges and setbacks, she was always persistent and positive about the progress. She is not only a wonderful advisor and mentor but a dear friend and confidant. I will undoubtedly miss her. Thanks go also to my committee members Dr. Paul Mueller and Dr. Philip Neuhoff for their advice and review of this thesis.

I am also very grateful for the financial support that was provided by the NSF SGR grant awarded to Dr. Ellen Martin.

Special acknowledgements go to Dr. George Kamenov for his patience and continuous help. This project would not have been completed without his guidance, suggestions, laboratory help, and assistance with analysis equipment. He is a true asset to this department and I was very lucky to have worked with him. Thanks go also to Dr. Ann Heatherington for her assistance with the TIMS. Thanks also go to Ken MacLeod for his help with the OAE portion of this project.

An appreciative thank you goes to Dr. Howard Scher for his guidance and help in the laboratory at a very early stage. He was definitely the force behind the start of this project and a number of the early analysis. I would also like to thank Derrrick Newkirk and the many others who have helped me in the laboratory.

Finally, I would like to thank my family and friends. Thanks go to Mary Blair for her unfaltering love and support. She is my dearest friend. Thanks go to Blair Plimpton

for being the first geologist in the family. Thanks go to David Sutton for his love and never- ending encouragement. Thanks go to my many wonderful friends in the Department of Geological Science at UF, especially to Jillian Hinds, Gillian Rosen, Warren Grice, Derrick Newkirk, Jane Gustavson, and Kelly McGowan for their friendship and laughter. Thanks go to Dr. Karen Harpp for her encouragement to continue on to graduate school. And last but not least thanks go to my many wonderful friends from Colgate University and from Baltimore, especially Miranda Clark for reading the following.

TABLE OF CONTENTS

page

ACKNOWLEDGMENTS iv

LIST OF TABLES viii

LIST OF FIGURES ix

ABSTRACT xi

CHAPTER

1 INTRODUCTION 1

2 GENERAL BACKGROUND 6

2.1 Isotope Systematics 6
2.1.1 Neodymium 6
2.1.2 Strontium 8
2.1.3 Carbon 9
2.2 General Ocean Circulation 10
2.3 Archives of Nd isotopes 11
2.4 Description of Sample Sites 16
2.4.1 DSDP Site 608 16
2.4.2 ODP Site 647 17
2.4.3 ODP Site 689 18
2.4.4 ODP site 690 18
2.4.5 ODP Site 886 19
2.4.6 ODP Site 982 19
2.4.7 ODP Site 1050 20
2.4.8 ODP Site 1090 20
2.4.9 ODP Sites 1258, 1259, 1260 20

3 METHODS 23

3.1 Sample Preparation 23
3.1.1 Fossil Fish Teeth Preparation 23
3.1.2 Fe-Mn Oxide Coating Preparation 23
3.2 Sr and Nd Column Chemistry 24
3.3 Nd Analysis 25
3.4 Major Element and REE Analyses from Fe-Mn oxide coatings 28

3.5 Sequential Extraction Procedure....29
3.6 Analysis of Nd and Sr isotopes, and Rare Earth Elements from Sequential Extractions....31
3.7 Sr Analysis....32

4 BACKGROUND FOR THE CRETACEOUS STUDY....34

4.1 General Climate Change and Tectonic Orientations....34
4.2 Cretaceous Ocean Circulation....35
4.3 Ocean Anoxic Events....36

5 RESULTS FROM THE CRETACEOUS OAE STUDY....43

6 DISCUSSION OF CRETACEOUS OAE STUDY....50

7 BACKGROUND ON EXTRACTION EXPERIMENTS....60

8 RESULTS OF THE FE-MN OXIDE COATING EXTRACTION PROCEDURE AND VALIDITY TESTS....62

8.1 Variations on the Extraction Procedure....62
8.2 Results from Southern Ocean Sites....65
8.3 Results from North Atlantic Sites....69
8.4 Results from Cretaceous Samples....72
8.5 Tests of Validity....73
8.5.1 REE Plots....74
8.5.2 Strontium Isotopes....78
8.5.3 Major Element Ratios....80
8.5.4 Sequential Extraction Procedure Results....84

9 DICUSSION OF EXTRACTION RESULTS FROM THE SOUTHERN OCEAN; NORTH ATLANTIC; AND CRETACEOUS AGE SAMPLES....91

9.1 Possible Lithologic Effects on the Extraction Procedure....91
9.2 REE Patterns of Fe-Mn oxide coatings....93
9.3 Sr Isotopes....95
9.4 Major Elements....97
9.5 Sequential Extraction....98
9.6 An Alternate Explanation....102

10 CONCLUSIONS....104

LIST OF REFERENCES....108

BIOGRAPHICAL SKETCH....121

LIST OF TABLES

Table		page
2-1	Nd Isotopic Data for Modern Seawater to Show the Variation in Values of Major Water Masses	7
5-1	Site 1258 mcd and $\delta^{13}C$	44
5-2	Sr and Nd Values from Cretaceous Samples from ODP Sites 886, 1050, 1258, 1259, 1260	48
6-1	REE Values from Fossil Fish Teeth Samples Before, During and After OAE2	52
8-1	Nd Isotopic Values from Fossil Fish Teeth and Fe-Mn Oxide Coatings from Southern Ocean ODP Sites 689, 690, and 1090	68
8-2	Nd Isotopic Values from Fossil Fish Teeth and Fe-Mn Oxide Coatings from North Atlantic DSDP and ODP Sites 608, 647, and 982	72
8-3	Nd Istopes from Fossil Fish Teeth and Fe-Mn Oxide Coatings from Sites 1258 and 1050.	73
8-4	REE Values from Fe-Mn Oxide Coatings	77
8-5	$^{87}Sr/^{86}Sr$ Values from Extracted Material and Foraminifera from Samples from ODP Sites 689, 690, 982, and 1090	80
8-6	Major Element Rations from Site 608, 647, 690, 1090, and 1258	82
8-7	$^{143/144}Nd$ values for Fossil Fish Teeth, Carbonate, Fe-Mn Oxide Coatings, and Residual Fractions from the Sequential Extraction Samples	86
8-8	87Sr/86Sr Values for Seawater, Carbonate, Fe-Mn Oxide Coatings, and Residual Fractions from the Sequential Extraction Samples	86
8-9	REE Values from Sites 608, 647, 689, 690, and 982 from Three Sediment Fractions	90
9-2	Percent Nd Contributed to the Bulk Sediment from the Carbonate, Fe-Mn Oxide, and Residual Fraction Separated during the Sequential Extraction Procedure	99

LIST OF FIGURES

Figure page

2-1 Variation of the $^{87}Sr/^{86}Sr$ ratio of seawater through the Cenozoic. 9

2-2 General Ocean Circulation model 11

2-3 ε_{Nd} from sites in the Atlantic sector of the Southern Ocean spanning 20 kyr to present, plotted with $\delta^{18}O$ values from the GRIP ice core and sea ice variations from the Western North Atlantic. 15

2-4 Modern plate reconstruction....16

2-5 Stratigraphic section of Cretaceous sequence for Site 1258 on Demerara Rise showing the three major lithostratigraphic intervals recovered: 21

3-1 The difference between the $\varepsilon_{Nd}(o)$ values of 11 samples measured on the TIMS and the NU-MC-ICP-MS. 27

4-1 Tectonic plate reconstruction at 90Ma showing the open connection between the Atlantic and Pacific Oceans 40

4-2 The seawater Sr isotope curve with 3 OAEs that coincide with perturbations in the Sr isotopic values....41

4-3 Relative ocean crust and plateau production over time. 41

4-4 Eustatic sea level curve of the last 200 Ma. 42

5-1 $\delta^{13}C$ and TOC % from ODP Site 1258 from 410-490 mcd. 43

5-2 $\varepsilon_{Nd}(t)$ and $\delta^{13}C$ values from Site 1258 from 370 to 490 mcd. 45

5-3 High resolution $\delta^{13}C_{org}$ with the $\varepsilon_{Nd(t)}$ values spanning OAE2 (420-428 mcd) from ODP Site 1258. 46

5-4 $\varepsilon_{Nd(t)}$ values from Site 886 in the Pacific Ocean, Sites 1259, 1258, and 1260 from Demerara Rise, and Site 1050 from Blake Nose spanning 65-103 Ma.....47

6-1 $^{87}Sr/^{86}Sr$ seawater curve from 85-100 Ma along with the Sr isotopic values from fossil fish debris collected from Site 1258. 51

5-3 REE plots of modern seawater compared to samples from before, during, and after OAE 2. 52

8-1 The difference of ε_{Nd} between fossil fish and Fe-Mn oxide coatings from samples of < 63 μm, 63-125 μm and >125 μm size fractions. S. 63

8-2 Difference of ε_{Nd} from obtained from fossil fish teeth and samples treated for 4, 2, and 1 hour extraction periods. 65

8-3 $\varepsilon_{Nd(o)}$ values from fossil fish teeth and Fe-Mn oxide coatings from the Southern Ocean Sites. 66

8-4 $\varepsilon_{Nd(o)}$ values from fossil fish teeth and Fe-Mn oxide coatings from DSDP Site 608 and ODP Site 647 from 5.5 to 9 and from 30 to 31 Ma. 70

8-5 $\varepsilon_{Nd(o)}$ values from fossil fish teeth and Fe-Mn oxide coatings from ODP Site 982 from 9 to 15 Ma. 71

8-6 $\varepsilon_{Nd(t)}$ values from fossil fish teeth and Fe-Mn oxide coatings from ODP Sites 1258 and 1090 from 77 to 102 Ma. 73

8-7 REE plot of four samples from ODP Site 690 74

8-8 REE plot of the average values from extracted coatings from the North Atlantic Sites 608, 647, and 982, the Cretaceous (Sites 1258 and 1050), and the Southern Ocean Sites 1090, 690, and 689... 76

8-9 Seawater Sr curve over the past 50 Ma plotted with $^{87}Sr/^{86}Sr$ values from extracted Fe-Mn oxide coatings. 79

8-10 Ti/(Fe+Mn) ratios of samples vs. the difference between ε_{Nd} values of the fossil fish teeth and the coatings from Sites 608, 647, 689, 690 , 982, 1090, and the Cretaceous samples from Sites 1050 and 1258. 82

8-11 $\varepsilon_{Nd(o)}$ and $^{87}Sr/^{86}Sr$ values from 8 sequential extraction samples 85

8-12 REE patterns from 8 sequential extractions. 88

8-13 REE patterns for 3 sediment fractions for sequential extractions. 90

9-1 Weight percent opal, carbonate, and terrigenous material from Site 1090 from 19.2 to 25.1 Ma plotted against the difference between ε_{Nd} values from fossil fish teeth and Fe-Mn oxide coatings. 92

9.2 Average sedimentation rate versus Nd concentration for Sites 608,647, 982, 689, 690, 1090, and 1258. 95

Abstract of Thesis Presented to the Graduate School
of the University of Florida in Partial Fulfillment of the
Requirements for the Degree of Master of Science

ND ISOTOPES:
INVESTIGATION OF CRETACEOUS OCEAN ANOXIC EVENT 2 AND
A SYSTEMATIC STUDY OF FE-MN OXIDE COATINGS
By

Susanna Whitman Blair

August 2006

Chair: Paul Mueller
Major Department: Geological Sciences

Nd isotopes in seawater are quasi-conservative water mass tracers and, therefore, can be used to reconstruct deep sea circulation through time, allowing scientists to further examine the link between ocean circulation and climate. This two-part study first explores circulation patterns in the North Atlantic during Late Cretaceous Ocean Anoxic Events (OAEs) using fossil fish teeth as an archive for Nd isotopes. Second, iron-manganese (Fe-Mn) oxide coatings on marine sediments are systematically tested as a potential new archive on Cenozoic timescales.

A high resolution Nd isotopic record was constructed for Site 1258 on Demerara Rise spanning OAE2 and the Mid-Cenomanian Event (MCE). Low resolution Nd isotopic records were also compiled from fossil fish teeth collected from ODP Sites 1259 and 1260 also on Demerara Rise, as well as Site 1050 (Blake Nose), and Site 886 (Central North Pacific). Data indicate that Nd isotopes are unaffected by diagenetic alteration. Average ε_{Nd} values of –15 before and after the OAEs at Site 1258 suggest that Demerara Rise was highly influenced by weathering off the South American continent. During OAE2 a very large, rapid increase of 8 ε_{Nd} units coincides with the increase in total organic carbon and the ~6$^{o}/_{oo}$ positive excursion in

$\delta^{13}C_{org}$. Competing causal theories for OAE2 attribute this anoxic event and the major shift in the global carbon budget to enhanced surface productivity or stagnation of the deep ocean. The rapid, positive increase in ε_{Nd} at Site 1258 approaches values observed at Blake Nose (subtropical North Atlantic) and in the Pacific around this time (ε_{Nd} = –4 to –6), indicate enhanced, rather than reduced, deep water circulation. This enhanced circulation may have been associated with increased rates of upwelling, contributing to surface productivity and increased carbon burial.

Fossil fish teeth are effective archives for Nd isotopes, yet they are not always present in sediment samples and are laborious to collect. Fe-Mn oxide coatings are present throughout time and space, can be accurately dated, and have proven to be reliable archives on Pleistocene time scales. Other studies have not had a method to test the accuracy of the oxide coating values. In this study ε_{Nd} results from these coatings were compared to fossil fish teeth values for samples as old as the Cretaceous. For ~90% of the samples from the Miocene to Eocene in the Southern Ocean (Sites 689, 690, and 1090) and North Atlantic (Sites 608, 647, and 982), as well as Cretaceous samples from Site 1258 the coatings and fish teeth yielded the same ε_{Nd} values.

A number of independent tests evaluated the selectivity and efficiency of the extraction procedure, including Sr isotopic analyses, REE patterns, and major element ratios. Sr isotopes were identified as a very conservative test. A sequential extraction procedure was also tested to determine the isotopic signature and REE patterns of various sediment fractions. It was concluded that terrigenous material in the sediments may affect the Sr isotopes, but not the ε_{Nd} values. Although these results indicate that Fe-Mn oxide coatings are a robust archive of deep sea Nd isotopes, it is necessary to test a few samples from each site against fossil fish teeh ε_{Nd} values. Preliminary results indicated that some of the Nd isotopic signal may also be coming from phosphates within the sediment. It can also be concluded that the rigorous cleaning procedure of fossil fish teeth prior to analysis is not necessary.

CHAPTER 1
INTRODUCTION

Throughout earth's history a number of climatic events have been linked to dramatic changes in ocean circulation. Examples include the correlation between the onset of the Antarctic Circumpolar Current, the thermal isolation of Antarctica, and the development of large ice sheets on Antarctica (Kennet, 1977; Scher and Martin, 2006). The correlation between the closure of the Central American Seaway (CAS) and the onset of modern thermohaline circulation, as well as Northern Hemisphere glaciation represents another example. By identifying changes to ocean circulation in the past scientists hope to better understand forcing mechanisms, rates of change, and possible effects of climate change. Global warming is quickly becoming one of the most important issues of our time. The melting of polar ice caps and permafrost, and the intense weather conditions across the globe have many concerned. By identifying major climatic changes in the past and understanding their forcing mechanisms we may be better prepared for future climate changes.

A conservative tracer for ocean circulation is required to evaluate to the role ocean circulation plays in the development of global climate on geologic timescales. Neodymium is one of the few possible tracers for this property. Neodymium has been used in a number of studies to evaluate changes in deep water circulation over a range of time scales (e.g. Ling et al., 1997; O'Nions et al., 1998; Winter et al., 1997; Frank anNions, 1998; Frank et al., 1999; Vance and Burton, 1999; Frank et al., 2003; Thomas et al., 2003; Martin and Scher, 2004; Piotrowski et al., 2005; Scher and Martin, 2006).

Different water masses can have distinct Nd isotopic values (Piepgras and Wasserburg, 1982 and 1987; Piepgras and Jacobsen, 1988; Bertram and Elderfield, 1993; Jeandel, 1993; Shimizu et al., 1994; Jeandel et al., 1998) because the residence time of Nd in the world's oceans is shorter than the mixing time of the ocean itself (Broecker and Peng, 1982; Elderfield and Greaves, 1982; Piepgras and Wasserburg, 1985; Jeandel et al., 1995; Tachikawa et al., 1999) and because the Nd isotopic signature is dominated by the local geology of the source regions. Unlike other potential tracers, such as $\delta^{13}C$ or Cd/Ca, Nd isotopes are not fractionated by biological processes or temperature. Tracking deep water Nd isotopes through time and space can lead to greater understanding of past deep ocean circulation patterns. In order to utilize this tool, an effective archive has to be identified that preserves the Nd isotope values over time. Some of the archives that have been used in paleoceanographic studies include ferromanganese (Fe-Mn) crusts and nodules, fossil fish teeth, and authigenic Fe-Mn oxide coatings (e.g. Albarede and Goldstein, 1992; Frank and O'Nions, 1998 and 1999; Martin and Haley, 2000; Frank et al., 2003; Thomas et al., 2003; Martin and Scher, 2004; Piotrowski et al., 2004; Scher and Martin, 2006).

This thesis presents two unique studies; one applies Nd isotopes from fossil fish teeth to study the relationship between ocean circulation and the development of Ocean Anoxic Events (OAEs) in the Cretaceous, and the second evaluates the potential of Fe-Mn oxide coatings on marine sediments as a possible archive for Nd isotopes on Cenozoic timescales.

The Cretaceous was a time of drastic changes in the world's oceans. One extreme event during this time was Ocean Anoxic Event 2 (OAE2), which is associated with large scale changes to the ocean's carbon budget (e.g. Schlanger and Jenkyns, 1976; Jenkyns,

1980, Arthur et al., 1988; Kuypers et al., 2002). This net burial of organic carbon around the Cenomanian-Turonian boundary occurred during the peak of the Cretaceous greenhouse climate interval. Widespread evidence for this event is present in all the world's oceans in the form of laminated, organic-rich silt and claystones virtually devoid of benthic fossils, indicating anoxic bottom waters over much of the seafloor. OAE2 is a global event and coincides with shifts in ocean chemistry, extinction of planktonic nannofossils (e.g. Leckie et al., 2002), the emplacement of the Caribbean large igneous province (LIP) (e.g. Kerr, 1998), and a highstand of sea level (e.g. Jenkyns, 1991); yet the ultimate cause of anoxia during this interval is still debated. The debate centers around whether the anoxic conditions that lead to the OAE2 were created by: 1) increased decay of organic carbon in response to enhanced surface productivity (largely a surface phenomenon), or 2) reduced ventilation and stagnation (largely a deep water phenomenon). Nd isotopes, which have been shown to effectively track ocean circulation, offer a unique opportunity to evaluate whether or not OAE2 was associated with changes in deep ocean circulation.

Nd isotopes from fossil fish teeth and debris were analyzed and compared to carbon isotopic data from OAE2 on the Demarara Rise (ODP Leg 207, Sites 1258, 1259, and 1260) in order to distinguish between proposed causal mechanisms. Nd isotopic data from Site 886 in the central north Pacific Ocean and Site 1050 from the subtropical north Atlantic (Blake Nose, Leg 171B) also helped constrain possible interpretations. Results from this study illustrate that there is a very dramatic response to OAE2 in the Nd isotopic record.

Although fossil fish teeth have proven effective for the generation of high resolution Nd isotope records on Cenozoic time scales (Martin and Haley, 2000; Martin and Scher, 2003; Thomas et al., 2003; Thomas, 2004) and the temporal resolution of Nd records from fossil fish teeth represents an enormous improvement relative to Fe-Mn crusts, the resolution is still not as high as traditional paleoceanographic proxies because the yield of teeth is highly variable. Moreover the method used to extract Nd from fossil fish teeth is very labor intensive. This project explores an alternative archive for creating these records. The dispersed, authigenic, Fe-Mn oxide coatings, common on marine sediments, have high concentrations of Nd and have been used to generate high resolution Nd isotope records on glacial-interglacial time scales (Rutberg et al., 2000; Bayon et al., 2002; Piotrowski et al., 2004). This project evaluates the preservation of initial Nd isotopes from Fe-Mn oxide coatings over Cenozoic time scales and seeks to identify a simple test of the integrity of the preserved signal.A reductive extraction procedure developed by Rutberg et al. (2000) and Bayon et al. (2002) to remove Fe-Mn oxide coatings was modified and applied to selected sediment samples of Miocene to Eocene age from Ocean Drilling Program (ODP) Sites 689, 690, and 1090 in the Southern Ocean and from DSDP (Deep Sea Drilling Program) and ODP Sites 608, 647, and 982 in the North Atlantic. To test the validity of the isotopic values obtained, the coating values have been compared with Nd isotopic values of contemporaneous fossil fish teeth. It is assumed throughout the study that the value obtained from the fossil fish teeth accurately reflects the Nd isotopic composition of the seawater at the time of deposition (Staudigel et al., 1985; Elderfiled and Pagette, 1986; Martin and Haley, 2000; Martin and Scher, 2004). This method of verifying the integrity of the signal preserved

in Fe-Mn oxide coatings is unique to this study. The sediment size fraction, extraction time, and extraction agents have been altered from the original Bayon procedure (Bayon et al., 2002) to obtain Nd isotopic values that match those of the fish teeth. The main concern with this extraction technique is possible contamination from the detrital material, which would undoubtedly alter the isotopic value. Less labor-intensive methods of verifying the integrity of the signal extracted from the oxide coatings have been tested. These tests were specifically designed to detect detrital contamination. The tests include studies of major element ratios, rare earth element (REE) patterns, and Sr isotopes. During the study a sequential extraction procedure was also applied to several samples to determine the Nd isotopic values of several distinct components: the fish teeth, carbonate, Fe-Mn oxide, and residual fractions of the sediment. The development of a reliable procedure for effectively extracting Fe-Mn oxide coatings from marine sediments would allow for a more continuous sampling of the ocean sediments and the development of a more complete reconstruction of ocean circulation through time.

CHAPTER 2
GENERAL BACKGROUND

2.1 Isotope Systematics

2.1.1 Neodymium

Neodymium is a lanthanide series element that has seven isotopes. ^{143}Nd is a radiogenic daughter product of ^{147}Sm produced by alpha decay with a half-life of approximately $1.06x10^{-11}$ years. The $^{143}Nd/^{144}Nd$ ratio is measured and commonly reported as ε_{Nd}. This notation allows small, but significant, variations in the isotopic ratio to be reported in whole numbers relative to a bulk Earth value (DePaolo and Wasserburg, 1976) and is determine by the equation below.

$$\varepsilon_{Nd}(o) = [(^{143}Nd/^{144}Nd)_{sample} / (^{143}Nd/^{144}Nd)_{CHUR} - 1] \times 10^4$$

Where CHUR (Chondritic Uniform Reservoir) is equivalent to the bulk Earth $^{143}Nd/^{144}Nd$ ratio or ~0.512638 (DePaolo and Wasserburg, 1976). Continental material has ε_{Nd} values of 0 to -50 while mid-ocean ridge basalts (MORB) have values of 0 to + 12 (Piepgras and Wasserburg, 1980).

Neodymium is a direct weathering product from the continents and generally reflects the relative ages and type of the weathered bedrock. The residence time of Nd in the world's modern oceans is ~1000 years (Elderfield and Greaves, 1982; Piepgras and Wasserburg, 1985; Jeandel et al., 1995; Tachikawa et al., 1999 and 2003), which is shorter than the total mixing time of the ocean (~1500 years; Broecker and Peng, 1982). The various ages and types of the weathered material in deep water source regions and

the relatively short mixing time of Nd in the oceans indicate that Nd isotopes can be used to track deep water masses.

Although Nd isotopes in seawater covary with other conservative tracers, such as salinity and silica (Rutberg et al., 2000; Goldstein and Hemming, 2003), Nd is not a perfect conservative tracer for water masses because the signal of ocean water masses can be altered by weathering inputs within a basin. Frank et al. (2003) termed Nd isotopes "quasi-conservative" water mass tracers due to this possible modification. One example of this effect is that Pacific waters have an ε_{Nd} value of ~-4 derived from relatively young Pacific Rim volcanic rocks despite the fact that most of the water masses flowing into the basin have ε_{Nd} values < -8. However, variations in ocean circulation can still be detected above this weathering signal (Piepgras and Jacobsen, 1988) (table 2-1). In comparison the North Atlantic, which is surrounded by old Pre-Cambrian cratons, has ε_{Nd} values of ~-13 to -14. Finally, the Indian Ocean has ε_{Nd} values of ~-8, which reflects the weathering input from surrounding landmasses, as well as a mixture of Atlantic and Pacific values (Piepgras and Wasserburg, 1979).

Table 2-1. Nd isotopic data for modern seawater to show the variation in values of major water masses

Water mass	**Modern ε_{Nd}**
AAIW (Antarctic Intermediate Water)	-7 to -8 [1]
AABW (Antarctic Bottom Water)	-9 [1]
PDW (Pacific Deep Water)	-4 [2]
NAIW (North Atlantic Intermediate Water)	-13 [3]
NADW (North Atlantic Deep Water)	-13.5 [3]

1.Jeandel, 1993; 2. Piepgras and Jacobsen, 1988; 3. Piepgras and Wasserberg, 1987

.

Neodymium is primarily sourced from continental sources including atmospheric dust, volcanic ash, resuspended detrital sediments, dissolved riverine input and river-borne particulates (Goldstein and Jacobsen, 1988; Bertram and Elderfield, 1993; Albarede et

al., 1997; Tachikawa et al., 1999 and 2003). Nd emitted at hydrothermal sources is thought to be scavenged almost immediately and therefore does not have an effect on waters beyond the immediate source area (Michard, 1983; German et al., 1990). Nd ions are relatively insoluble and very particle reactive, thus the concentration of Nd in seawater is fairly low, ~4 pg/g in the deep water. Nd is quickly scavenged by detritus, fecal pellets and oxide coatings in the water column and deposited on the ocean floor.

2.1.2 Strontium

Strontium isotopes have been used in this study as a chronostratigraphic tool as well as an independent test of the validity of the Nd isotopic value of the extracted Fe-Mn oxide fraction. The Sr isotopic value of the ocean is a function of a number of inputs; crustal weathering by riverine systems, which have radiogenic $^{87}Sr/^{86}Sr$ values (~0.7119), mantle derived material from hydrothermal venting with non-radiogenic values of ~0.7035 (Palmer and Edmond, 1989), and pore water diffusion which introduces Sr with the isotopic ratio of old marine carbonates (Hess et al., 1986; Hodell et al., 1990).

Strontium has a residence time in the oceans on the order of several million years (Hodell et al., 1994), which creates a homogeneous ocean with respect to $^{87}Sr/^{86}Sr$ at any one time in earth's history. The major sink for Sr is carbonate precipitation, because the Sr^{2+} ion can easily replace Ca^{2+}. Extensive work has been done to document the changes in Sr over the past 50 Ma (figure 2-1). Strontium isotopes illustrate a general increasing trend throughout the Cenozoic making them a fairly effective tool for chemostratigraphy.

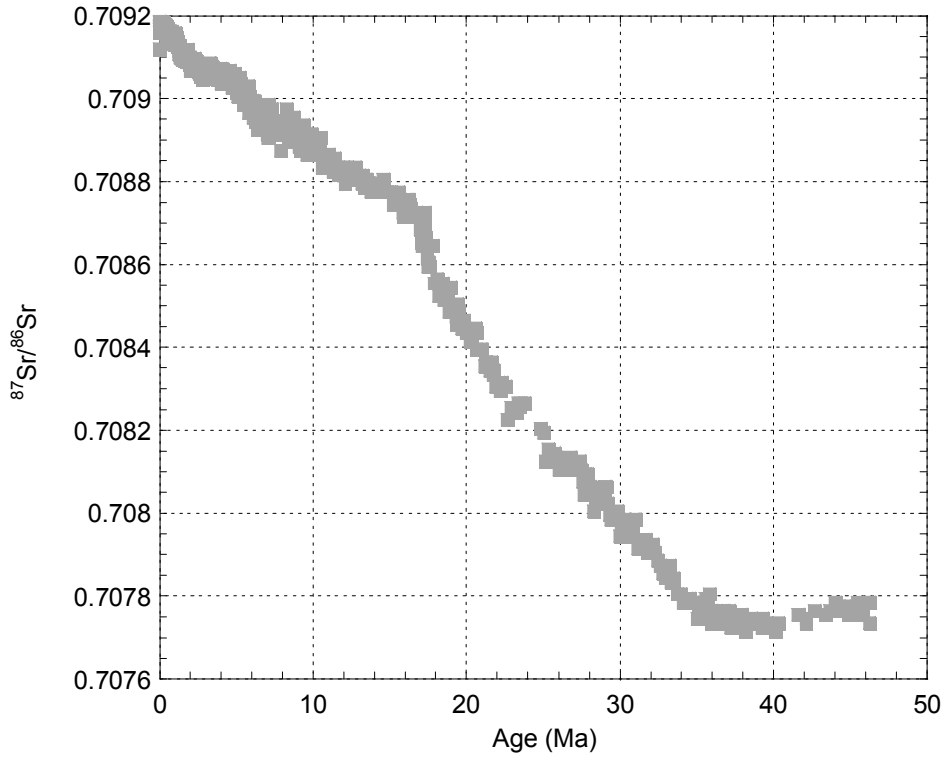

Figure 2-1. Variation of the $^{87}Sr/^{86}Sr$ ratio of seawater through the Cenozoic. Data from Hodell and Woodruff, 1994; Farrel, 1995; Mead and Hodell, 1995; Martin et al., 1999.

2.1.3 Carbon

Carbon isotopes extracted from ocean sediments are used to track carbon transfers into and within oceanic reservoirs. Carbon moves through these reservoirs as organic carbon, which consists of both living and dead matter, and inorganic carbon, which is primarily dissolved ions, but can also include atmospheric CO_2. Marine foraminifera have preserved inorganic carbon throughout the geologic record and are commonly used as an archive for carbon isotopes. Carbon isotopes are fractionated during photosynthesis because living organisms preferentially incorporate ^{12}C instead of ^{13}C into their tissue. This fractionation shifts the $\delta^{13}C$ value of organic matter toward more negative, ^{12}C enriched values, relative to that of inorganic carbon (Goodney et al., 1980), leaving the oceans enriched in ^{13}C. During times of increased primary productivity in the oceans the

$\delta^{13}C_{org}$ of foraminifera and bulk organic matter shifts toward more positive values. In this study carbon isotopic ratios in bulk organic matter are interpreted to represent the global signal of net organic burial and provide an independent record of the position of OAE2.

Carbon isotopes can also be used as a tracer of water mass age. In young deep waters that have recently been at the surface, such as modern North Atlantic Deep Water (NADW), $\delta^{13}C$ is more positive, reflecting the recent ventilation of surface waters influenced by extensive photosynthesis. As this water circulates and becomes older ^{12}C is progressively returned to the water through organic decay and the $\delta^{13}C$ becomes more negative. Carbon is considered a non-conservative water mass tracer because it can be altered by changes in productivity. It provides information about how long the deep water has been away from the surface and the extent of surface productivity, but it does not record information about the source region of the deep water.

2.2 General Ocean Circulation

The modern ocean circulation model is relatively well constrained and is controlled by the sinking of cold, saline water in the high latitudes. Highly simplified, the cycle begins as NADW sinks in the North Atlantic, due to its cold temperature and high salinity, both of which make this water relatively dense. This water mass makes its way to the Southern Atlantic where it mixes with Antarctic Bottom Water (AABW), which is formed around Antarctica, because of the cold temperatures and high salinities associated with sea ice formation. These water masses combine and continue east in a circumpolar current, flow into the Indian Ocean and into the Pacific, and eventually return through the Drake Passage and the Indonesian Seaway as intermediate and surface waters. This process is referred to as the global conveyor (Broecker and Peng, 1982) (Figure 2-2).

Cooling and sinking of warm NADW keeps Europe relatively warm for its latitude. The rate of conveyor cycling is approximately 10^3 years (Broecker and Peng, 1982).

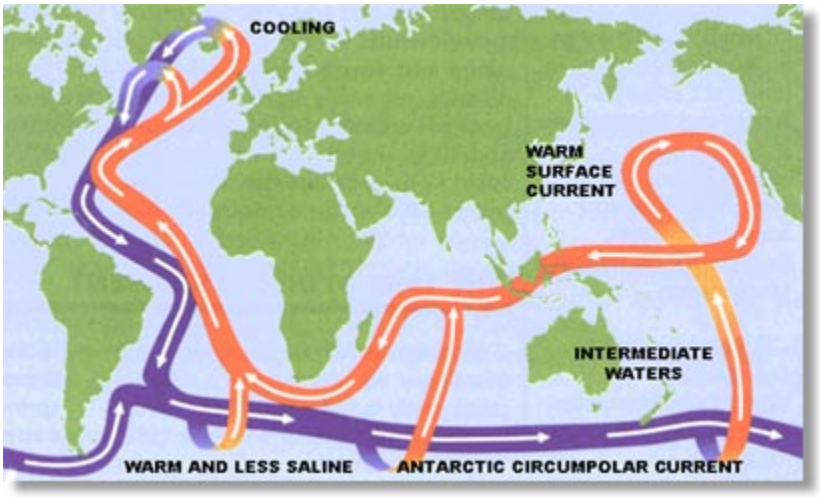

Figure 2-2- General Ocean Circulation model, adapted from Broecker and Peng, 1982. (www.metoffice.gov.uk)

This ocean circulation pattern has evolved through geologic time. Some of the factors that control the deep ocean circulation pattern include openings and closings of oceanic gateways, as well as changes in the thermal gradient and conditions in source regions. The Late Cretaceous circulation, specifically, was very different from today's; at that time the North Atlantic had recently opened, creating isolated basins between sills and fractures in the ocean floor (Bonatti et al., 1994; Jones et al., 1995; Handoh et al., 1999).

2.3 Archives of Nd isotopes

To determine the Nd value of seawater in the past a physical storehouse or archive has to be identified that incorporates Nd from the seawater into its structure and maintains its integrity through burial and diagenesis. In order to reconstruct ε_{Nd} changes this archive must be found throughout space and time, and must be datable. Identified

archives include biogenic carbonate, ferromanganese (Fe-Mn) oxide crusts and nodules, phosphates (particularly fossil fish teeth), and Fe-Mn oxide coatings.

Biogenic carbonates have been used as an archive for many other chemical proxies (ex. strontium, carbon, and oxygen isotopes); however, the concentration of Nd in carbonates is very low, on the order of a few ppm, because Nd^{3+} is the wrong size and charge for the carbonate structure (Palmer and Elderfield, 1985). Early studies that attempted to extract Nd from planktonic foraminifera found that 90% of the Nd was in the Fe-Mn coating with only 10% in the carbonate (Palmer and Elderfield, 1985). Nd values obtained from un-cleaned foraminifera yielded $^{143}Nd/^{144}Nd$ values similar to those of Fe-Mn crusts from a similar location and time period (Palmer and Elderfield, 1985). Other studies have suggested that after intensive redox cleaning the Nd isotopic value of planktonic foraminifera records the surface water value (Vance and Burton, 1999). It is, however, unclear if any cleaning can remove all of the coating and produce isotopic values purely from the carbonate (Pomies, 2000). Although foraminifera are abundant throughout the world's oceans it is unclear whether they can be used as effective recorders of either surface or deep-ocean water compositions.

Fe-Mn oxide crusts and nodules have proven to be effective archives for Nd ue to high concentrations of Nd, ~50 pm (Piepgras and Wasserburg, 1979). There have been a number of successful studies illustrating that these crusts record deep water Nd values through time (e.g. Albarede and Goldstein, 1992; Burton and Ling, 1997; Frank and O'Nions, 1998, Frank et al., 2002). However, there are a few drawbacks to using crusts and nodules. These deposits have exceedingly slow accumulation rates (on the order of 1-10mm/Myr; Segl et al., 1984; Puteanus and Halbach, 1988) and their sparse

distribution does not always allow for global sampling (Abouchami et al., 1997; Burton et al., 1997 and 1999; Ling et al., 1997; O'Nions et al., 1998; Frank et al., 1999; von Blanckenburg and O'Nions, 1999; Frank et al., 2002). The slow growth rate also makes dating this archive very difficult. $^{10}Be/^{9}Be$ and Co have been used to date these crusts (Frank, 1999); however, this work requires numerous assumptions and Os isotope chemostratigraphy recently highlighted the errors of some of these age models (Klemm et al., 2005). Since the growth rate is exceedingly slow the Nd isotopic values of these crusts can record long term trends of ocean water circulation and have provided important end member values for many water masses, but they do not record rapid shifts in circulation associated with many climate events. (Table 2-1).

Phosphates, especially apatites in the form of conodonts and fossil fish teeth, have proven to be effective archives for Nd isotopes, (Elderfield and Pagett, 1987; Keto and Jacobsen, 1987 and 1988; Martin and Macdougall, 1995; Martin and Haley, 2000; Thomas et al., 2003; Martin and Scher 2004; Thomas, 2004; Scher and Martin, 2006). The hydroxyfluorapatite structure of fossil fish teeth contains 100-1000 ppm Nd, which is incorporated into the teeth soon after they are deposited on the ocean floor and still in contact with deep ocean water (Wright et al., 1984; Shaw and Wasserburg, 1985; Staudigel et al., 1985; Martin et al., 1995, Martin and Haley, 2000; Martin and Scher, 2004). Evidence to support this idea include: 1) fish teeth and Fe-Mn crusts from the same water mass preserve the same isotopic value (Martin and Haley, 2000), 2) REE patterns from fossil fish teeth are the same as those for seawater (Elderfield and Pagett, 1986; Reynard et al., 1999), 3) teeth that were found in variable lithologies and pore fluids, but deposited in the same bottom water have the same isotopic value (Martin and

Haley, 2000), 4) the concentration of Nd in teeth does not increase or decrease with depth or age of sediments (Bernat, 1975; Elderfield and Pagett 1986; Staudigel et al., 1985; Grandjean et al., 1987), and 5) teeth that have been deposited in areas of slow sedimentation and therefore exposed to seawater longer, commonly have higher Nd concentrations (Elderfield and Pagett, 1986; Staudigel et al., 1986; Martin and Scher, 2004).

Fossil fish teeth, like Fe-Mn crusts, do effectively record the Nd isotopic signal of bottom water; yet, unlike crusts, teeth can be easily dated with the surrounding sediment using paleomagnetism, biostratigraphy, chemostratigraphy, and orbital tunning. Because of this, relatively high-resolution records can and have been produced. Most recently, fossil fish teeth have been used to create a Nd isotopic record of the Southern Ocean in an effort to constrain the timing of the opening of the Drake Passage, allowing for a deepwater connection from the Pacific into the Atlantic (Scher and Martin, 2004 and2006). While fossil fish teeth have been used to produce records with higher resolution than the records produced from Fe-Mn crusts, there are quite a few drawbacks to their use as an Nd archive. The process of picking them from sediments and cleaning them is very time intensive and, more importantly, fossil fish teeth are not widely distributed temporally and spatially throughout the world's oceans, leaving large gaps in some records.

Another recently explored archive for Nd isotopes is authigenic Fe-Mn oxide coatings (Rutberg et al., 2000 and Bayon et al., 2002; Piotrowski et al., 2004). Although early work with uncleaned planktonic foraminifera determined that these coatings

recorded ocean water Nd isotopic values (Palmer and Elderfield, 1985), this archive has only recently been further investigated.

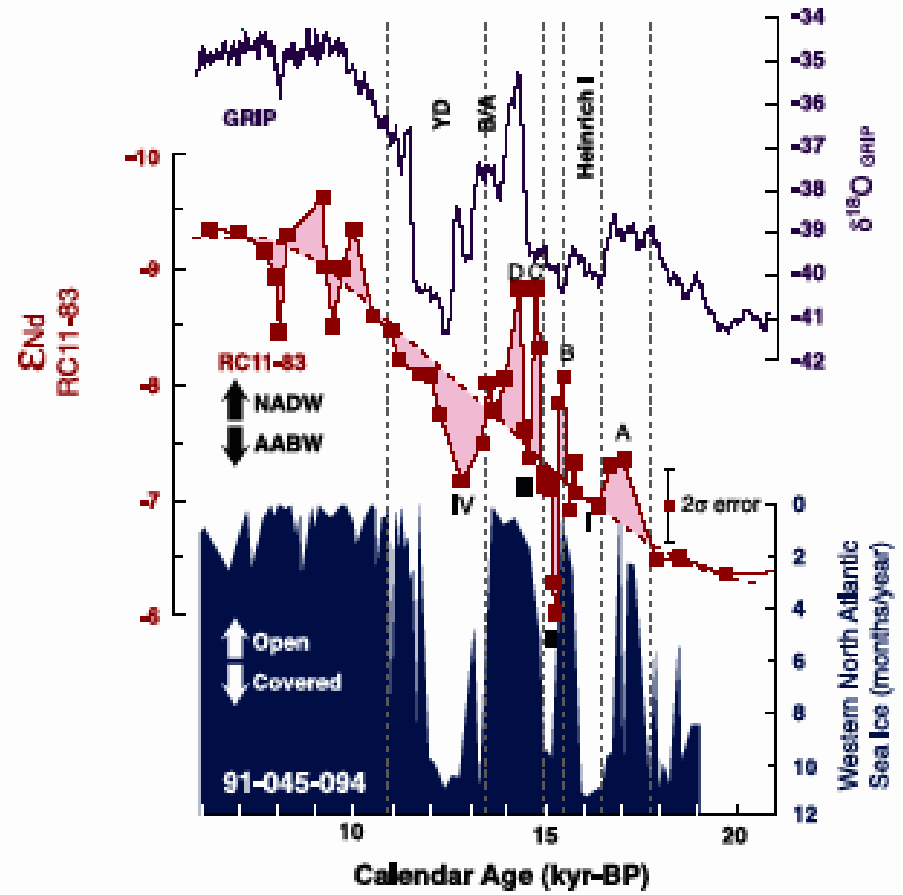

Figure 2-3. ε_{Nd} from sites in the Atlantic sector of the Southern Ocean spanning 20 kyr to present, plotted with $\delta^{18}O$ values from the GRIP ice core and sea ice variations from the Western North Atlantic. Variations in the Nd isotopic record are interpreted to be changes in the strength of NADW and AABW production over interglacial and glacial timescales. During glacial periods ε_{Nd} values are more radiogenic due to a greater influence of AABW to this site, oxygen isotope values are more negative representing cooler climate, and there is more sea ice covering the Western North Atlantic (adapted from Piotrowski et al., 2004).

These coatings occur as a thin veneer of Fe and Mn oxide on the surface of ocean sediments worldwide and throughout time. Work by Hein et al. (1997) has shown the mineralogy of Fe-Mn crust to be both ferruginous vernadite and Mn-feroxyhyte. This coating is essentially a dispersed accumulation of the same material that is concentrated

in Fe-Mn crusts and nodules. Using Pleistocene and younger sediments from the South Atlantic, it has been shown that these coatings do, in fact, record variations in the flow of NADW to the Southern Ocean during interglacial/glacial cycles (Rutberg et al., 2000 and Bayon et al., 2002; Piotrowski et al., 2004). Piotrowski et al. (2004) demonstrated that Nd isotopic values obtained from Fe-Mn coatings even preserve a record of changes in deep water circulation on millennial time scales (Figure 4). It has yet to be determined if this archive can be used for much older sediments.

2.4 Description of Sample Sites

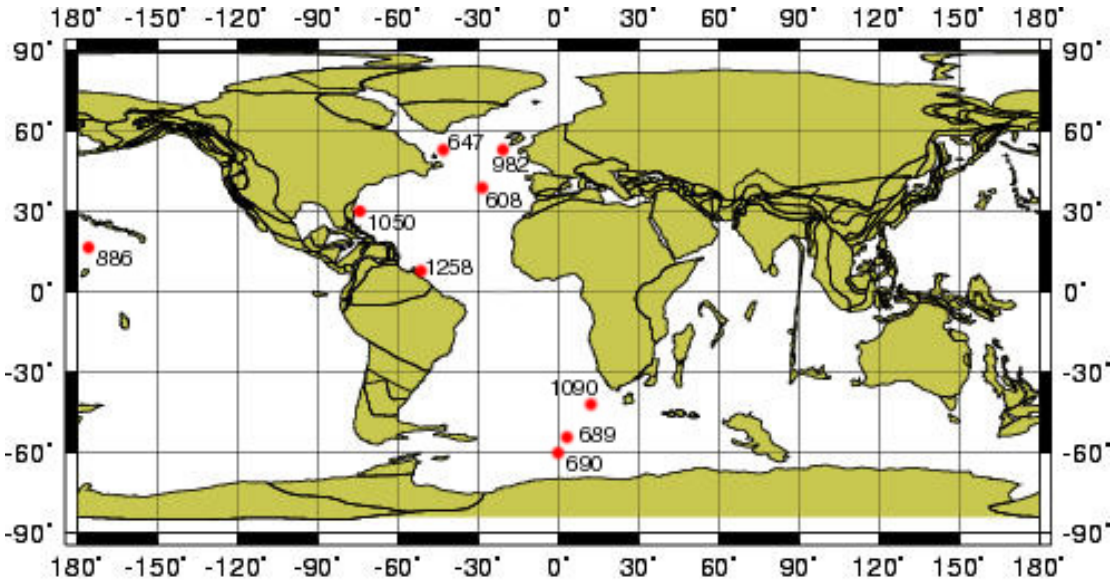

Figure 2-4. Modern plate reconstruction from the Ocean Drilling Stratigraphic Nework (www.odsn.de) with DSDP and ODP site locations used in this study. Sites 1259 and 1260 are located in the same area as Site1258.

2.4.1 DSDP Site 608

DSDP Site 608 (42°50.205'N, 23°05.252'W, 3541.8 m water depth is located on the southern sife of the King's Trough tectonic complex, which is about 700km northeast of the Azores (figure 2-4). Hole 608 was drilled to a depth of 530.9 m into to upper middle Eocene sediments. Samples used for this study ranged from 119.23 to 208.05 mbsf. The section sampled is primarily white foraminiferal nannofossil ooze, with a

carbonate range of 90-95%. The sedimentation rate for this section is 34 m/m.y. and the age range if from 3.9 to 8.9 Ma. A smear slide summary from hole 608 core 20 indicates that calcareous nannofossils comprise 78% of the lithology, along with 20% quartz and 2% foraminifers (Ruddiman et al., 1987).

2.4.2 ODP Site 647

ODP site 647 (53°19.876'N, 45°15.717'W, 3862 m water depth) is located in the southern Labrador Sea off the southern tip of the Gloria Drift and was drilled to further investigate deep ocean circulation between the Arctic and the North Atlantic (figure 2-4). Penetration at Hole 647A was to a depth of 736 m. Sediments used in this study range in ages from 7.3 to 30.6 Ma with corresponding depths ranging from 116.5 to 158.4 mbsf. The samples cover 3 different lithologic units, IIA, IIB, and IIIA. Unit IIA, from 116-119 mbsf is a silty clay underlain by nannofossil clay. This unit contains a significant proportion of nannofossils and towards the bottom becomes a nannofossil clay with scattered iron/ manganese nodules. The top section (40cm) is composed of 70% clay and 25% quartz silt at the top and 70% clay and 25% nannofossils in the bottom section, with minor amounts of mica and pyrite. Unit IIB spans from 119 to 135.4 mbsf and consists of two subunits. The upper subunit consists is composed of a 65% - 75% silty clay with 30% quartz including diatoms and spicules. The lower subunit consists of 90% clay minerals and minor amounts of quartz silt and mica. There is little to no biogenic carbonate in this section. The percent carbonate for both units is less than 20% throughout with a sedimentation rate of 46 m/m.y. Finally Unit IIIA consists of a nannofossil clay and contains both carbonate and biogenic silica. The biogenic component is 25%-50% and remaining is clay. The average carbonate % for Unit IIIA is 35% with a sedimentation rate of 16 m/m.y. (Shipboard Scientific Party, 1987)

2.4.3 ODP Site 689

ODP site 689 (64°31.009'S, 03°05.996'E, 2080 m water depth of 2080 m) was drilled during Leg 113 on Maud Rise, which is a topographic high in the Weddell Sea (figure 2-4). The deepest drill depth was 297.3m in hole 689B. The sediment sampled for this project ranged from 60 to 160 mbsf, which equates to an age range of 18 to 40 Ma. From 60 to 72 mbsf the main sediment type is very white to white diatom nannofossil ooze. The sediment from 72-160 mbsf is dominated by calcareous nannofossils with radiolarians decreasing downwards through the section. Carbonate percentages throughout the sampled section range from 51.2-98.5% with an average of ~88% $CaCO_3$. Clay is highly variable throughout the section, with some areas that have little to no clay content and others that have 60-90% smectite. Sedimentation rates range from 7 m/m.y. for 18-23 Ma, 4 m/m.y. for 25-33 Ma, and 4.5 m/m.y. for 33-40 Ma (Shipboard Scientific Party, 1988)

2.4.4 ODP site 690

ODP site 690 (65°9.629'S, 1°12.296'E, 2914 m water depth) was also drilled during Leg 113 to Maud Rise in the Southern Ocean (figure 2-4). The deepest hole was 690B, which recovered 213.4 m. The sediment used in this project ranged from a depth of 54 to 114mbsf, with ages of 25 to 45 Ma. Lithology from 54-93 mbsf consists of light grey diatom-bearing nannofossil ooze. Sediment from 93-114 mbsf is almost exclusively composed of calcareous biogenic sediment, which is primarily white to very pale brown foraminifer-bearing nannofossil ooze. Throughout the sampled section there are common (15-30%) to very abundant (60-90%) chlorite, kaolinite, illite, and smectite sections. Carbonate ranges from 50-85% throughout the sampled section. The sedimentation rate for 51-93 mbsf is 5.5 m/m.y (Shipboard Scientific Party, 1988).

2.4.5 ODP Site 886

ODP Site 886 (44°41.384'N, 168°14.400'W, 5713 m water depth) is located on the eastern edge of the Chinook Trough (figure 2-4). For hole C, which was sampled for this study, only recovered 72.4 m sediment, but the oldest sediment is Late Cretaceous in age. Sediment for this project ranged from 64.4 to 70.1 mbsf with ages ranges from 70.1 to 81 Ma (ages were determined using Os isotopes) (Ravizza, personal communication). The lithology of this section is primarily light to dark brown clay and is described as the "classic North Pacific 'red' clay". The clay contains 10-30% accessory minerals of authigenetic and/or digenetic origin. There are ferro-manganese crusts and nodules throughout the section (Shipboard Scientific Party, 1993).

2.4.6 ODP Site 982

ODP Site 982 (57°31.002'N, 15°51.993'W, 1134 m water depth) is located on the Rockall Plateau, which is about halfway between Iceland and Ireland (figure 2-4). It is a shallow platform at about 1000 m water depth, yet the hole was drilled in a bathymetric low on the plateau. Drilling reached a depth of 614.9 mbsf in hole B. Samples were taken from depths of 361.6 to 509.7 mbsf with ages ranging from 10.8 to 15.2 Ma. Lithology of this section consists primarily of nannofossil ooze with very minor variations. There are occasional layers of ash and ooze-chalk, but these were avoided during sampling. Calcareous nannofossils were the most abundant, while diatoms and radiolarians were very sparse and there were barren intervals throughout the section. Calcium carbonate averages about 90% throughout the sampled interval. Sedimentation rates throughout the section average about 35 m/m.y. (Shipboard Scientific Party, 1996).

2.4.7 ODP Site 1050

ODP Site 1050 (30°5.9953'N, 76°14.0997W, 2296.5 m water depth) located on Blake Nose, on the eastern margin of the Blake Plateau which is due east of Northern Florida (figure 2-3). Samples for this study were taken from 490 to 597 mbsf, which represents ages of 77 to 101 Ma. The samples were taken from Units IV and VI, as defined by the initial reports. Unit 4 extends to 491 mbsf and ranges from a calcareous claystone with nannofossils present to a nannofossil chalk with clay. Unit 6 extends from 501 to 606 mbsf and is composed of nannofossil chalk or limestone with variable amounts of clay and claystone. The sedimentation rate for most of this section is ~10 m/m.y. The carbonate ranges from 30 to 90 weight percent throughout these sequences but is generally higher from 500 to 600 mbsf (Shipboard Scientific Party, 1998).

2.4.8 ODP Site 1090

OPD site 1090 (42°54.814'S, 8°53.998E, 3702 m water depth) is located on the southern flank of the Agulhas Ridge (figure 2-4). The sediments used in this study ranged from 73 to 163 mbsf, with an age range of 16.6 to 12.0 Ma. The lithology is similar throughout the sampled section and consists of a mud bearing diatom ooze to a mud- and diatom- bearing nannofossil ooze and chalk. The carbonate weight percent is highly variable ranging from 0-80 wt%, but averages to about 30%. Opal averages to ~15% and terrigenous material is ~55% throughout the sampled section. The sedimentation rate is about 10 m/m.y. (Shipboard Scientific Party, 1999).

2.4.9 ODP Sites 1258, 1259, 1260

ODP Site 1258 (9°26.000'N, 54°43.999'W, 3192 m water depth), 1259 (9°17.999'N, 54°11.998'W 2354 m water depth), and 1260 (9°15.948'N, 54°32.633'W, 2549 m water depth) are all located on Demerara Rise, off Suriname, South America

(figure 2-4). Site 1258 is the deepest site on the western slope of the rise. This site was the most heavily sampled of the three for this project. Samples were collected from 375-450 mbsf, representing an age range of 80-96 Ma. The lithology of the sampled section spans Units III-V, as denoted by the initial reports (Figure 2-5). Unit III (325- 385 mbsf) is a calcareous nannofossil clay, with an average of ~65 weight percent carbonate. Unit IV ranges from 385-445 mbsf and is composed of laminated black shale and limestone. Color variations between these two sediment types record increasing and decreasing carbonate content, which ranges from 5-95 wt%. Finally Unit V is composed of phosphatic calcareous clay with organic matter. The sedimentation rate across all these lithologies is ~3 m/m.y. (Erbacher et al., 2004).

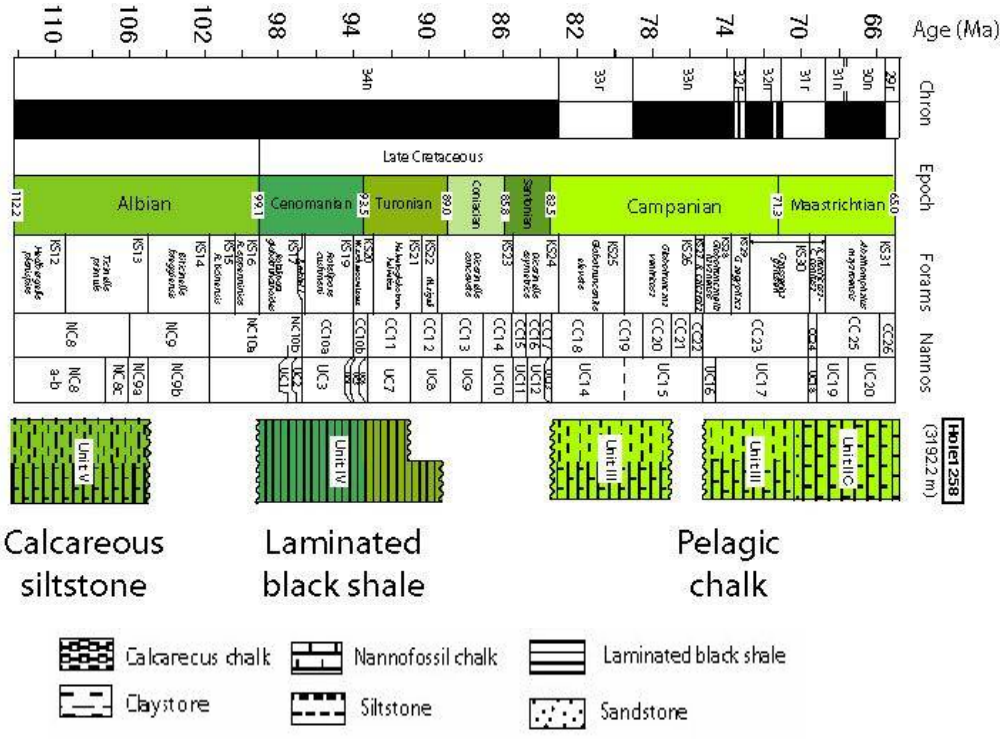

Figure 2-5. Stratigraphic section of Cretaceous sequence for Site 1258 on Demerara Rise (Erbacher et al., 2004) showing the three major lithostratigraphic intervals recovered: early Cenomanian and older faulted, synrift siltstones and claystones, Cenomanian-early Campanian laminated "black shales", and Campanian-Paleogene chalk and clayey chalk.

Site 1259 is located on the north facing slope of the rise. Samples were taken from a depth of 441-470.5 with relative ages of 66-70 Ma. The lithology of this section is composed of nannofossil chalk with clay and calcareous debris with calcareous siltstone and glauconitic claystone. The carbonate content in this section constitutes ~80 wt% of the sediments and the sedimentation rate is ~4.5 m/m.y. (Erbacher et al., 2004).

Finally, site 1260 is on the northwest facing side of the slope. Sampling from this site ranged from 356-386 mbsf representing ages of 70 to 75 Ma. The lithology is nannofossil chalk with foraminifera to calcareous claystone. The carbonate in this section ranges from 45-80 wt%. The sedimentation rate is 4.3 m/m.y. (Erbacher et al., 2004).

CHAPTER 3
METHODS

3.1 Sample Preparation

3.1.1 Fossil Fish Teeth Preparation

Sediment used for all analyses was obtained from DSDP or ODP. Fossil fish teeth were handpicked from the >125 μm size fraction of 50-60 cc samples. The teeth were cleaned following the oxidative/reductive technique developed by Boyle (Boyle, 1981; Boyle and Keigwin, 1985). This procedure removes Fe-Mn oxide coatings on the teeth that could alter the isotopic ratios. Fossil fish teeth have Nd concentrations that range from 100 to 1000 ppm and analysis can be performed on samples as small as 8 ng Nd. From each sediment sample 40 μg or more of teeth, which is generally 3 or more teeth, were collected and cleaned. The teeth were dissolved in aqua regia to remove any organics remaining after the cleaning process. After drying down the teeth were redissolved in 30 μl of 1.8 N HCl before they were processed through two cation exchange columns to isolate Sr and Nd.

3.1.2 Fe-Mn Oxide Coating Preparation

Upon retrieval from ODP core repositories, sediment was thoroughly cleaned through 63 μm sieves with deionized water. The sediment samples consist of 0.25 to1 g of >63 μm size fraction of dry sediment, which was placed into a 50 ml centrifuge tube. An initial 20 ml of buffered acetic acid solution was added to each sample and the sample was agitated on an electric shaker until there was no longer a reaction. (ie. the carbonate no loner reacted). The sample was then centrifuged and the initial 20 ml of acid was

decanted. Then another 10-20 ml of buffered acetic acid solution was added and this process was repeated until there was no longer a reaction and all the carbonate had been removed. Samples were then sieved using distilled water through 63 μm sieves to remove any remaining clay particles that may have been inside any of the carbonate tests. Samples were then centrifuged and the water was decanted. Next, 10-15 ml of 0.02 M Hydroxylamine Hydrochloride (HH) solution was added to each sample to reduce the oxide coatings. Each sample was then agitated for 1.5 hours and centrifuged for 0.5 hours. The supernatant was removed and placed in clean 50 ml centrifuge tubes, which were centrifuged again to remove any residual particulate matter. The HH solution was then removed and divided into two aliquots , one for isotopic analyses and the second for major element and REE analyses.

3.2 Sr and Nd Column Chemistry

Fish teeth samples and Fe-Mn oxide samples were passed through 2 columns to effectively separate Sr and Nd from the samples. The first column, or Primary column, used Mitsubishi cation exchange resin with an HCl eluent and isolated Sr as well as the bulk REE. The REE cut was dried down and loaded onto the second column, or the REE column. This column, which separates Nd from other isobars, was packed with Mitsubishi cation exchange resin and methylactic acid was used as an eluent. Total procedural blanks are ~10 pg of Nd and 100 pg Sr. A second type of REE column was used for the extracted coating samples. This procedure used an HCl elution with quartz columns packed with Teflon beads, which are coated with bis-ethylhexyl phosphoric acid to separate Nd and Sm from the other REE.

Four of the Cretaceous fish teeth and fish debris samples used in this study were spiked and analyzed for Sm to determine the $^{147}Sm/^{144}Nd$ ratios preserved in the teeth. The range of $^{147}Sm/^{144}Nd$ values from teeth and fish debris from ODP sites 1050 and 1258 is 0.125, which correlates to corrections of 0.67-0.87 ε_{Nd} units for this age and agrees well with values reported by Scher and Martin (2004), Thomas et al. (2004) and Puceat et al. (2005). The $^{147}Sm/^{144}Nd$ was also measured on the extracted coating samples and yielded the same correction. Samples from these sites were corrected and plotted as $\varepsilon_{Nd(t)}$. For all other samples in this study $\varepsilon_{Nd(o)}$ values were used. For these same spiked samples the concentration of Nd in the fish teeth samples ranged from 200-700 ppm, which is well within the range reported for fish teeth (Martin and Scher, 2004). These concentrations obtained on the TIMS from spiked samples were compared to the Nd concentrations obtained on the Element by REE analysis on the fish teeth and the two techniques produced values that fell well within error of one another.

3.3 Nd Analysis

The Nd from small (<200 μg) fish teeth samples were analyzed on a Micromass Sector 54 Thermal Ionization Mass Spectrometer (TIMS) at the University of Florida (UF). Using dynamic mode Nd was measured as NdO, which increases the efficiency of the analysis. The samples were loaded on zone refined Re filaments using silica gel as a loader. All ratios are normalized to $^{146}NdO/^{144}NdO = 0.722254$. Ideally NdO was then analyzed for 200 ratios at .5 V ^{142}NdO, but for very small samples the voltage was set as low as 0.25 V and as few as 100 ratios were counted in order to obtain a measurement. Errors for all samples are noted in data tables and graphs. The $^{143}Nd/^{144}Nd$ value for

repeat analyses of the JNdi-1 standard is 0.512102 ± 0.000014 (2σ). This uncertainty corresponds to ± 0.27 ε_{Nd} units.

Larger fish teeth samples (>200 μg) and extracted coating samples were analyzed on a Nu Plasma Multi-Collector - Inductively Coupled Plasma – Mass Spectrometer (MC-ICP-MS) at the University of Florida (UF). 0.5 ml of 2% HCl was added to each dry sample, then 10 μl was removed and placed in a sampling beaker. An additional 0.99 ml of 2% HCl was added to this aliquot and the concentration of the sample was then tested on the MC-ICP-MS. Ideally 2-5 V of ^{143}Nd was analyzed, and each sample was diluted appropriately after the first test measurement. The instrument and typical operating conditions are described in Belshaw et al. (1998). All ratios were normalized to ^{146}Nd/^{144}Nd = 0.7129 to correct for fractionation. Baselines were measured by ESA (electrostatic analyzer) deflection of the beam. Under static mode, using the instrument software both wet plasma using a micromist nebulizer and dry plasma using a desolvating nebulizer (DSN) were used as uptake systems. Only fairly large samples (>70 ppb) can be analyzed with wet plasma. When using the DSN a correction factor of 0.000028 or 0.2 ε_{Nd} unit was applied to samples to make them equate with results using the wet plasma method. Some samples were measured using time-resolved analysis (TSA), which produces very precise results with a very small sample size over a much shorter period of time (Kamenov, unpublished). This method was developed during the data collection of this project, and, therefore, was only applied for the later analyses. For this method on-peak-zeros were measured for 30 seconds just before sample introduction. Data were acquired in series of 0.2 seconds integrations over an average of a 60 second uptake time.

Both TIMS and MC-ICP-MS methods of Nd isotopic analyses were used for data collection of both fish teeth and Fe-Mn oxide coatings. To compare the results a correction factor was applied to all data collected on the MC-ICP-MS. Over a day of data collection on the MC-ICP-MS the JNdi-1 standard was run 5-10 times and averaged. The difference between this daily averaged value and the 0.512102 value obtained from the TIMS was used as a correction factor for all data collected on that day. The 2σ error varied daily, falling between .25 and .6 ε_{Nd} units. Error bars on data plots reflect the external run error correctly for each machine and each correction method. Due to variability internal to the MC-ICP-MS it is difficult to develop an overall long-term calibration. To test the correction method used in this study 11 samples were analyzed on both instruments and the corrected results all fell within error of one another (figure 3-1).

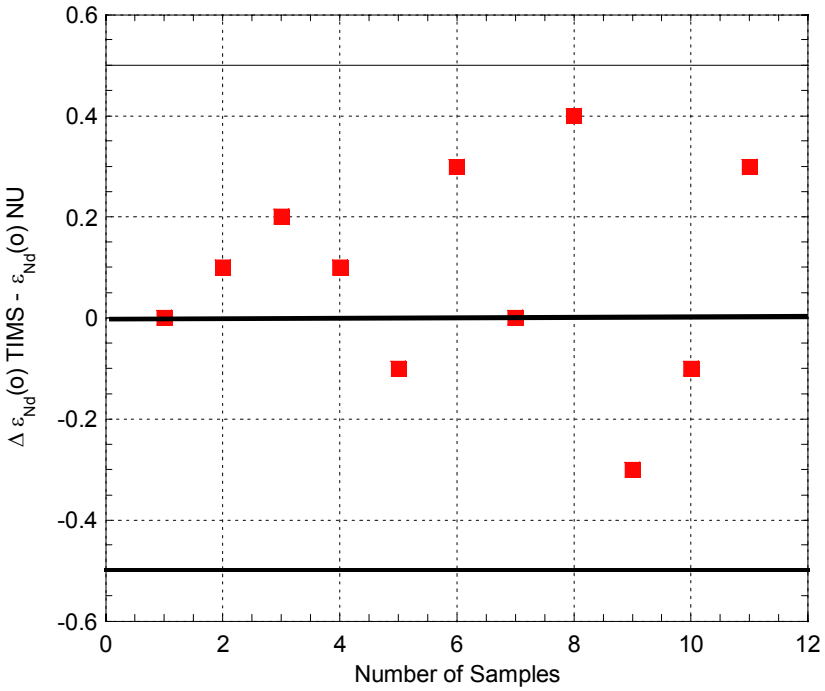

Figure 3-1. The difference between the $\varepsilon_{Nd}(o)$ values of 11 samples measured on the TIMS and the NU-MC-ICP-MS. The line at 0.0 represents samples that yielded identical values. The fine lines at 0.5 and -0.5 outline the typical error envelope based on TIMS analyses.

3.4 Major Element and REE Analyses from Fe-Mn oxide coatings

The portion of the extracted coating not used for the isotopic analysis was used for major element ratios and REE patterns. After the samples were dried down they were dissolved in 4 ml of 5% HNO_3 and left tightly capped on a hot plate overnight. Approximately 200 μl of the 4 ml was diluted with ~4 ml of 5% HNO_3 (for a final dilution of ~2000 times) for analysis on the Element 2 ICP-MS at UF. Each sample had an uptake time of 1 minute and a wash time of 2 minutes. All REE were analyzed in Medium Resolution mode, while ^{24}Mg, ^{27}Al, ^{49}Ti, ^{55}Mn, and ^{56}Fe. ^{23}Na and ^{39}K were analyzed in High Resolution mode. Four runs and four passes or a total of 16 measurements per isotope were performed. For the major elements the error was ± 5% and the blank is negligible. USGS whole rock standards ENDV, as well as a NOD-A and NOD-P (manganese nodules standards using Axelsson et al., 2002 for the dissolution method) and an in-house standard of AGV were used as correction factors for both majors and REEs. Data were normalized first in the Results Editor by checking and adjusting the calibration curves and second using a drift corrector. The drift corrector, commonly one of the above standards, was run every 5-8 samples and samples were adjusted to compensate for any drift during a given analysis. To do this a correction factor was found between the drifts at either end of sample set and then this correction factor was multiplied by the unknown sample value and the position of that sample in the sequence relative to the other samples. Samples measured for major elements were also corrected using the NOD-A and NOD-P USGS standards. Using the counts for each sample reported by the instrument the major element ratios were determined. To correct these ratios the known standard NOD values were divided by the measured NOD values

and all of the unknown sample values were multiplied by these counts to concentration conversion. A known standard was not identified for the analysis, all standards and samples were run as unknowns corrected as described. The reported REE for each sample was then normalized to the weight of the starting sediment sample and to PAAS (Post-Archean Australian Shale) (Taylor and McLellen, 1985). The error for REE elements is ± 5% and the blank is negliable.

3.5 Sequential Extraction Procedure

The goal of this procedure was to effectively separate the different fractions of marine sediments and obtain REEs and Sr and Nd isotopic values and concentrations for each fraction (Bayon et al., 2002). Samples of 0.75 g – 0.5 g were weighed out and the weight was recorded, then each sample was placed in a 50 ml pre-weighed centrifuge tube. Using a technique similar to that of the extraction procedure defined above, the carbonate fraction was first removed by adding 40 ml of acetic acid to the centrifuge tube. The weight of this liquid was accurately recorded for each sample so that concentrations could be calculated. The sample was agitated until there was no longer a reaction with the carbonate. The sample was then centrifuged and two aliquots of 5 ml each of the acetic acid were removed and set aside. One of these samples was used for REE and major element concentrations and the other was dried down and used for column chemistry and isotopic analysis. The remaining acid was discarded.

Four times (4x) distilled water was added to the remaining solid material, the sample was shaken, centrifuged, and the water decanted. This step was repeated twice to remove all of the acetic acid. The sample was then dried in an oven overnight to remove any remaining water and reweighed after it was completely dry. The weight difference between the initial and final weights was assumed to represent the weight of the

carbonate. Once dry, approximately 10 g of 1M HH solution was added to each sample. Samples were placed in 75^{o} C water bath for three hours and agitated every 30 minutes (Bayon et al., 2002). This method of extraction was used, as opposed to the one described above for removal of the Fe-Mn oxide coating for Nd analyses, because Bayon et al. (2002) determined that this technique removed the whole of the oxide coating more effectively, leaving the detrital fraction clean for analysis. Once the three hour extraction procedure was complete the sample was centrifuged and again two 5 ml samples were removed, one for elemental concentrations and the other was dried for isotopic analyses. The remaining solution was discarded and the sample was rinsed twice with 4x distilled water as described above.

The sample was again placed in the oven to dry. In a preliminary study hydrogen peroxide was used to remove the organic fraction of each sample. In many cases there was a violent effervescence that caused the loss of some of the sediment. When REE were measured on this fraction the concentrations were up to three orders of magnitude lower than the values from the other sediment fractions. Also there seemed to be no distinct REE pattern for the organics. The organic removal step was subsequently eliminated and the data presented in this study does not include a distinct organic fraction.

After the HH step, rinsing, and drying, the remaining sample was removed from the oven and weighed in the pre-weighed centrifuge tube to determine the amount of sediment residue. This residue was then powdered using a mortar and pestle and the sample was split into two portions, one for REE and one for isotopic analysis. For REE analysis 0.05 g were removed and placed into a beaker containing a drop of 4x water.

One ml of concentrated HF and 2 ml of concentrated HNO_3 were then added to each of the REE samples to dissolve the particulates and then the beakers were tightly capped. The samples were heated in an oven at 100ºC for 24-48 hours, then uncapped and placed on a hot plate to evaporate. After the samples were dry, 4 g of 5% HNO_3 was added to each. The day before analysis the samples were left on a hotplate uncapped to dry overnight, then removed and allowed to cool before analysis. For isotopic analysis 0.1 g of sample was removed and placed in a beaker. To this 1-2 drops of HNO_3 and 3 ml of HF are added and placed on a hotplate for 2 days. Samples are removed and dried down on a hotplate. Once dry, 2 ml of 6 N HCl is added to the sample to turn it into chloride salts. The sample was left on the hotplate overnight, opened and allowed to dry prior to column chemistry.

3.6 Analysis of Nd and Sr isotopes, and Rare Earth Elements from Sequential Extractions

For REE patterns samples were analyzed on the ICP-MS using the method described above for major elements and REE. The weight of the acetic acid or HH solution and the dilutions were accounted for in the software when analyzing each sample. The reported values are REE concentrations normalized to PAAS (Taylor and McLellen, 1985).

The second aliquots of samples were dried down and used for isotopic analysis. Preliminary tests showed that preparation of the carbonate fraction for column chemistry was fairly difficult. The samples formed a gelatinous mass (probably a calcium chloride substance) that would not fully dissolve in the small amount of 0.75 N HCl used to load samples onto the columns. Once the samples were loaded a carbonate cap commonly formed at the top of the resin inhibiting the flow of the eluents. To avoid this problem

the sample was run through the primary columns twice. For the first pass the sample was dissolved in 1 ml of 1.7 N HCl and added to the column in 250 μl increments. After the sample was loaded 5 ml of 1.7 N HCl is added to remove most of the Ca. This cut was discarded and 4.5 ml of 4.5 N HCl was added to remove the remaining sample including Sr and REEs. This cut was then dried down and run back through primary columns using the normal procedure as explained above. The Sr and REE cuts were both collected. The REE cut was passed through the same columns that were used to elute Nd from the extracted coatings.

Analysis of the HH aliquot followed the procedure described above for the other samples treated with HH. The first column eluted Sr and the REEs. Traditional Sr and REE cation columns were used with AG50W-X12, 200-400 mesh resin with a 3.5N HCl acid eluent. Both the Sr and REE cuts from the first column were dried down, and the REE cuts were passed through REE columns, to elute Nd, using the procedure defined above for the extracted coatings. Sr isotopes were analyzed using the TIMS and Nd isotopes were analyzed using the TRA procedure on the Nu MC-ICP-MS.

3.7 Sr Analysis

Sr was isolated by two different methods, depending on whether the archive of Sr was fish teeth, Fe-Mn oxide coatings, or foraminifera. The Sr from fish teeth and Fe-Mn oxide coating samples was collected from the primary columns as described above, during the elution to separate Sr and REE. Sr isotopes were also extracted from foraminifera for dating purposes. Foraminifera were handpicked from >125 μm size fraction of 50-60 cc samples. The concentration of Sr in forams is ~1000 ppm and the smallest sample that can be analyzed is ~50 μg Sr. Forams from each sample were

individually broken open and cleaned by sonication with water and methanol. Foraminifera were then dissolved with HCl and dried down. Sr was eluted using Sr Spec resin and 4x H_2O following the technique of Pin and Bassin (1992).

Sr cuts from both types of samples were dried down and analyzed on a Micromass Sector 54 TIMS at UF. Samples were loaded onto Tungsten filaments using Ta_2O_5 and analyzed for 200 ratios at an intensity of 1.5V ^{88}Sr. Fractionation was corrected to $^{86}Sr/^{88}Sr$ at 0.1194. The $^{87}Sr/^{86}Sr$ value for repeat analyses of the NBS-987 standard is 0.712025 ± 0.000023 (2σ). The procedural blank for Sr is ~100 pg.

CHAPTER 4
BACKGROUND FOR THE CRETACEOUS STUDY

4.1 General Climate Change and Tectonic Orientations

Extreme climatic, tectonic, and sea level changes made the Cretaceous a very dynamic and unique time in earth's history, and all may have had a direct effect on ocean circulation. The Cenomanian was a relatively cool period, but gradually warmed into the greenhouse conditions of the Cretaceous Thermal Maximum (CTM) during the Turonian. This was the warmest interval of the last 150 Ma and the peak of the last greenhouse interval (Frakes, 1994). This interval was characterized by: 1) drastic increases in poleward heat transport (e.g. Barron et al., 1993; Berner, 1994; Barron et al., 1995; Frakes, 1994); and 2) CO_2 levels that were four times modern values (Poulsen et al., 1999). Models suggest that poleward heat transport also increased from 15-30% to explain the reduced equator to pole gradient during the Turonian (Poulsen et al., 1999). The intense changes in climate, especially the thermal maximum, cannot be directly related to changes in ocean circulation, but there is undoubtedly some correlation in terms of changes in circulation patterns and heat transport (e.g., Brass, 1982; Arthur, 1987; Calvert and Pederson, 1990; MacLeod and Huber, 1996; Frank et al., 1999; Erbacher et al., 2001; Wilson and Norris, 2001; Leckie et al., 2002; Poulsen et al., 2003; Erbacher et al., 2005; MacLeod et al., 2005).

Tectonically the Cretaceous was marked primarily by the opening of the North Atlantic Ocean beginning in the Albian. The opening caused large-scale alterations in wind patterns and ocean circulation, and brought about changes to global surface

temperatures. Since circulation was fairly restricted the thermal gradients were low which hindered heat transport. It has been shown through model simulations that the opening of the North Atlantic, and the gateway between the North and South Atlantic oceans, could have been a factor in the development of the thermal maximum, as well as reorganization of ocean circulation and changes to regional climate systems (Poulsen et al., 2003). During the Turonian midlatitude Westerlies developed along with a 1-15^{o} warming in the polar regions (Bice and Marotzke, 2001). Simultaneously, the opening of this seaway reduced the regional equator-to-pole temperature gradient by as much as 15^{o} C. This caused cooling at the equator, and possible production of warm saline bottom water (Poulsen et al., 1999).

4.2 Cretaceous Ocean Circulation

Both changes to plate configuration and changes in global surface temperatures seemed to effect ocean circulation to some degree, however it is very difficult to constrain this circulation. Using general circulation models there is evidence that the opening of the gateway between the North and South Atlantic in the Late Albian, had a large effect on circulation (e.g. Barron and Peterson, 1989). Prior to this opening there were extremely warm and saline conditions in both the North and South Atlantic Oceans. After the opening there is evidence that Antarctic Bottom Waters fed into the Atlantic, as well as the Pacific and Indian Oceans, driving thermohaline circulation in these basins (Haupt and Seidov, 2001; Poulsen et al., 2001). Contrary to this conclusion, the presence of warm saline bottom waters originating at low latitudes has been identified by comparing $\delta^{18}O$ values of planktonic and benthic foraminifera (e.g., MacLeod and Huber, 1996; Barrera and Savin, 1999).

By the Maastrichtian there is also evidence of intermediate and deep water forming in the high-latitude Southern Ocean and the northern Atlantic which flowed throughout the ocean basins inferred from changes in $\delta^{13}C$ from benthic foraminifera (e.g., Frank et al., 1999; D'Hondt and Arthur, 2002). The limited number of deep sea drill sites that penetrated to this age and concerns about preservation of carbon and oxygen isotopes limit what can be determined from these methods. Modeling simulations produce results that are also contrary to the above conclusions suggesting that there was no deep water connection between the North and South Atlantic oceans until after the Cenomanian (Handoh et al., 2003). Needless to say, there are very few constraints on ocean circulation throughout the Cretaceous.

The Mid-Cretaceous opening of the North and South Atlantic Oceans created a complicated ocean bathymetry. There is evidence of secluded basins (e.g. Demarara, Sierra Leone, and Guinea) and large sills that could have interrupted deep sea circulation (Jones et al., 1995). There were also large offset fracture zones and transverse ridges, which may have restricted flow (Bonatti et al., 1994; Handoh et al., 1999).

4.3 Ocean Anoxic Events

In addition to the large perturbations in temperature and CO_2 and critical plate reconfigurations, the Cretaceous is marked by dramatic perturbations to the global carbon budget recorded as ocean anoxic events (OAEs). Theses events are distinguished by ocean-wide and regional changes from normal pelagic sediments to organic-rich black shales, which were deposited in oxygen deficient waters. They are recognizable by large increases in total organic carbon content and a large positive $\delta^{13}C$ excursion in both organic and inorganic carbon (e.g., Arthur et al., 1990; Bralower et al., 1994). Other

evidence of large-scale changes to ocean chemistry is illustrated by extinctions of some nannoplankton species, which are attributed to these anoxic events (e.g. Wonders et al., 1980; Kuhnt et al., 1986; Jarvis et al., 1988; Erbacher and Thurow, 1997). Six distinct OAEs have been recognized throughout the Late Cretaceous (OAE1a-d, OAE2, and OAE3), two of which can be identified on a global scale, OAE1a and OAE2. These events represent relatively brief periods of time (10^5-10^6 years) (e.g. Sageman et al., 2006) and must have been caused by large scale changes to the ocean environment, yet the ultimate cause is still highly debated.

OAE2, or the Bonarelli Event, which falls at the Cenomanian – Turonian boundary about 93.5 Ma falls right at the height of the Cretaceous greenhouse and represents the largest perturbation to the global carbon cycle in the last 250 Ma. It is characterized by laminated organic-rich silt and claystone with no evidence of benthic fossils. Although this event has been studied in numerous global localities, the cause of anoxia during this OAE, as well as all the others is still unknown. The prevailing theories simply stated are that the anoxia can be attributed to either: 1) a surface down phenomenon, such as a sharp increase in surface productivity, or 2) a bottom up phenomenon, denoted by deep water stagnation that could lead to enhanced preservation.

The surface down argument states that the warm humid conditions of the Cretaceous led to enhanced physical weathering of the continents and an accompanying increased delivery of nutrients to the ocean, resulting in enhanced surface productivity and organic carbon burial (e.g., Pederson and Calvert, 1990; Calvert and Pederson, 1992; Erbacher and Thurow, 1997; Wonders, 1980; Kuhnt et al., 1986; Jarvis et al., 1988; Weissert 1989). Other models called on enhanced upwelling (Kolonic et al., 2005) or

volcanic production of nutrients in a surface plume (Sinton and Duncan, 1997; Snow et al., 2005), but the premise is the same; excess surface productivity generated an organic rain rate than exceeded the capacity of the deep ocean to oxidize the material.

The opposing mechanism for OAE formation calls upon enhanced preservation due to changes in deep water properties, notably warmer bottom water temperatures, lower oxygen concentrations, and/or slower deep circulation leading to stagnation. This model is based on the assumption that high sea level and changes to thermohaline circulation caused a decrease in the subsurface oxygen concentration and subsequent expansion of the oxygen minimum zone (OMZ) (e.g. Bralower and Thierstein, 1984; Herbin et al., 1986), which resulted in the increased burial of organic carbon (e.g., de Greciansky, 1984; Arthur, 1990). Changes to circulation could have been caused by warmer surface water temperatures at the poles, which decreased the formation of cold bottom water and increased the amount of warm, high salinity bottom waters that formed at lower latitudes (Sinton and Duncan, 1997). Alternatively, ocean circulation models suggest that deep water continued to form in the high latitudes as the water there was still cooler than at the lower latitudes although it was warmer than modern high latitudes (Bice et al., 2001)

Benthic foraminifera $\delta^{18}O$ values support the idea of warmer bottom water temperatures at this time, ~20^{o}C compared to ~12^{o}C during the late Albian (Huber et al., 2002) and 2^{o}C today. This warm water would contain less dissolved oxygen, and might indicate more stagnant deep water circulation (Savin, 1977; Erbacher, 2001). Sageman and Meyers (2002) illustrated that peaks in $\delta^{13}C$ values can precede or follow the peaks for total organic carbon (TOC) for OAE2. This suggests the anoxia does not simply result from oxygen depletion due to high organic carbon rain rates. Herrle et al. (2003)

examined the forcing mechanism of black shale formation during OAE1 and found variations between oxygen isotopes, and calcareous nannoplankton, palynomorph, and benthic foraminifera assemblages that reflect changes to climatic conditions. The study concluded that these variations were caused by feedback mechanisms within a monsoonal climate system, which involve warm/humid and cool/dry cycles. They argue that the black shale formation and deep water anoxia occurred during humid conditions when high precipitation and low evaporation resulted in decreased deep water formation and stagnation.

Another popular theory for the cause of anoxia focuses on changes in ocean and atmospheric chemistry caused by the eruption of large igneous provinces (LIPS), namely the Caribbean province and/or an increase in hydrothermal activity associated with increased ocean crust production, both of which coincide with OAE2 (Arthur et al., 1997; Weissert, 1989; Larson, 1991; Sinton and Duncan, 1997; Kerr, 1998; Jones et al., 2001; Brumsack, 2005; Snow et al., 2005). Weissert (1989) argues that increased subsurface volcanism put excess CO_2 into the atmosphere, which in turn accelerated continental weathering increasing the supply of nutrients to the oceans. Another argument suggests that the subsea eruption was so large that the buoyant hydrothermal plume brought limiting nutrients in the form of dissolved metals to the surface of the ocean, resulting in drastically increased surface productivity (Sinton and Duncan, 1997; Snow et al., 2005). These LIPS eruptions are believed to have been 3 orders of magnitude larger than the largest mid-ocean ridge event (Sinton and Duncan, 1997) and the increase in O_2 consumption by the oxidation of sulfides and metals could have overwhelmed the poorly oxygenated water below the mixed layer leading to brief periods of seawater anoxia and

the extinction of some bottom dwelling organisms. Plate reconstructions for this time highlight an open gateway in the current Caribbean region, connecting the Atlantic and Pacific (Lawver et al., 1994; figure 4-1). This configuration would have assured that events in the Pacific influenced at least the northern Atlantic (Sinton and Duncan, 1997).

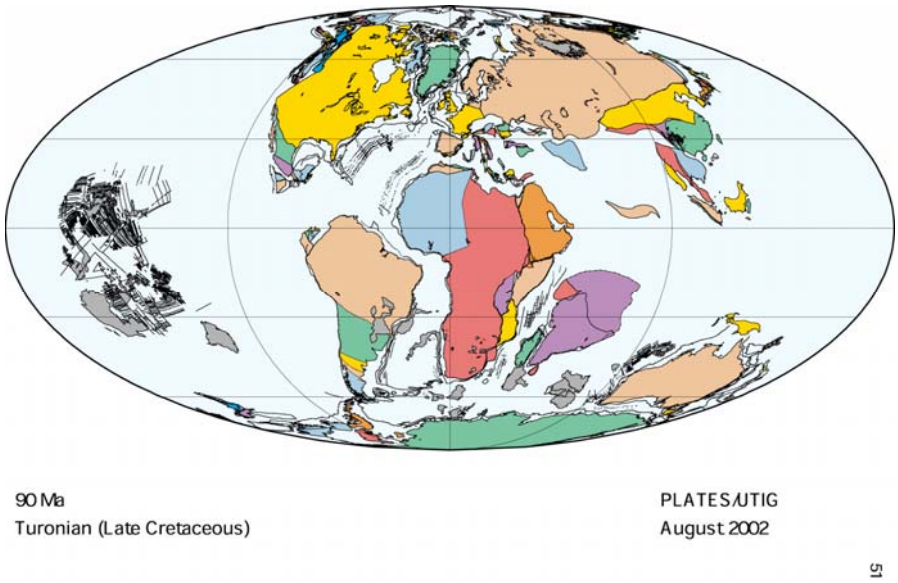

Figure 4-1. Tectonic plate reconstruction at 90Ma showing the open connection between the Atlantic and Pacific Oceans (Lawver et al., 1994)

Interestingly, a number of the OAEs throughout the Mesozoic coincide with large perturbations to the Sr isotopic curve (figure 4-2). The OAEs that occurred during the Jurassic, the Early Aptian, and the Cenomanian-Turonian (OAE2) all have sharp nonradiogenic excursions in the $^{87}Sr/^{88}Sr$ value (Jones and Jenkyns, 2001). The most probable cause for these excursions is the increase in hydrothermal activity associated with the eruption of LIPS and crust production (figure 4-3). Given that OAE events punctuate a long interval of increased crustal production, Jones and Jenkyns (2001) suggest that the increased nutrients and CO_2 from these out-gassing events simply preconditioned the oceans for anoxia, but there had to be another simultaneous variable, such as sea level change, that pushed the ocean into complete anoxia.

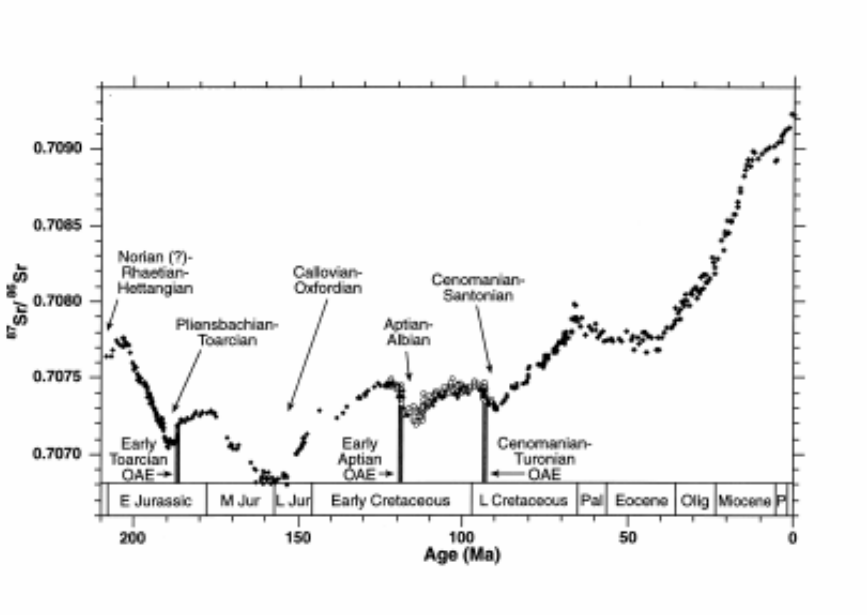

Figure 4-2. The seawater Sr isotope curve with 3 OAEs that coincide with perturbations in the Sr isotopic values (from Jones and Jenkyns, 2001).

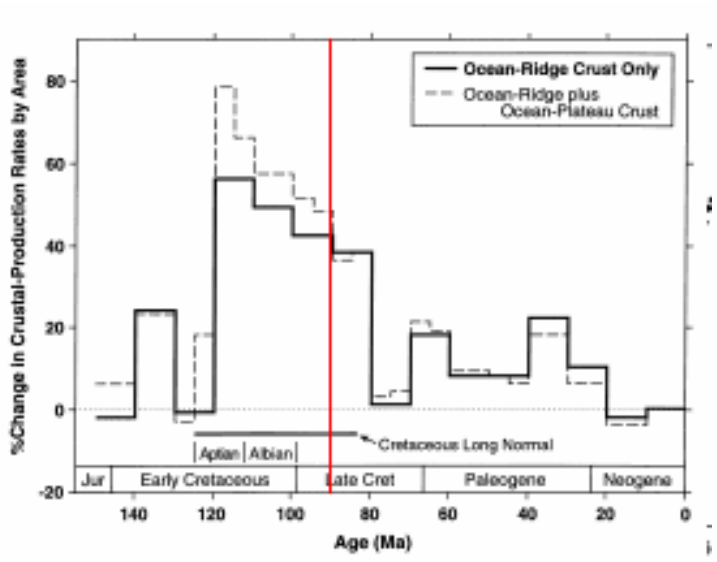

Figure 4-3. Relative ocean crust and plateau production over time. The line represents the position of OAE2 (adapted from Jones and Jenkyns, 2001). Production rates from 120 to 80 Ma are higher than the preceding or subsequent intervals.

A dramatic sea level rise (Figure 4-4) also coincides with OAE2 and OAE3 and increased ocean crust production (Haq et al., 1988; Jenkyns, 1991). Erbacher and Thurow (1997) proposed that this increase in sea level drowned carbonate platforms,

thereby leaching nutrients into the oceans, which in turn caused an increase in primary productivity. Given that OAEs are isolated, relatively short events, Jones and Jenkyns (2001) proposed that global warming associated with hydrothermal activity and crust production may have preconditioned the ocean, while sea level rise provided the final trigger for the event.

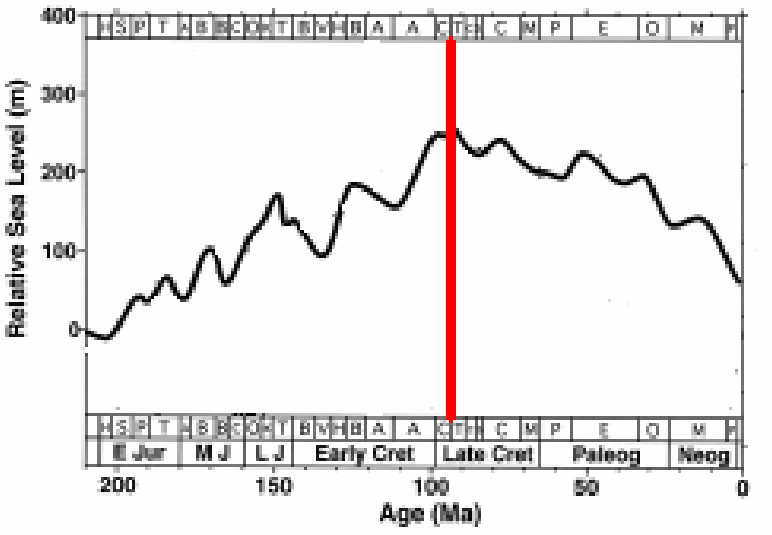

Figure 4-4. Eustatic sea level curve of the last 200 Ma. The line represents the position of OAE2 and correlates fairly well to a sea level high stand (adapted from Jones and Jenkyns, 2001).

Among the many theories for enhanced anoxia during the Late Cretaceous, the most popular theories rely on 1) increased productivity or 2) increased preservation as a function of a change in circulation, and it has been difficult to distinguish between the two. Nd isotopes have been shown to effectively record changes in ocean circulation independent of changes in productivity. By obtaining a record of Nd values over an anoxic interval, it may be possible to test whether changes in deep ocean circulation were related to periods of anoxia. If there is no change in Nd values it could be imply that OAEs were caused chiefly by an increase in surface production.

CHAPTER 5
RESULTS FROM THE CRETACEOUS OAE STUDY

The $\delta^{13}C_{org}$ values measured at site 1258 on Demerara Rise (figure 2-4) record the large positive excursion typical of OAEs during both OAE2 and the Mid-Cenomanian event (figure 5-1; table 5-1). This work will primarily focus on the OAE2, which spans from 422.26 to 423.81 mcd, but the Mid-Cenomanian Event (MCE), another anoxic event, is also clearly distinguishable at 448.18 mcd. Both events record excursions of ~6 ‰ (MacLeod, unpublished data), which is the same shift documented by Erbacher et al. (2006). The total organic carbon (TOC) jumps from ~13% to nearly 30% during OAE2 (figure 5-1).

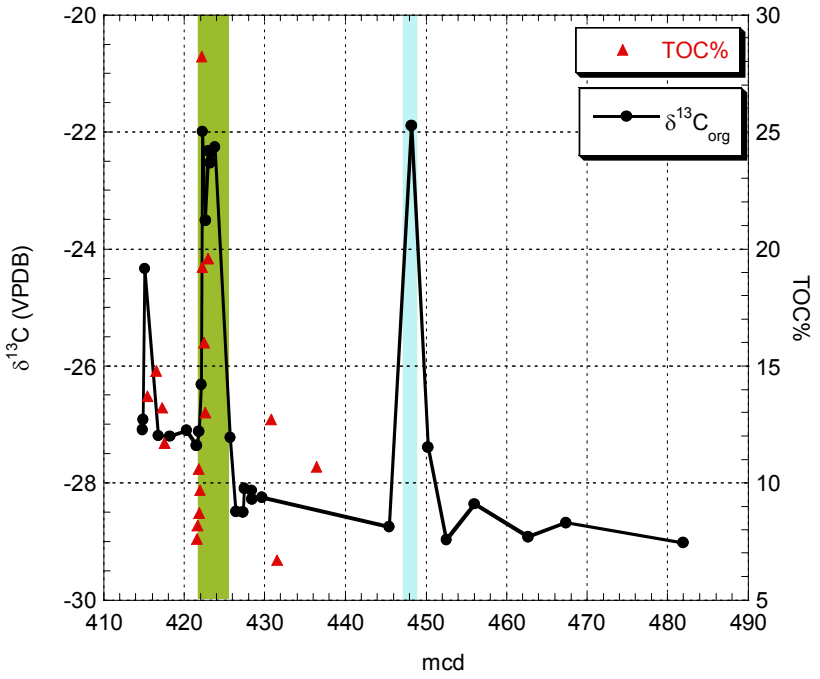

Figure 5-1. $\delta^{13}C$ and TOC % from ODP Site 1258 from 410-490 mcd. The green box from 422-424 mcd represents OAE2 and the aqua box is the MCE spanning from 448 to 453 mcd.

Table 5-1. Site 1258 mcd and $\delta^{13}C$

mcd	$\delta^{13}C$ vs VPDB	
414.78	-27.09	
414.83	-26.92	
415.11	-24.33	
416.77	-27.19	
418.24	-27.20	
420.29	-27.10	
421.51	-27.36	
421.81	-27.12	
422.09	-26.31	
422.26	-21.99	
422.62	-23.51	
422.96	-22.32	**OAE2**
423.22	-22.53	
423.81	-22.25	
425.71	-27.22	
426.44	-28.48	
427.32	-28.50	
427.48	-28.09	
428.30	-28.12	
428.36	-28.27	
429.60	-28.24	
445.43	-28.75	
448.18	-21.89	**MCE**
450.22	-27.39	
452.53	-28.97	
456.04	-28.36	
462.68	-28.92	
467.33	-28.68	
481.87	-29.02	

Unpublished data from McLeod.

To determine whether there was a change in ocean circulation associated with OAE2 and the MCE in the North Atlantic $\varepsilon_{Nd(t)}$ was measured for Site 1258 over the interval encompassing both carbon isotope shift. Neodymium isotopes were sampled from 375 to 480 mcd at fairly low resolution, averaging about every 30 kyr. The $\varepsilon_{Nd(t)}$ values prior to MCE and between the MCE and OAE2 were fairly nonradiogenic with values as low as -16 and as high as -13 ε_{Nd} units (figure 5-2; table 5-2). The largest anomaly prior to OAE2 is the large peak that coincides with the MCE at 448.18 mcd

where the $\varepsilon_{Nd(t)}$ value spikes to -10.6. After OAE2 $\varepsilon_{Nd(t)}$ values drop back to nonradiogenic values of -13.5 to -17.8.

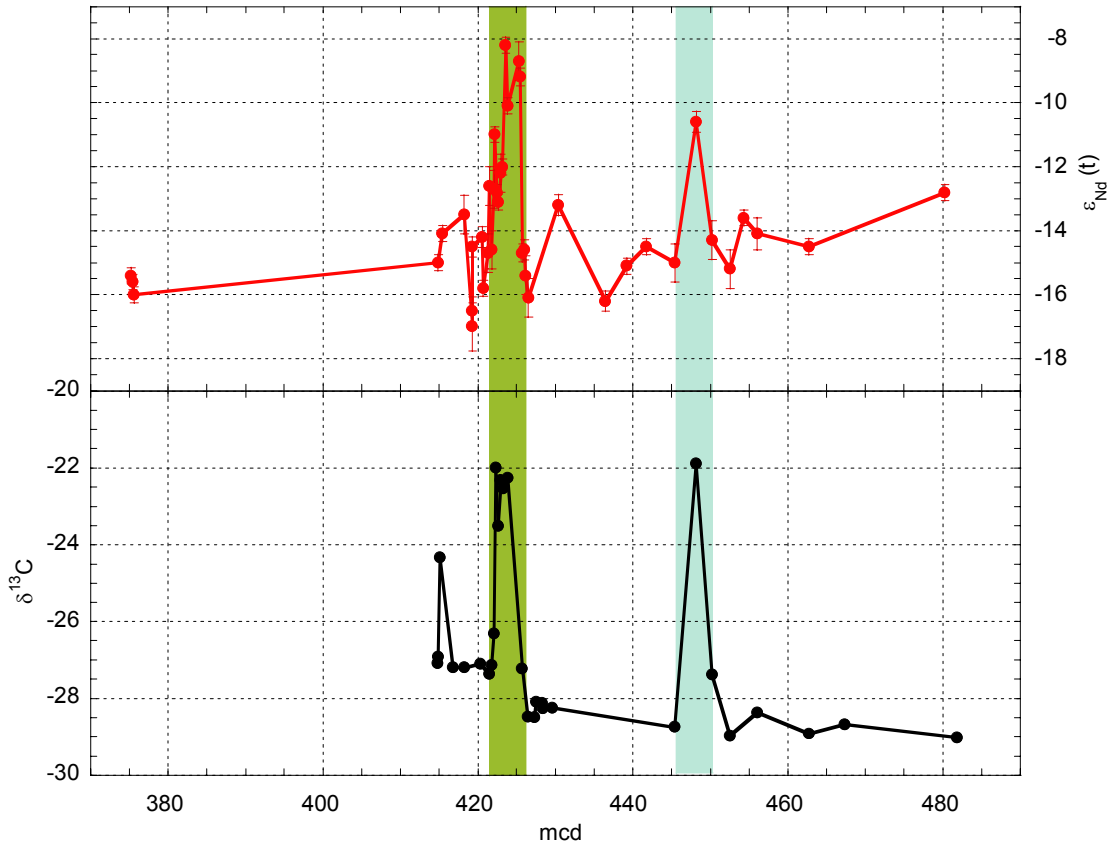

Figure 5-2. $\varepsilon_{Nd}(t)$ and $\delta^{13}C$ values from Site 1258 from 370 to 490 mcd. The green box represents OAE2 and the aqua box represents the MCE.

During OAE2 $\varepsilon_{Nd}(t)$ values increase dramatically by nearly 8 ε_{Nd} units peaking at -8.2. This transition occurred fairly rapidly and is tightly correlated to high resolution $\delta^{13}C_{org}$ results for the same core (Erbacher et al.,2005) (figure 5-3). The rate of increase at the start of the event is very similar between the two proxies and the peak of each falls within 130 cm; ε_{Nd} peaks at the onset of the event at 425.29 mcd and $\delta^{13}C_{org}$ peaks at 425.16 mcd. Based on $\delta^{13}C_{org}$ Erbacher (2005) defines the anoxic interval between 422

to 426 mcd. The ε_{Nd} excursion falls almost precisely within these limits (421.8 to 426 mcd) and the small discrepancy that exists may be a function of sampling frequency.

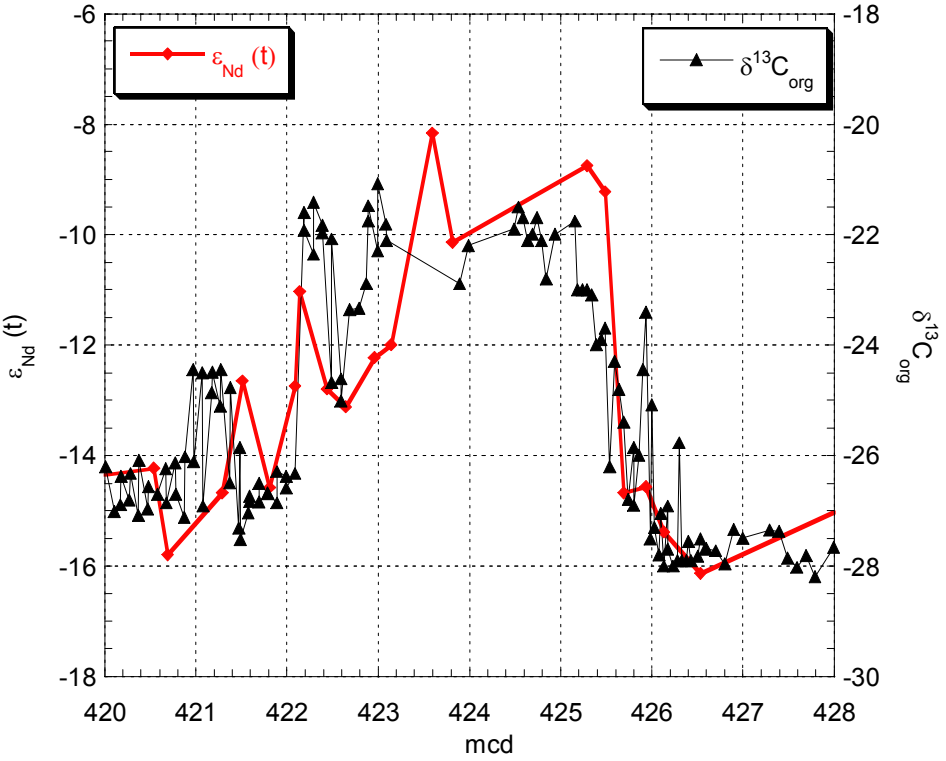

Figure 5-3. High resolution $\delta^{13}C_{org}$ from Erbacher et al., 2005 with the $\varepsilon_{Nd(t)}$ values spanning OAE2 (420-428 mcd) from ODP Site 1258.

To determine the distribution of Nd isotopes during the Mid-Cretaceous fish tooth or fish debris samples were also analyzed from Site 886 in the Pacific Ocean and Site 1050 at Blake Nose (figure 2-4). Low resolution sampling from these sites illustrates that values from 70 to 81 Ma at Site 886 were more radiogenic than any other site sampled in this study, ranging from -4 to -5.5 (figure 5-4; table 5-2). Samples from 95 to 102 Ma at Blake Nose (Site 1050) also yielded relatively radiogenic $\varepsilon_{Nd}(t)$ values of -5, but ranged down to –9.5 at 77 Ma.

Sites 1259 and 1260 with present water depths of 2354 mbsl and 2549 mbsl respectively represent shallower locations than Site 1258 (present water depth of 3192

mbsl). Samples were analyzed from these sites to determine whether the very negative ε_{Nd} values observed at Site 1258 were unique. From ~66 to 71 Ma Site 1259 yielded values that ranged from -15 to -16.5 ε_{Nd} units. Site 1260 samples yielded relatively consistent values around -16 from 70 to 75 Ma. At 70 Ma data points from 1260 and 1259 are within error of one another at a value of -15.85 ε_{Nd} units.

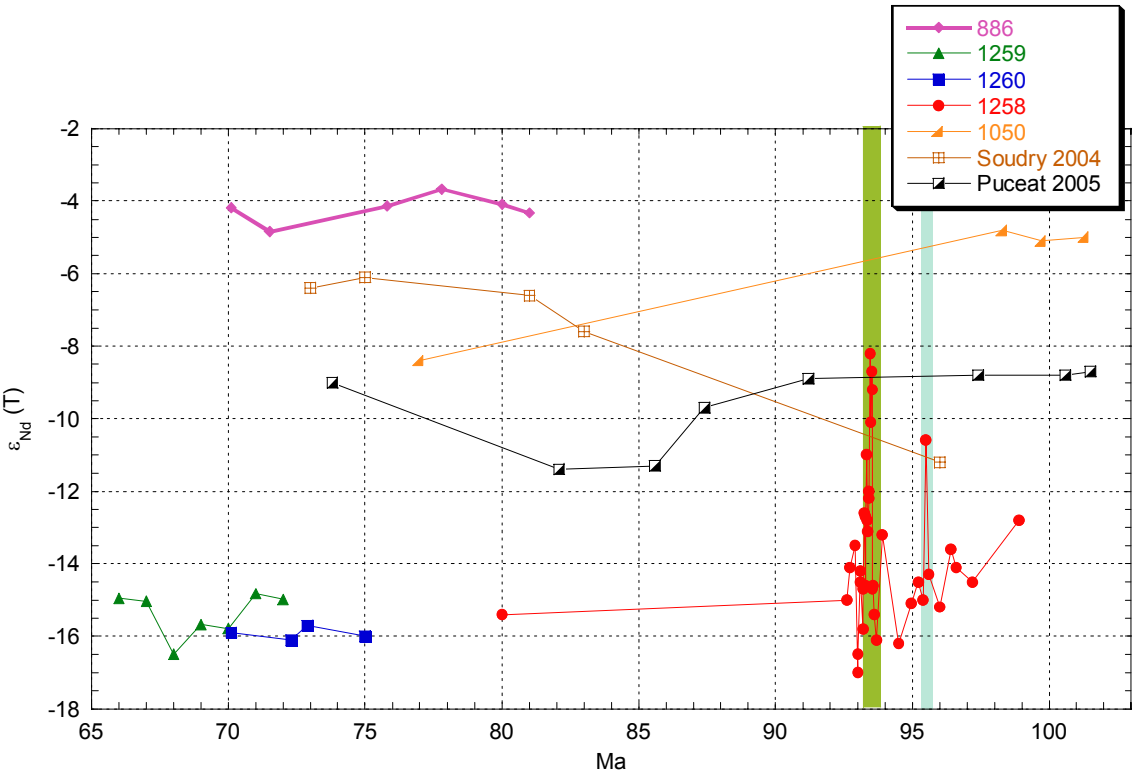

Figure 5-4. $\varepsilon_{Nd(t)}$ values from Site 886 in the Pacific Ocean, Sites 1259, 1258, and 1260 from Demerara Rise, and Site 1050 from Blake Nose spanning 65-103 Ma. The green box represents OAE2 and the aqua box shows the position of the MCE. Additional data includes ε_{Nd} values from the Negev in Israel (Soudry et al., 2004) and Tethyan values from France (Pucaét et al., 2005).

Table 5-2. Sr and Nd values from Cretaceous Samples from ODP Sites 886, 1050, 1258, 1259, 1260

Sample name	mcd	Age (Ma)[1]	$^{87}Sr/^{86}Sr$[2]		$^{143/144}Nd$[3]	$\varepsilon_{Nd(o)}$[4]	$\varepsilon_{Nd(t)}$[5]		$^{147}Sm/^{144}Nd$
Pacific									
886-C 8-1 60	64.40	70.1	0.70795 ±	2.3E-05					
886C 8-1 112.5	64.90	71.5			0.512389	-4.86	-4.19 ±	0.25	
886-C 8-2 122.5	66.50	71.5	0.70796 ±	2.3E-05	0.512356	-5.51	-4.84 ±	0.25	
886C 8-3 122.5	68.00	75.8			0.512392	-4.80	-4.13 ±	0.25	
886C 8-4 122.5	69.50	77.8			0.512415	-4.35	-3.68 ±	0.25	
886-C 8-5 113	70.93	80	0.70812 ±	2.3E-05	0.512395	-4.75	-4.08 ±	0.25	
886C 8-6 52	71.82	81			0.512382	-4.99	-4.32 ±	0.25	
Atlantic/Blake Nose									
1050 20-1 33	490.63	77.00			0.512179	-8.95	-8.44 ±	0.25	
1050 27-2 103	558.25	98.30			0.512349	-5.64	-4.77 ±	0.25	
1050 29-2 102	577.45	99.73			0.512334	-5.93	-5.06 ±	0.25	
1050 31-2 103	596.65	101.30			0.512337	-5.87	-5.00 ±	0.25	
Atlantic/DemeraraRise									
1258A 38-1 105A	375.20	80.00			0.511804	-16.27	-15.44 ±	0.25	
1258A 42R -1 8	414.83	92.62	0.70758 ±	2.3E-05	0.511824	-15.88	-15.01 ±	0.25	
1258A 42R-1 65	415.40	92.67	0.70753 ±	2.3E-05	0.511872	-14.95	-14.08 ±	0.25	
1258A 42R-3 60	418.24	92.90			0.511899	-14.42	-13.55 ±	0.60	0.1250
1258B 45R-1 95	419.28	93.04	0.70755 ±	2.3E-05	0.511724	-17.83	-16.96 ±	0.75	
1258B 45R-1 95	419.28	93.04			0.511748	-17.36	-16.49 ±	0.43	
1258B 45R-1 96	419.29	93.05			0.511849	-15.39	-14.52 ±	0.32	
1258B 45R-3 36	420.54	93.10			0.511864	-15.10	-14.23 ±	0.32	
1258B 45R-3 51	420.69	93.18	0.70759 ±	2.3E-05	0.511783	-16.67	-15.80 ±	0.25	
1258A 42R-5 12	421.29	93.21			0.511841	-15.55	-14.68 ±	0.60	
1258A 42-6 2	421.51	93.24			0.511945	-13.52	-12.65 ±	0.60	
1258A 42-6 32	421.81	93.28			0.511846	-15.45	-14.58 ±	0.60	0.1256
1258A 42-6 60	422.09	93.29			0.511940	-13.62	-12.75 ±	0.60	
1258A 42R-6 65	422.14	93.32	0.70757 ±	2.3E-05	0.512028	-11.90	-11.03 ±	0.25	
1258A 42R-6 95	422.44	93.35	0.70757 ±	2.3E-05	0.511938	-13.66	-12.79 ±	0.25	
1258A 42R-6 115	422.64	93.37	0.70759 ±	2.3E-05	0.511921	-13.99	-13.12 ±	0.25	
1258A 42R-7 7	422.96	93.40			0.511967	-13.09	-12.22 ±	0.60	
1258A 42R-7 25	423.14	93.42	0.70760 ±	2.3E-05	0.511978	-12.87	-12.00 ±	0.25	
1258A 42R-7 70	423.59	93.46	0.70760 ±	2.3E-05	0.512175	-9.03	-8.16 ±	0.25	
1258A 42R-7 92	423.81	93.48	0.70774 ±	2.3E-05	0.512074	-11.01	-10.14 ±	0.25	
1258C 17X-1 85	425.29	93.52			0.512145	-9.62	-8.75 ±	0.60	
1258C 17X-1 105	425.49	93.53			0.512120	-10.10	-9.23 ±	0.28	
1258C 17X-1 125	425.69	93.55			0.511841	-15.55	-14.68 ±	0.28	
1258C 17X-2 10	425.93	93.57			0.511847	-15.43	-14.56 ±	0.32	
1258C 17X-2 30	426.13	93.60			0.511805	-16.25	-15.38 ±	0.60	
1258C 17X-2 70	426.53	93.70			0.511766	-17.01	-16.14 ±	0.60	
1258B 47R-1 23	430.40	93.90			0.511917	-14.06	-13.19 ±	0.32	
1258B 48R-1 111	436.45	94.50			0.511764	-17.05	-16.18 ±	0.32	
1258B 49R-1 44	439.20	94.97	0.70760 ±	2.3E-05	0.511822	-15.92	-15.05 ±	0.25	
1258B 49R-3 30	441.73	95.21			0.511853	-15.32	-14.45 ±	0.25	
1258A 45R-2 57	445.43	95.40			0.511822	-15.92	-15.05 ±	0.60	0.1262
1258A 46R-1 0	448.18	95.50			0.512049	-11.49	-10.62 ±	0.32	
1258A 46R-2 68	450.22	95.60			0.511859	-15.20	-14.33 ±	0.60	0.1218
1258A 46R-4 33	452.53	96.00			0.511812	-16.11	-15.24 ±	0.60	
1258A 47R-1 12	456.04	96.59	0.70764 ±	2.3E-05	0.511873	-14.93	-14.06 ±	0.50	

Table 5-2. Continued

1258C 27R-2 0	480.29	98.93	0.70755 ±	2.3E-05	0.511935	-13.71	-12.84 ±	0.25
1258C 32R-CC	505.95	101.00	0.70759 ±	2.3E-05				
1259								
1259B 13R-1 114	441.91	66.00			0.511837	-15.63	-14.96 ±	0.32
1259B 13R-7 40	442.60	67.00			0.511833	-15.70	-15.03 ±	0.32
1259B 14R-2 90	452.06	68.00			0.511758	-17.17	-16.50 ±	0.32
1259B 15R-1 76	458.90	69.00			0.511800	-16.35	-15.68 ±	0.32
1259B 15R-3 58	459.03	70.00			0.511794	-16.46	-15.79 ±	0.32
1259B 15R-6 70	459.64	71.00			0.511844	-15.49	-14.82 ±	0.32
1259B 16R-1 56	470.98	72.00			0.511836	-15.64	-14.97 ±	0.32
1260								
1260A 39R-1 78	357.12	70.10	0.70772 ±	2.3E-05	0.511788	-16.58	-15.91 ±	0.25
1260A 40R-1 109	369.05	72.30	0.70770 ±	2.3E-05	0.511776	-16.81	-16.14 ±	0.25
1260A 40R-3 104	372.00	72.90	0.70771 ±	2.3E-05	0.511801	-16.33	-15.66 ±	0.25
1260A 42R-2 77	389.89	75.00	0.70766 ±	2.3E-05	0.511783	-16.68	-16.01 ±	0.25

[1.] Ages for Site 886 from Ravizza, unpublished data.; for Site 1050 from Shipboard Scientific Party, 1998; and for Sites 1258, 1259, 1260 from Erbacher, 2004.

[2.] Measured $^{87}Sr/^{86}Sr$ of the NBS-987 standard = 0.7120250 ± 0.000023 (2σ) and normalized to $^{86}Sr/^{88}Sr$ = .1194

[3.] $^{143/144}Nd$ values are normalized to Jndi-1 average on the day the samples were analyzed and are then normalized to Jndi-1 = 0.512103 (TIMS average)

[4.] $\varepsilon_{Nd(o)} = [(^{143}Nd/^{144}Nd)_{sample}/(^{143}Nd/^{144}Nd)_{CHUR}-1] \times 10^4$

[5.] $\varepsilon_{Nd(t)} = [(^{143}Nd/^{144}Nd)_{sample(t)}/(^{143}Nd/^{144}Nd)_{CHUR(t)}-1] \times 10^4$ using $^{147}Sm/^{144}Nd$

CHAPTER 6
DISCUSSION OF CRETACEOUS OAE STUDY

The ε_{Nd} values for the Cretaceous study were derived from fossil fish teeth and fish debris. An important consideration for material of this age is whether these values represent contemporaneous bottom waters, as they do for younger samples (e.g. Staudigel et al., 1985; Martin and Scher, 2004), or if the values have been influenced by diagenetic alteration. There are several lines of evidence to suggest that the shift seen in the ε_{Nd} values at Site 1258 does, in fact, represent a change in ocean water mass. Firstly, the lithology across the OAE2 and the MCE intervals is consistent. For 15 Ma throughout the Cenomanian and Turonian thinly laminated, organic- rich black shales were deposited, with no change in lithology. The primary lithologic boundary occurs instead in the Late Campanian; however, background values are the same before and after this change. Thus, there is no lithologic change associated with the large shift in Nd isotopes, and no Nd isotopic change associated with the lithologic boundary.

Secondly, the large positive excursion in the Nd isotopes could be created by diagenetic alteration from young volcanic material. To test this theory Sr isotopes were analyzed from the fish teeth and debris, with the expectation that alteration in the presence of volcanic ash would produce a corresponding shift in the $^{87}Sr/^{86}Sr$ value toward less radiogenic values. Strontium isotopes measured in fossil fish teeth from Site 1258 are much more radiogenic than the $^{87}Sr/^{86}Sr$ seawater curve. Figure 6-1 illustrates that the Sr isotopes preserved in the fish debris are shifted toward continental values rather than young volcanics.

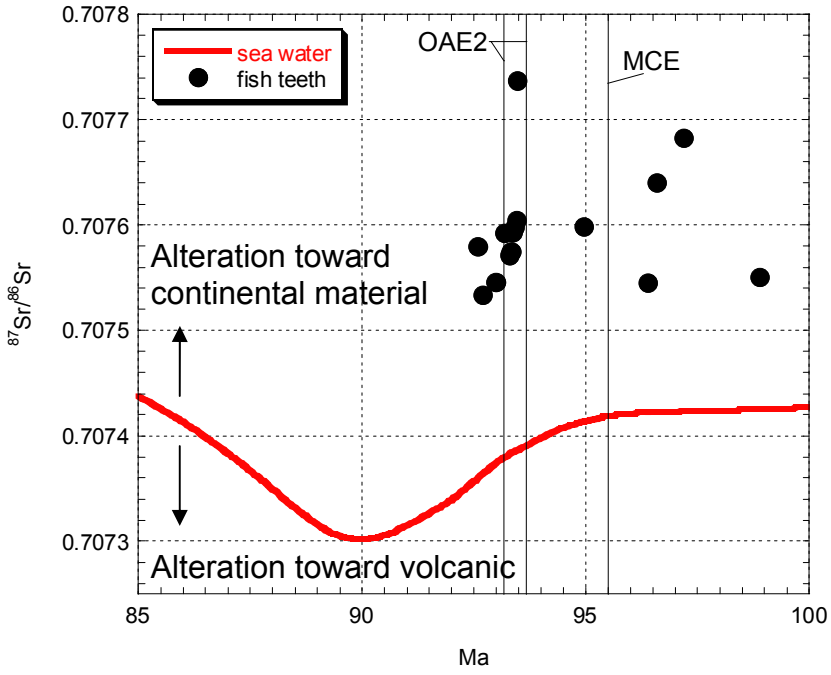

Figure 6-1. $^{87}Sr/^{86}Sr$ seawater curve from 85-100 Ma (Jones and Jenkyns, 2001) along with the Sr isotopic values from fossil fish debris collected from Site 1258.

REE patterns measured on fish teeth and debris provide further support for the lack of diagenetic alteration. REE were measured from samples before, during, and after OAE2 to determine if there was any change across this interval. If the anomaly were caused by diagenesis (suggesting that the excursion during the event was the product of young volcanic input), the REE patterns from before and after the excursion might be expected to be different from the pattern during the event. In particular, samples affected by diagenesis in the sedimentary environment would be expected to have flatter REE patterns typical of shale or terrestrial inputs, when normalized to PAAS. However, all of the samples have MREE enrichment relative to shale, suggestive of REE fractionation into apatite (figure 6-3) (e.g. Reynard et al., 1998) and do not seem to be influenced by volcanics, which would be recorded as an enriched HREE pattern. All the samples also have a similar Ce anomaly indicating that they were deposited under similar redox conditions (Grandjean et al., 1987; Lecuyer et al., 2004).

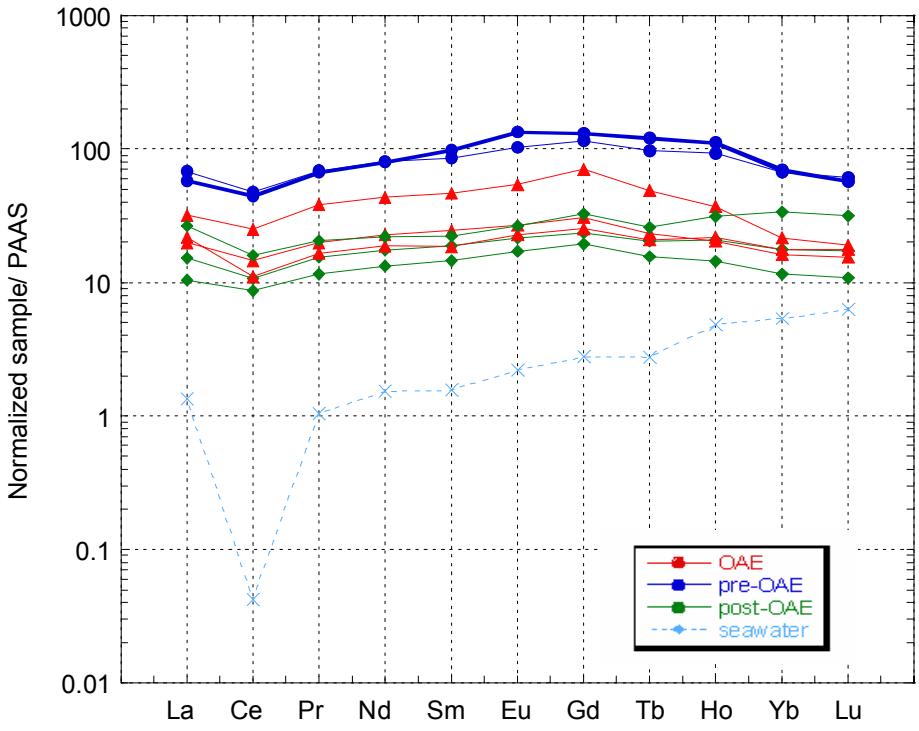

Figure 5-3. REE plots of modern seawater (De Baar, 1985) compared to samples from before, during, and after OAE 2. All profiles are normalized to PAAS shale (Taylor and McLellen, 1985). REE pattern for modern seawater from 3000 m (De Baar et al., 1985).

Table 6-1. REE values from Fossil Fish Teeth Samples from Before, During and After OAE2

Sample	La	Ce	Pr	Nd	Sm	Eu	Gd	Tb	Ho	Yb	Lu
Before	31.627	25.021	38.072	43.610	46.467	53.721	70.377	48.386	36.923	21.381	19.013
Before	19.783	14.621	19.929	22.743	24.579	26.793	30.578	23.436	20.399	16.058	15.377
Before	21.763	11.017	16.478	18.864	18.523	22.857	25.400	20.858	21.670	17.769	17.697
During	67.776	47.387	68.525	80.871	85.371	103.068	115.327	97.000	92.685	66.885	61.319
During	57.743	44.318	67.019	79.922	98.529	134.449	131.601	120.295	111.479	69.611	57.463
After[1]	26.329	15.998	20.565	22.116	22.190	26.310	32.652	25.814	31.092	33.689	31.451
After	15.304	10.725	15.453	17.590	18.638	21.386	23.660	20.456	20.849	17.741	17.354
After	10.477	8.667	11.607	13.316	14.463	17.076	19.479	15.609	14.354	11.517	10.835

Notes: [1]Sample values multiplied by 10
Error is ± 5%

Finally, diagenetic alteration of the Nd isotopes might be expected to coincide with lithologic boundaries. The Late Cretaceous section measured for this study has a very consistent lithology of black shale, which continues from 92.6 to 98.5 Ma and crosses the Cenomanian-Turonian boundary and OAE2. The largest change in lithology in the interval of interest occurs at 415 mcd at the hiatus/condensed interval that separates the

black shale from chalk (figure 2-3). There are undoubtedly changes in diagenetic conditions across this boundary, yet the ε_{Nd} values are unaffected (figure 4-2)

The $\varepsilon_{Nd(t)}$ values reported at Demerara Rise, from Sites 1258, 1259, and 1260, before and after OAE are extremely nonradiogenic (-14 to -17). These values are lower than any other values reported over this time period, suggesting that there was a separate and distinct water mass bathing this site. Published ε_{Nd} values for the Late Cretaceous include values of -2.5 to -5.5 for the central Pacific (Thomas, 2004; Frank et al., 2005) and values of -7 to -12 for the Tethys (Stille and Fisher, 1990; Soudry et al., 2004; Pucéat et al., 2005). Values from Pucéat (2005) and Soudry (2004) are plotted on figure 5-4 and represent a distinct water mass from the one bathing Demerara Rise before and after the anoxic events. However during the events the excursions at Site 1258 are similar to, although slightly less radiogenic than, these Tethyan water masses. The background values reported in this study are also lower than the modern North Atlantic, which has the most nonradiogenic value for a major modern water mass, with values of about -13 (e.g. Piepgras and Wasserberg, 1987; Lacan and Jeandel, 2005), and lower than any other reported ε_{Nd} value for a major water mass in the Cenozoic (Burton et al., 1997; Ling et al., 1997; O'Nions et al., 1998; Burton et al., 1999; Frank, 2002; Thomas et al., 2003; Scher and Martin, 2004; Soudry et al., 2004; Thomas, 2004; van der Flierdt et al., 2004; Frank et al., 2005; Scher and Martin, 2006).

During the Late Cretaceous the North Atlantic was a young ocean with large sills and ridges that could have restricted deep circulation (Bonatti et al., 1994; Jones et al., 1995; Handoh et al., 1999). In particular, there is evidence that there was no deep connection between the North and South Atlantic at this time (Kennett, 1982; Frank and

Arthur, 1999). The nonradiogenic values from Demerara suggest that this may have been a relatively isolated basin that was affected by proximal weathering from the South American continent. Local weathering of the Trans-Amazonian Proterozoic Shield or the Archean Guiana Highland would have introduced nonradiogenic Nd into the bottom waters in this region (White and Dupré, 1985). This idea of an isolated basin around Demerara is further supported by the ε_{Nd} values at Blake Nose that are much more radiogenic over this period, suggesting they may have been influenced by the open flow between the North Atlantic and the Pacific (figure 5-4).

The most intriguing aspects of the ε_{Nd} data from Demerara Rise are the large ε_{Nd} positive excursion of 8 units and the close, if not exact, correlation to the $\delta^{13}C_{org}$ excursion during OAE2, as well as the MCE. OAE2 spans about 4 m of sediment at Site 1258 and is believed to represent 563-601 k.y. based on an orbitally tuned record (Sageman et al., 2005). Given that the ε_{Nd} excursion is not the result of diagenetic processes, the most likely cause is a change in deep water circulation at this site during the anoxic event. This conclusion argues against the theory that OAE2 is caused by an increase in primary production (e.g., Pederson and Calvert, 1990; Calvert and Pederson, 1992; Erbacher and Thurow, 1997 Wonders, 1980, Kuhnt 1986, and Jarvis, 1988, Weissert 1989), as productivity alone would not alter the ε_{Nd} value. In addition, the Nd isotopic evidence that Demerara Rise is located in an isolated basin before and after OAE2 argues that OAE2 is not the product of increase in preservation caused by deep water stagnation (Savin, 1977; Erbacher, 2001). Instead the ε_{Nd} changes at this site indicate a rapid onset of mixing or changes to flow patterns concurrent with changes to the carbon isotopes. Any theory for the formation of OAE2 must take into account the

shift to radiogenic ε_{Nd} values over the event and the correlation to the positive shift in $\delta^{13}C$ values, which implies an increase in productivity and/or preservation. There are few hypotheses presented in the literature that would explain both of these proxies.

One possible explanation of the data is that the sea level transgression across the Cenomanian- Turonian boundary (Jones and Jenkyns, 2001) may have led to a connection between deep waters at Demerara Rise and Blake Nose. Mixing between the Blake Nose endmember (-5) and the Demerara endmember (-16) could produce the observed excursion value of up to –8 ε_{Nd}. In terms of $\delta^{13}C$, the sea level rise would have drowned continental shelves thereby releasing nutrients into the ocean and leading to increased productivity, which in turn caused the anoxia (Haq et al., 1988; Jenkyns, 1980; Jenkyns, 1991). Thus, a rise in sea level could explain both the enhanced deep water circulation and increased surface productivity. Jenkyns (1980) found evidence of rapid sea level rise in both the Western Interior Seaway (WIS) and in Northern Europe associated with both OAE2 and OAE3. The transgressive events appeared to have relatively short durations similar to those of the OAEs; however, the ages were poorly constrained. Although the highstands in the WIS and Northern Europe seem to peak during OAE2, the global sea level record peaks at the end of the event (Jenkyns, 1980). An additional problem with this theory is that every sea level rise is not associated with an OAE and some of the OAEs (e.g. OAE1c) are not associated with a sea level transgression (Jones and Jenkyns, 2001). In this scenario, the ocean at the time of the Cretaceous OAEs must have been preconditioned by some other mechanism so that sea level rise could have such a dramatic effect.

Another proposed mechanism for OAEs is the drastic increase in ocean crust production or Caribbean LIP formation (Sinton and Duncan, 1997; Jenkyns and Jones, 2001; Leckie et al., 2002; Snow et al., 2005). This eruption would have: 1) increased CO_2, which in turn would lead to an increase in primary production and continental weathering, and 2) increased nutrients associated with hydrothermal venting or enhanced continental weathering, thereby leading to increased production (Vogt, 1989; Erba, 1994; Kerr, 1998; Jones et al., 2001; Leckie et al., 2002; Snow et al., 2005). This increase in productivity would account for the increased $\delta^{13}C_{org}$ values and the increased organic rain would lead to anoxia. In terms of Nd, the ε_{Nd} value of oceanic basalt is ~+10, thus the shift in Nd isotopes observed at Demerara Rise could reflect the input from basalt weathering or hydothermal inputs. There are two assumptions associated with this theory. Firstly, there would have to be an open gateway for mixing between the deep or intermediate water directly affected by the eruption and the water at Demerara Rise. Elemental abundances measured by Orth in the WIS, the Atlantic, and Pacific show large peaks during OAE2 that are indicative of increased seafloor spreading and hydrothermal processes. These anomalies are larger in the west and get smaller toward the east traveling from the Pacific into the Atlantic (1993). This west to east trend possibly indicates a west to east circulation pattern, thus connecting the eruption site (equatorial eastern Pacific) with Demerara Rise. The second assumption is that the anoxic conditions would have prevented the quantitative removal of Nd from hydrothermal vents sites. In modern oceans Nd is effectively removed at hydrothermal vent sites by Fe-Mn hydroxides (Michard et al., 1983; German et al., 1990), and is not circulated into the

ocean; however, the situation may have been very different under anoxic deep water conditions.

The problem with the LIP and increased sea floor production hypothesis is that it has been established that the basin surrounding Demerara rise was effectively isolated from other deep water masses (e.g. the one at Blake Nose), thus the eruption had to have a major effect on the surface water in order for it to affect deep to intermediate waters at Demerara. Otherwise some other process would have had to be coincident with the eruption of the LIPS and increase in ocean crust production, such as sea level rise or a change in upwelling. A greater problem is that there were two pulses of volcanism from the Caribbean LIP, as recorded in the WIS (Snow et al., 2005). Due to limited correlation between the WIS and Demerara Rise it is difficult to determine whether the two peaks seen in the Nd record, at 423.5 and 425.5 mcd, could be an effect of the two volcanic pulses. The pulses of volcanic activity identified by Erbacher (2004) do not correlate to peaks in the Nd record. There is also no evidence for a volcanic event associated with the mid-Cenomanian event for which there are similar shifts in $\delta^{13}C$ and ε_{Nd}.

The final hypothesis that could explain the positive excursions in both the $\delta^{13}C$ and the ε_{Nd} values across OAE2 is a change in the upwelling pattern at Demerara Rise. Upwelling would effectively bring nutrient rich waters from depth causing an increase in productivity directly leading to a positive excursion in $\delta^{13}C_{org}$ and the deposition of black shales (e.g. Handoh, 2003). Upwelling could also cause increased mixing as the upwelled water is replaced by intermediate or deep water from a different location, in this case possibly the more radiogenic waters that bathed Blake Nose and/or the Pacific. Changes in trace metal abundances in black shales from OAE2 exhibit signatures that are

indicative of coastal upwelling (Brumsack, 2005). It has also been suggested that volcanic processes may have generated a buoyant plume that initiated upwelling (Vogt, 1989).

Work by Kolonic et al. (2005) supports the theory that wind-driven upwelling is a mechanism for driving nutrient-rich waters to the surface to increase productivity. His recent work off the northwest coast of Africa found black shale formations interbedded with thin layers of carbonate sediment, suggestive of oxic conditions, and attributes these lithologic changes to the alternating position of the Intertropical Convergence Zone (ITCZ). Movement of the ITCZ can cause periods of arid conditions when it is located at a more southerly position, followed by extremely humid conditions, when the convergence migrates to the north. This atmospheric driven oceanographic change is supported by modeling experiments across the Cenomanian- Turonian boundary (Flögel, 2002). A modeling experiment of a proposed Tethyan circumglobal current also predicts seasonal monsoonal events (Bush and Philander, 1997). The modern analogue to this movement of the ITCZ is seen on the west coast of the African continent. During the northern hemisphere summer there are strong northerlies, which move the ITCZ north causing moist air to move inland over the continent. During the northern hemisphere winter the northerlies are weak, the ITCZ is in its more southern position, and dry air flows off the continent from the north leading to a more arid climate. When the ITCZ is in a more southerly position the weaker trades allow for upwelling along the coast. If this same idea is used on the South American continent there would be little to no upwelling on the east coast when the ITCZ is in a more northerly position and enhanced upwelling when it is in a more southerly position. Today, the movement of the ITCZ is a seasonal

change, so it is difficult to use this mechanism to explain a 10^6 year event. Kolonic (2005) invokes the idea of an orbital control on the location of the ITCZ ωιτη α στρονγ 100,000 ψεαρ εχχεντριχιτψ σιγναλ, ψετ φυρτηερ τεστ ωουλδ βε νεεδ το προωε τηισ.

Φυρτηερ ινωεστιγατιον ισ ρεθυιρεδ το χονστραιν τηε χαυσε οφ τηισ γλοβα λ ανοξιχ εωεντ, ψετ τηε $\delta^{13}C$ and ε_{Nd} records are undoubtedly linked. Therefore, the mechanism for anoxia must combine both productivity in the water column as well as enhanced intermediate to deep water mixing. Significantly, these data argue against the theory of stagnation as the cause for anoxia.

CHAPTER 7
BACKGROUND ON EXTRACTION EXPERIMENTS

Rutberg et al. (2000) first demonstrated that Nd extracted from extracted Fe-Mn oxide coatings was an effective tracer for ocean circulation on Pleistocene timescales. Their Nd isotopic record from a core in Cape Basin confirmed previous ideas that NADW production decreased during cold marine isotope stages stages 2 and 4 (e.g. Mix et al., 1985; Oppo and Fairbanks, 1987; Charles et al., 1992). Their procedure designed to selectively extract the Fe-Mn oxide coatings was modified from Chester and Hughes (1967) and used buffered acetic acid to remove the carbonate fraction followed by a 0.02 M hydroxylamine hydrochloride (HH) solution to reduce the Fe-Mn oxide fraction. Using this procedure Piotrowski et al. (2004) developed the record presented above to track millennial time scale changes in the strength of NADW over the last 20 kyr (figure 2-3).

The procedure used by Rutberg et al. (2000) was further tested by Bayon et al. (2001) in a study of the Last Glacial Maximum (last 30 kyr) from a different core in the Cape Basin. This study was designed to isolate the detrital fraction as well as the Fe-Mn oxide fraction of a marine sediment sample. Both of these fractions were then used to identify changes in ocean circulation. The continental sources of the detrital fraction provided information about the provenance of this material and possible water current directions, while Nd isotopes were extracted from the Fe-Mn oxide fraction. A number of variations in the technique were developed in order to completely isolate the detrital and Fe-Mn fractions. These variations included changes to the strength of the HH

solution, heating the sample during extraction, and removing the organic fraction prior to extraction. In the most effective procedure, an acetic acid wash was used to remove the carbonate fraction and a 0.5 M HH solution was used to remove the Fe-Mn oxide fraction, similar to Rutberg et al. (2000); however, they determined that using a HH solution with a lower molarity (0.04) did not remove the whole of the Fe-Mn oxide fraction and the Nd isotopic value of the detrital fraction was shifted toward seawater values. Each variation on the extraction procedure was systematically tested using Sr isotopes and REE patterns. It was assumed that the Nd isotopes were accurately recording the value of deep water when the Sr isotopes yielded appropriate seawater values. REE patterns of the various fractions are distinctly different and were used to verify whether the Fe-Mn oxide and detrital fraction were effectively separated from one another. This study was the first to systematically test the acetic acid wash and HH solution procedure. In conclusion, the detrital fraction could be effectively separated from the Fe-Mn oxide portion, but it proved very difficult to isolate the oxide portion with no effect from either the detritus, carbonate or the organic fractions.

CHAPTER 8
RESULTS OF THE FE-MN OXIDE COATING EXTRACTION PROCEDURE AND VALIDITY TESTS

8.1 Variations on the Extraction Procedure

The main goal of this portion of this project was to determine if it was possible to obtain Nd isotopic values from Fe-Mn oxide coatings that reflect seawater values on Cenozoic time scales. Bayon et al. (2000), Rutberg et al. (2000), and Piotrowski et al. (2004) demonstrated that extraction techniques are effective on younger timescales, but there is yet to be a systematic study of older sediments. To test the validity of the Nd isotopic values obtained from the extracted coatings in this study, they were compared to values from contemporaneous fossil fish teeth, assuming that the Nd isotopic value obtained from the fish teeth was correct. The extraction procedure by Rutberg et al. (2000) was the initial procedure used for this study, and it was subsequently modified.

The main concern with any extraction procedure is the removal of material other than the desired Fe-Mn oxide coating. Contamination from detrital material is likely to have an effect on the ε_{Nd} value obtained, altering it toward more or less radiogenic values depending on the source. Detrital in this case refers to any clay or other terrigenous material as well as any particulate contamination from volcanic sources or hydrothermal processes. The first steps taken to minimize detrital contamination were to alter the grain size used for extraction, the molarity of the HH solution, and the length of the extraction time.

The first variable tested was the grain size of the sediment. A previous study by Scher et al. (2003), on samples from ODP Site 1090, determined that extracting coatings from the <63 μm size fraction in many cases did not give ε_{Nd} values that fell within error of the values obtained from fossil fish teeth (Figure 8-1). The less than 63 μm fraction is composed chiefly of clay material, and although the particles may have oxide coatings, the chances of obtaining seawater values are greater if this possible contaminant can be eliminated. The 63-125 μm and >125 μm size fractions were also tested. A number of samples from each of those two size fractions were extracted and analyzed. It was determined that there was no distinguishable difference between samples of 63-125 μm and >125 μm size fraction samples (Figure 8-1). Samples used in the remainder of this study consist of >63μm size fraction of sediment.

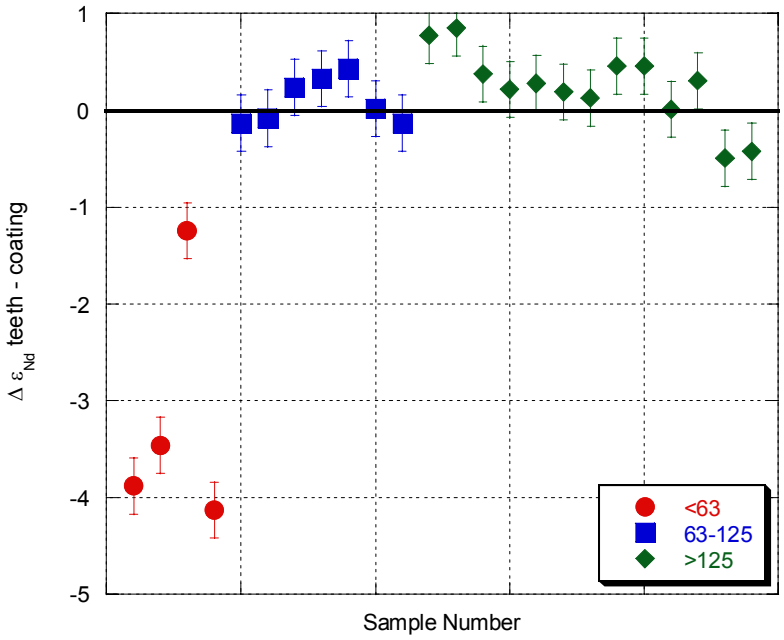

Figure 8-1. The difference of ε_{Nd} between fossil fish and Fe-Mn oxide coatings from samples of < 63 μm (circles), 63-125 μm (squares) and >125 μm (triangles) size fractions. Samples with a difference less than 0.5 ε_{Nd} units are assumed to agree within error for the TIMS.

The other variable tested was the length of time the HH solution remained on the sediment. For this test all samples were extracted with a 0.5M HH solution. Work by Bayon et al. (2001) determined that 1M HH solution removed nearly all the Fe-Mn oxide coating on marine sediment, leaving the remaining detrital material clean, which was their targeted material. By using a lower molarity HH solution, enough of the coating was removed for this study, but there was less chance of contamination from the remaining detrital material. Although the solution was weaker, an additional test was set up to determine whether it would have the same effect as the stronger solution if it were left on the samples for an extended length of time. To test this, sequential sediment samples were treated for 4, 2, and 1 hour time intervals. As figure 8-2 illustrates, samples treated for 1-2 hours fell within error of the contemporaneous fossil fish teeth samples more often than samples treated for 4 hours. Several of the samples that were treated for 4 hours did not give ε_{Nd} values that were close to the values obtained from the fish teeth. In these cases the HH solution must have removed nearly all the Fe-Mn oxide coating and reacted with some of the detrital material, thus altering the isotopic signal towards more less radiogenic values indicating contamination from a continental source. A possible source of this contamination might be cations from exchangeable sites on the clays. As a result, samples used in this study were treated for 1.5- 2 hours with a 0.5 M HH solution.

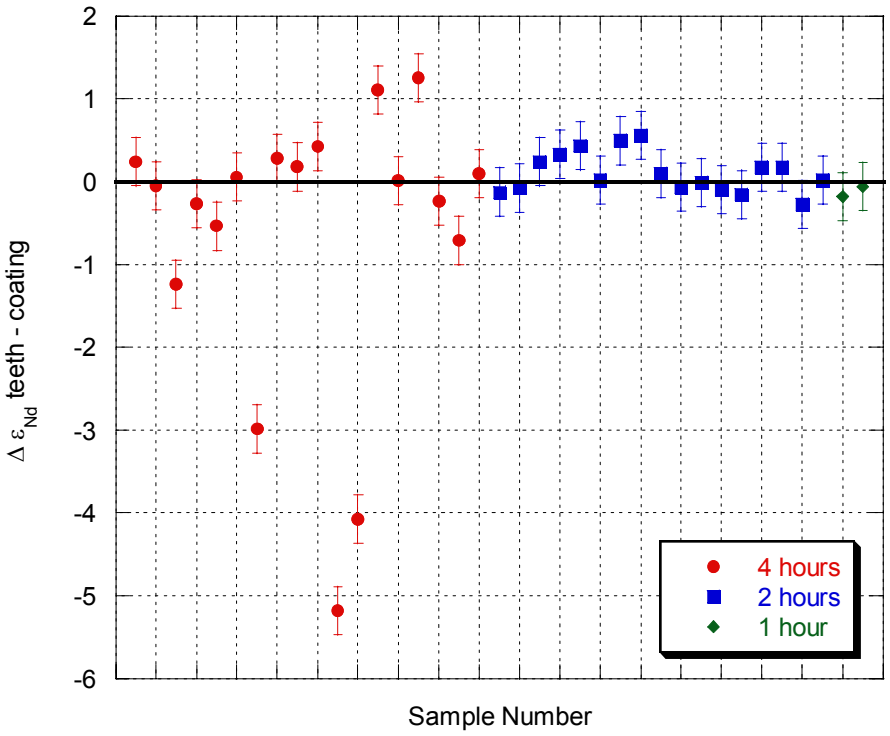

Figure 8-2. Difference of ε_{Nd} from obtained from fossil fish teeth and samples treated for 4 (diamonds), 2 (squares), and 1 (triangles) hour extraction periods.

8.2 Results from Southern Ocean Sites

Samples of fish teeth and Fe-Mn oxide coatings from 15-40 Ma (Miocene to Eocene) were analyzed from Sites 689, 690, and 1090 in the Southern Ocean (see figure 2-6 for site locations). The ε_{Nd} values from fish teeth for Site 689 range from -7.7 to -9.1 and values from Fe-Mn oxide coatings range from -7.7 to -9.7 (table 8-1). Out of 27 samples from Site 689 4 (15%) did not fall within error of the fossil fish teeth (figure 8-3A); however, all coatings were less radiogenic than the teeth. The ages of samples from Site 690 range from 26 to 44 Ma (Oligocene to Eocene) with ε_{Nd} values for teeth ranging from -8.7 to -10.2 (table 8-1). Values for the coatings range from -8.2 to -10.5 and out of 23 samples 5 (~22%) values from oxide coatings did not fall within error of the fossil fish teeth (figure 8-3B). All but one of the samples that fell outside of error of the fish teeth was less radiogenic than the corresponding teeth value. Site 1090 teeth and coating

samples range in age from 17-25 Ma (Miocene to Oligocene), ε_{Nd} values from fossil fish teeth range from -7 to -8.3 and coating values range from -6.9 to -8.3 (table 8-1). Out of 17 samples all coating samples fell within error of ε_{Nd} values obtained from fossil fish teeth (figure 8-3C). Thus, in the Southern Ocean 88% of the ε_{Nd} values obtained from Fe-Mn oxide coatings fell within error of the values obtained from the fossil fish teeth. The greatest discrepancy between the extracted coatings and fish teeth is 1.5 ε_{Nd} units, and the average offset is 0.9 ε_{Nd} units.

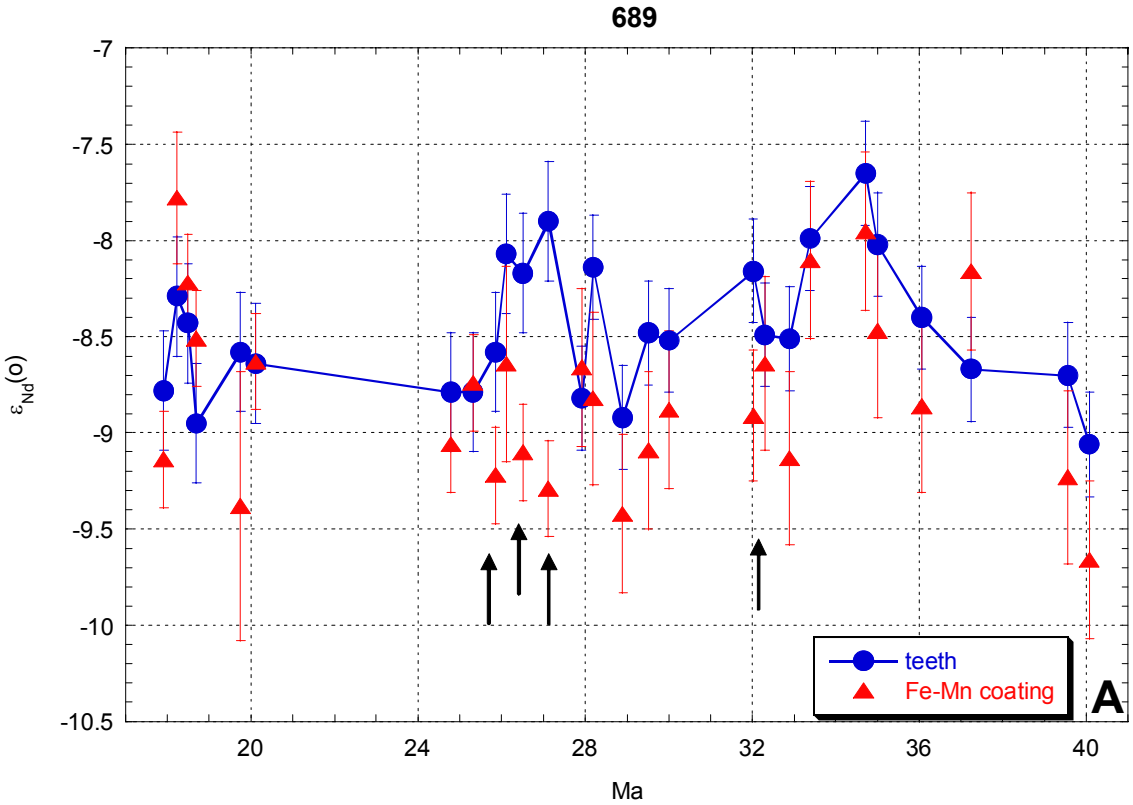

Figure 8-3 $\varepsilon_{Nd(o)}$ values from fossil fish teeth (blue circles) and Fe-Mn oxide coatings (red triangles) from the Southern Ocean Sites. A-689, B- 690, and C. 1090. Arrows on the plots for 689 and 690 highlight the Fe-Mn oxide coatings that did not fall within error of the teeth.

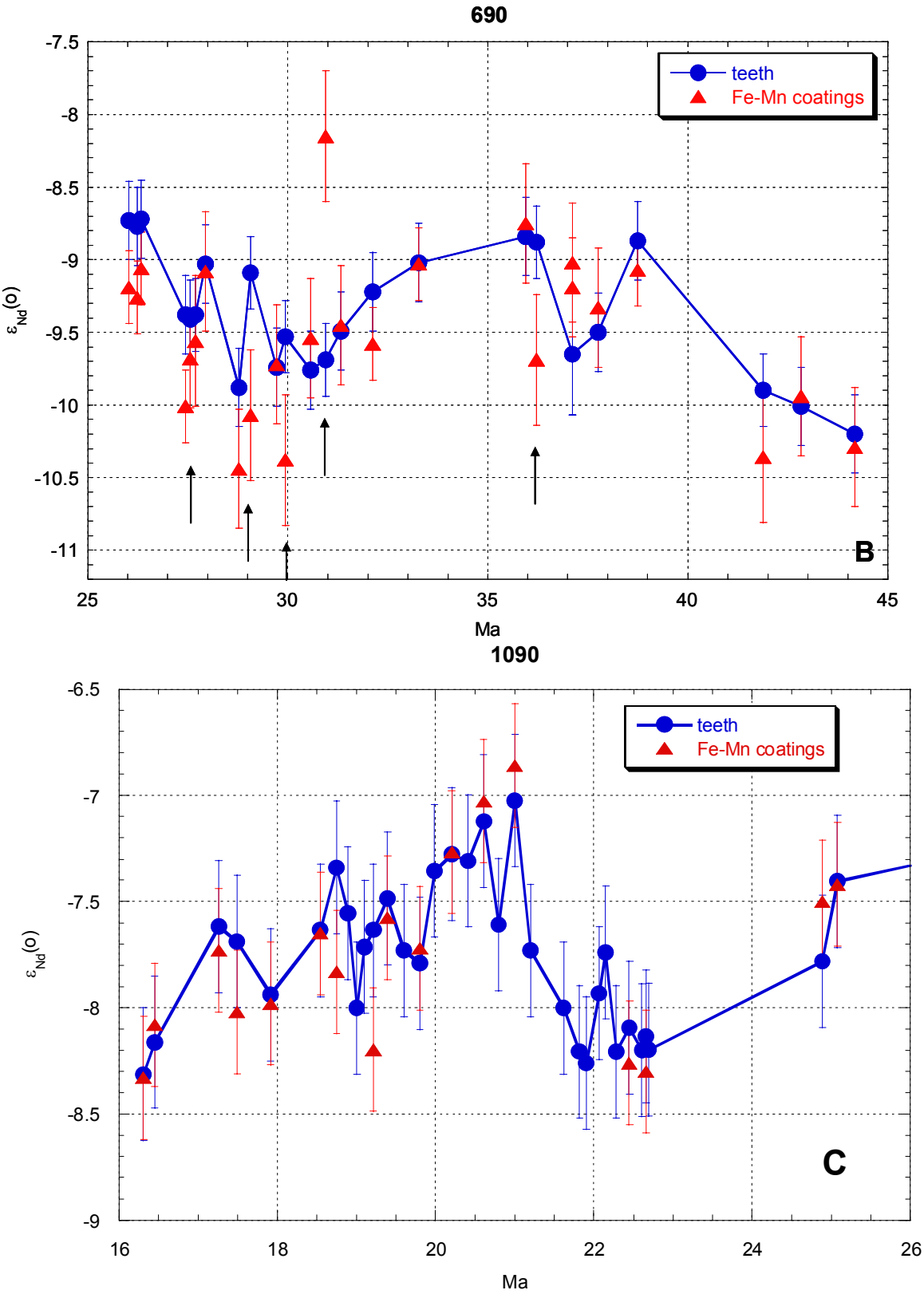

Figure 8-3 A-C continued.

Table 8-1. Nd isotopic values from Fossil Fish Teeth and Fe-Mn Oxide Coatings from Southern Ocean ODP Sites 689, 690, and 1090

			Coatings[2]		Teeth[4]	
Sample	**mbsf**	**Age (Ma)[1]**	**143/144**	**$\varepsilon_{Nd(o)}$[3]**	**143/144**	**$\varepsilon_{Nd(o)}$**
689B						
689 7-6 18	60.590	17.91	0.51217	-9.14 ± 0.25	0.512188	-8.78 ± 0.31
689 7-6 121	61.610	18.23	0.512239	-7.78 ± 0.34	0.512213	-8.29 ± 0.31
689 8-1 84	63.340	18.49	0.512217	-8.22 ± 0.25	0.512206	-8.43 ± 0.31
689 8-2 83.5	64.840	18.69	0.512202	-8.51 ± 0.25	0.512179	-8.95 ± 0.31
689 8-3 4	65.540	19.75	0.512157	-9.38 ± 0.70	0.512198	-8.58 ± 0.31
689 8-3, 129	66.790	20.11	0.512196	-8.63 ± 0.25	0.512195	-8.64 ± 0.31
689 8-3, 140	66.900	24.79	0.512173	-9.06 ± 0.25	0.512187	-8.79 ± 0.31
689 8-5, 111.5	69.610	25.32	0.51219	-8.74 ± 0.25	0.512187	-8.79 ± 0.31
*689 9-1, 26	72.360	25.85	0.512165	-9.22 ± 0.25	0.512198	-8.58 ± 0.31
689 9-2, 7	73.670	26.11	0.512170	-8.64 ± 0.51	0.512224	-8.07 ± 0.31
*689 9-3, 62.5	75.720	26.51	0.512171	-9.10 ± 0.25	0.512219	-8.17 ± 0.31
*689 9-6, 63	80.230	27.13	0.512162	-9.29 ± 0.25	0.512233	-7.90 ± 0.31
689 10-3, 116.5	85.865	27.91	0.512194	-8.66 ± 0.41	0.512186	-8.82 ± 0.27
689 10-5 26	87.960	28.20	0.512186	-8.82 ± 0.45	0.512221	-8.14 ± 0.27
689 11-2, 46	93.260	28.90	0.512155	-9.42 ± 0.41	0.512181	-8.92 ± 0.27
689 11-5, 106	98.360	29.51	0.512172	-9.09 ± 0.41	0.512203	-8.48 ± 0.27
689 12-2, 7.5	103.920	30.00	0.512183	-8.88 ± 0.41	0.512201	-8.52 ± 0.27
*689 13-1, 127.5	111.880	32.02	0.512181	-8.91 0 0.34	0.512220	-8.16 ± 0.27
689 13-2 107	113.170	32.30	0.512195	-8.64 ± 0.45	0.512203	-8.49 ± 0.27
689 13-4 82	115.920	32.89	0.512170	-9.13 ± 0.45	0.512202	-8.51 ± 0.27
689 13-6, 60	118.700	33.38	0.512223	-8.10 ± 0.41	0.512228	-7.99 ± 0.27
689 14-3, 104	124.240	34.71	0.51223	-7.95 ± 0.41	0.512246	-7.65 ± 0.27
689 14-4 82-88	125.550	35.00	0.512204	-8.47 ± 0.45	0.512227	-8.02 ± 0.27
689 15-4 45	134.850	36.05	0.512184	-8.86 ± 0.45	0.512207	-8.40 ± 0.27
689 16-3, 46	142.860	37.24	0.51222	-8.16 ± 0.41	0.512194	-8.67 ± 0.27
689 17-7 51-57	158.640	39.55	0.512165	-9.23 ± 0.45	0.512192	-8.70 ± 0.27
689 18-2, 60	160.900	40.07	0.512143	-9.66 ± 0.41	0.512173	-9.06 ± 0.27
690B						
690 7-4,83	54.205	26.03	0.512167	-9.19 ± 0.25	0.512191	-8.73 ± 0.27
690 7-5,87	57.240	26.24	0.512163	-9.26 ± 0.25	0.512189	-8.77 ± 0.27
690 7-6, 34	58.210	26.34	0.512174	-9.06 ± 0.25	0.512191	-8.72 ± 0.27
*690 8-3, 121	64.280	27.44	0.512125	-10.01 ± 0.25	0.512157	-9.38 ± 0.27
690 8-4,67	65.240	27.56	0.512142	-9.68 ± 0.34	0.512156	-9.41 ± 0.27
690 8-5 17	66.245	27.69	0.512148	-9.56 ± 0.45	0.512157	-9.38 ± 0.25
690 8-6, 67	68.240	27.94	0.512173	-9.08 ± 0.41	0.512175	-9.03 ± 0.27
690 9-3, 148	74.255	28.78	0.512103	-10.44 ± 0.41	0.512131	-9.88 ± 0.27
*690 9-5 148	77.250	29.06	0.512122	-10.07 ± 0.45	0.512172	-9.09 ± 0.25
690 10-2, 136	82.230	29.72	0.51214	-9.72 ± 0.41	0.512139	-9.74 ± 0.27
*690 10-3 87	83.240	29.94	0.512106	-10.38 ± 0.45	0.512149	-9.53 ± 0.25
690 10-4, 135	85.225	30.57	0.512149	-9.54 ± 0.41	0.512138	-9.76 ± 0.27
*690 10-5 84	86.215	30.95	0.512220	-8.15 ± 0.45	0.512141	-9.69 ± 0.25
690 10-6, 35	87.215	31.33	0.512154	-9.45 ± 0.41	0.512151	-9.49 ± 0.27
690 11-1, 18	89.250	32.12	0.512147	-9.58 ± 0.25	0.512166	-9.22 ± 0.27
690 11-3, 17	92.250	33.27	0.512175	-9.03 ± 0.25	0.512175	-9.02 ± 0.27
690 11-4, 68	94.250	35.95	0.51219	-8.75 ± 0.41	0.512185	-8.84 ± 0.27
*690 11-5 17	95.240	36.22	0.512141	-9.69 ± 0.45	0.512183	-8.88 ± 0.25

Table 8-1. Continued

690 11-7, 17	98.240	37.11	0.512176	-9.02 ±	0.41	0.512143	-9.65 ± 0.42
690 11-7, 17 rep	98.240	37.11	0.512167	-9.19 ±	0.34	0.512143	-9.65 ± 0.42
690 12-1, 146	100.230	37.76	0.51216	-9.33 ±	0.41	0.512151	-9.50 ± 0.27
690 12-3, 146	103.230	38.75	0.512173	-9.07 ±	0.25	0.512183	-8.87 ± 0.27
690 12-6 94	107.210	41.88	0.512107	-10.36 ±	0.45	0.512131	-9.90 ± 0.25
690 12-7, 47	108.240	42.83	0.512128	-9.94 ±	0.41	0.512125	-10.01 ± 0.27
690 13-3, 74	112.210	44.18	0.51211	-10.29 ±	0.41	0.512115	-10.20 ± 0.27
1090							
1090D 8-2, 138	73.190	16.31	0.512211	-8.33 ±	0.27	0.512212	-8.31 ± 0.27
1090D 8-3, 48	73.790	16.45	0.512224	-8.08 ±	0.27	0.512220	-8.16 ± 0.27
1090D 8-6, 38	78.190	17.26	0.512242	-7.73 ±	0.27	0.512247	-7.62 ± 0.27
1090E 8-4, 133	80.080	17.49	0.512227	-8.02 ±	0.27	0.512244	-7.69 ± 0.27
1090D 9-2, 5	82.980	17.91	0.512229	-7.98 ±	0.27	0.512231	-7.94 ± 0.27
1090E 9-2, 137	87.980	18.54	0.512246	-7.65 ±	0.27	0.512247	-7.63 ± 0.27
1090E 9-4, 48	90.090	18.75	0.512237	-7.83 ±	0.29	0.512262	-7.34 ± 0.27
1090D 10-3, 5	93.980	19.21	0.512218	-8.20 ±	0.29	0.512247	-7.63 ± 0.27
1090D 10-4,35	95.780	19.39	0.512250	-7.58 ±	0.29	0.512254	-7.49 ± 0.27
1090E 10-4, 36	99.930	19.80	0.512242	-7.72 ±	0.29	0.512239	-7.79 ± 0.27
1090D 11-3, 90	103.930	20.20	0.512265	-7.27 ±	0.29	0.512265	-7.28 ± 0.27
1090E 11-3, 122	108.230	20.61	0.512278	-7.03 ±	0.29	0.512273	-7.12 ± 0.27
1090D 12-2, 130	112.330	21.00	0.512286	-6.86 ±	0.29	0.512278	-7.02 ± 0.27
1090D 13-4, 39	123.680	22.45	0.512215	-8.26 ±	0.29	0.512223	-8.09 ± 0.27
1090E 13-3, 8	125.890	22.66	0.512213	-8.30 ±	0.29	0.512221	-8.13 ± 0.27
1090E 16-5, 116	160.920	24.88	0.512254	-7.50 ±	0.29	0.512239	-7.78 ± 0.27
1090D 17-3, 34	163.120	25.08	0.512258	-7.42 ±	0.29	0.512258	-7.40 ± 0.27

[1.] Ages for Site 689 from Mead and Hodell, 1995; Spiess, 1990; Shipboard Scientific Party, 1988. Ages for Site 690, Shipboard Scientific Party, 1988; and for Site 1090 are from Scher, 2006.

[2.] $^{143/144}$Nd values are normalized to Jndi-1 average on the day the samples were analyzed and then normalized to Jndi-1 = 0.512103 (TIMS average).

[3.] Fossil fish teeth data from Scher, 2005.

[4.] $\varepsilon_{Nd(o)} = [(^{143}Nd/^{144}Nd)_{sample}/(^{143}Nd/^{144}Nd)_{CHUR}-1] \times 10^4$

* indicates samples whose coating and teeth were not within error of one another.

8.3 Results from North Atlantic Sites

Fish teeth samples and extracted coatings from contemporaneous sections were analyzed from North Atlantic DSDP Site 608 and ODP Sites 647 and 982. Due to the scarcity of teeth in samples from Site 608 only 2 samples were analyzed. The ε_{Nd} values of the teeth from these two samples are -11.07 and -12.30. Coatings for both of these samples fall outside the error window at -9.66 and -11.28 respectively (table 8-2 and figure 8-4). Four samples were analyzed from Site 647 and ε_{Nd} values of the teeth range from -9.93 to -11.61, while Fe-Mn oxide coating values range from -9.66 to -11.28 (table

8-2). All four of these samples fell within error of the contemporaneous fish teeth (figure 8-4). For all of the samples analyzed from these two sites the coating samples were consistently more radiogenic than the fish teeth samples.

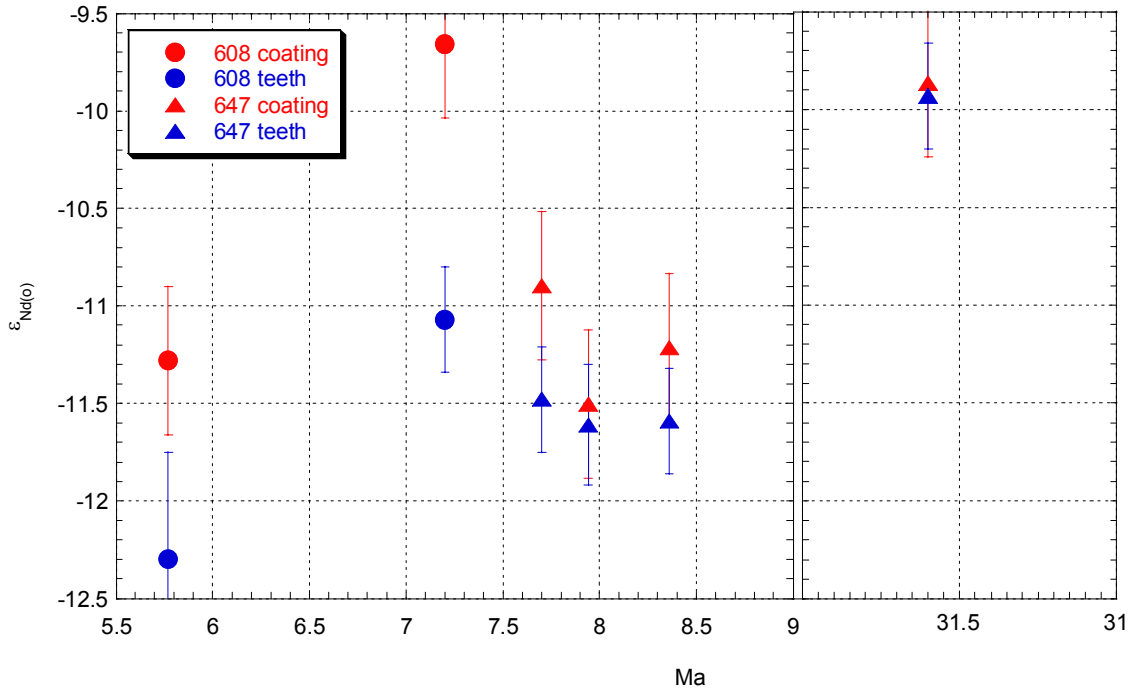

Figure 8-4 $\varepsilon_{Nd(o)}$ values from fossil fish teeth and Fe-Mn oxide coatings from DSDP Site 608 (circles) and ODP Site 647 (triangles) from 5.5 to 9 and from 30 to 31 Ma.

Twelve samples were analyzed from ODP Site 982 spanning from 9.2 to 14.4 Ma. Fossil fish teeth as well as phosphate pieces or fish debris (commonly bones or scales) were analyzed for three of the samples. The ε_{Nd} values obtained from the two types of phosphates are indistinguishable, implying that when fish teeth are absent from a sample, phosphate fish debris can be used instead (table 8-2). The ε_{Nd} values from the fish teeth and debris range from -8.13 to -10.86, and the oxide coating values range from -8.66 to -10.61, with all of the values falling within error of the teeth (table 9-2). In these samples the coating values are not consistently more or less radiogenic than the teeth (figure 8-5).

Of all the samples analyzed in the North Atlantic (all 3 localities) 88% of the values obtained from coating samples agreed with the values obtained for the teeth.

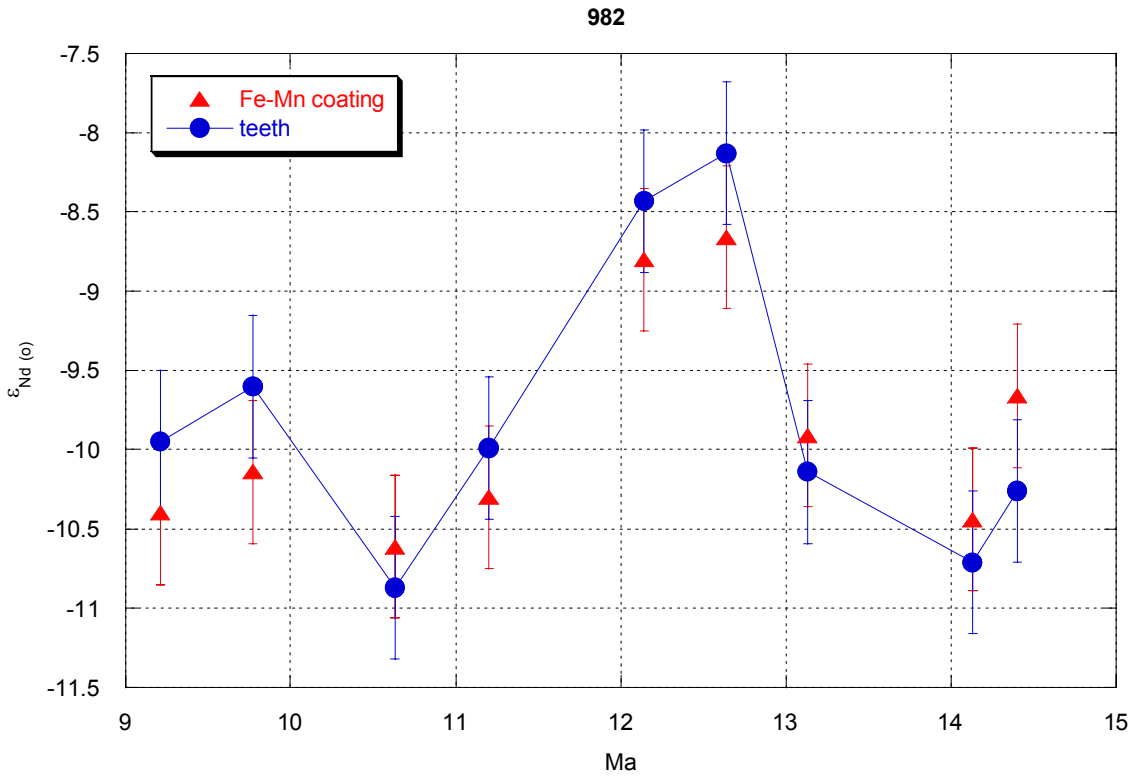

Figure 8-5. $\varepsilon_{Nd(o)}$ values from fossil fish teeth (blue circles) and Fe-Mn oxide coatings (red triangles) from ODP Site 982 from 9 to 15 Ma.

Table 8-2. Nd isotopic values from Fossil Fish Teeth and Fe-Mn Oxide Coatings from North Atlantic DSDP and ODP Sites 608, 647, and 982

			Coatings [4]		Teeth	
Sample	mbsf	Age (Ma)[3]	$^{143/144}Nd$	$\varepsilon_{Nd(o)}$ [5]	$^{143/144}Nd$	$\varepsilon_{Nd(o)}$
608						
*608 17-1, 102.5	152.000	5.77	0.51206	-11.28 ± 0.38	0.512008	-12.30 ± 0.55
*608 20-2, 10.5	177.300	7.20	0.512143	-9.659 ± 0.38	0.512070	-11.07 ± 0.27
647						
647 13-1, 104	117.010	7.70	0.512079	-10.9 ± 0.38	0.512049	-11.48 ± 0.27
647 13-1, 133	117.300	7.94	0.512048	-11.5 ± 0.38	0.512043	-11.61 ± 0.31
647 13-2, 34.5	117.815	8.36	0.512063	-11.21 ± 0.38	0.512044	-11.59 ± 0.27
647 17-1, 62	155.390	30.40	0.512132	-9.864 ± 0.38	0.512129	-9.93 ± 0.27
982						
982 34-1 52.5A[1]	307.150	9.21	0.512105	-10.40 ± 0.45	0.512128	-9.95 ± 0.45
982 34-1 52.5B[2]	307.155	9.21	0.512105	-10.40 ± 0.45	0.512110	-10.30 ± 0.45
982 36-1 12	326.310	9.77	0.512118	-10.14 ± 0.45	0.512146	-9.60 ± 0.45
982 39-5 22.5A	355.825	10.63	0.512094	-10.61 ± 0.45	0.512081	-10.87 ± 0.45
982 39-5 22.5B	355.825	10.63	0.512094	-10.61 ± 0.45	0.512101	-10.48 ± 0.45
982 41-5 5.5B	375.103	11.20	0.512110	-10.30 ± 0.45	0.512126	-9.99 ± 0.45
982 43-3 103.5A	394.205	12.14	0.512187	-8.80 ± 0.45	0.512206	-8.43 ± 0.45
982 45-2 27.5B	413.175	12.64	0.512194	-8.66 ± 0.45	0.512221	-8.13 ± 0.45
982 47-1 62B	432.260	13.13	0.512130	-9.91 ± 0.45	0.512118	-10.14 ± 0.45
982 51-1 17.5A	470.615	14.13	0.512103	-10.44 ± 0.45	0.512089	-10.71 ± 0.45
982 51-1 1 spiked	470.615	14.13	0.512103	-10.44 ± 0.45	0.512102	-10.46 ± 0.45
982 52-4 2 spiked	480.675	14.40	0.512143	-9.66 ± 0.45	0.512112	-10.26 ± 0.45

[1] A samples are values from fossil fish teeth

[2] B samples are values from phosphate pieces, commonly fish debris such as scales or bone.

[3] Ages for Site 608 are from Ruddiman et al., 1987; for Site 647 Shipboard Scientific Party, 1987; and for 982 Shipboard Scientific Party, 1996.

[4] $^{143/144}Nd$ values are normalized to the Jndi-1 average on the day the samples were analyzed and then normalized to Jndi-1 = 0.512103 (TIMS average)

[5] $\varepsilon_{Nd(o)} = [(^{143}Nd/^{144}Nd)_{sample}/(^{143}Nd/^{144}Nd)_{CHUR}-1] \times 10^4$

* indicates samples whose coating and teeth values were not within error of one another.

8.4 Results from Cretaceous Samples

As one final test, this extraction procedure was performed on four samples from Cretaceous sediments (80-102 Ma) from ODP Sites 1050 and 1258. The ε_{Nd} value for the fish teeth from the one sample from Site 1258 was -15.44 and the value from the coating was -16.05. From Site 1050 fish teeth values range from -5.00 to -8.44 and coating values range from -5.56 to -8.93 (table 8-3). The coating values of all four samples fell within error of the values obtained from the fish teeth and are not consistently more or less radiogenic than the teeth values (Figure 8-6).

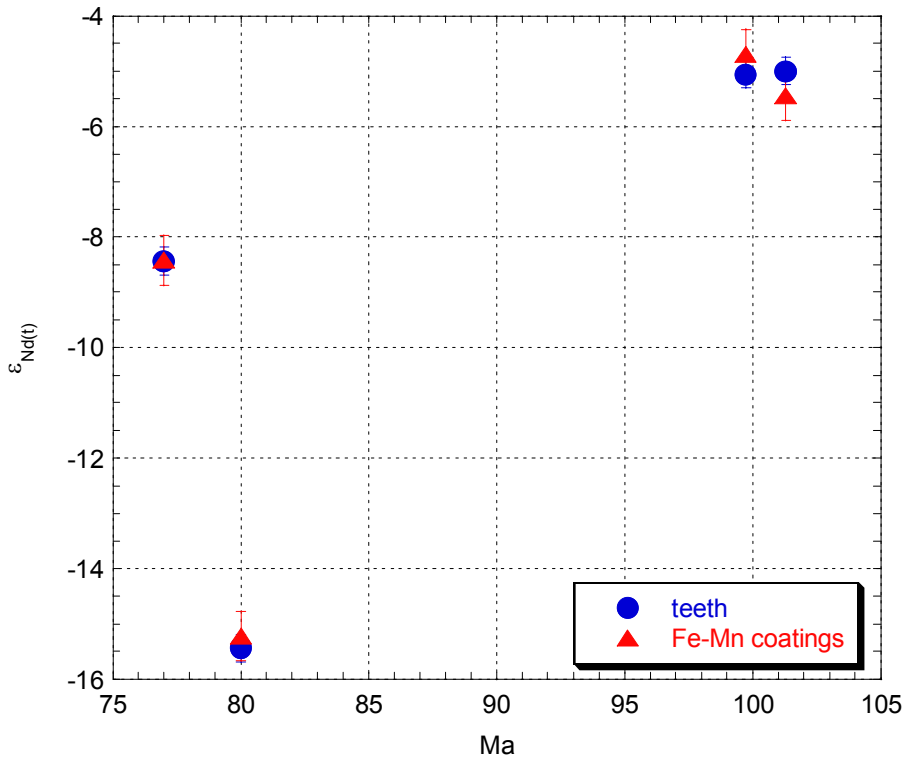

Figure 8-6. $\varepsilon_{Nd(t)}$ values from fossil fish teeth (blue circles) and Fe-Mn oxide coatings (red triangles) from ODP Sites 1258 and 1090 from 77 to 102 Ma.

Table 8-3. Nd istopes from Fossil Fish Teeth and Fe-Mn Oxide Coatings from ODP Sites 1258 and 1050.

			Teeth[2]					Coatings			
Sample	mcd	Age (Ma)[1]	$^{143/144}$Nd	$\varepsilon_{Nd(o)}$[3]	$\varepsilon_{Nd(t)}$[4]			$^{143/144}$Nd	$\varepsilon_{Nd(o)}$	$\varepsilon_{Nd(t)}$	
1258 38-1 105	375.20	80.00	0.511804	-16.27	-15.44	±	0.25	0.511815	-16.05	-15.22	± 0.45
1050 20-1 33	490.63	77.00	0.512179	-8.95	-8.44	±	0.25	0.512180	-8.93	-8.42	± 0.45
1050 29-2 102	577.46	99.73	0.512334	-5.93	-5.06	±	0.25	0.512353	-5.56	-4.69	± 0.45
1050 31-2 103	596.65	101.30	0.512337	-5.87	-5.00	±	0.25	0.512314	-6.32	-5.45	± 0.45

1. Ages for Site 1258 are from Erbacher, 2004 and for Site 1050 from Shipboard Scientific Party, 1998.
2. $^{143/144}$Nd values are normalized to Jndi-1 average on the day the samples were analyzed and then normalized to Jndi-1 = 0.512103 (TIMS average).
3. $\varepsilon_{Nd(o)} = [(^{143}Nd/^{144}Nd)_{sample}/(^{143}Nd/^{144}Nd)_{CHUR}-1] \times 10^4$
4. $\varepsilon_{Nd(t)} = [(^{143}Nd/^{144}Nd)_{sample(t)}/(^{143}Nd/^{144}Nd)_{CHUR(t)}-1] \times 10^4$ using $^{147}Sm/^{144}Nd$

8.5 Tests of Validity

Although a majority ~90% of the extracted Fe-Mn oxide coatings do fall within error of the contemporaneous fossil fish teeth, some do not and the scope of the next portion of the project was to determine whether there is a test other than analyzing fish teeth that could be used to identify coating samples with accurate ε_{Nd} values. If successful, the goal

was that these tests could be used in place of the more time consuming, complicated and expensive analyses of fossil fish teeth. Tests for the integrity of the coatings include REE plots, Sr isotopes, and major element ratios, which were all expected to detect possible contamination.

8.5.1 REE Plots

REE plots for different geological materials are very distinct; continental material, basalts, fish teeth, and Fe-Mn oxide coatings all produce unique REE profiles. The goal was to determine whether the REE patterns for extracted coating samples that did not match the ε_{Nd} value of the fossil fish teeth were distinct from those that did agree with the teeth data.

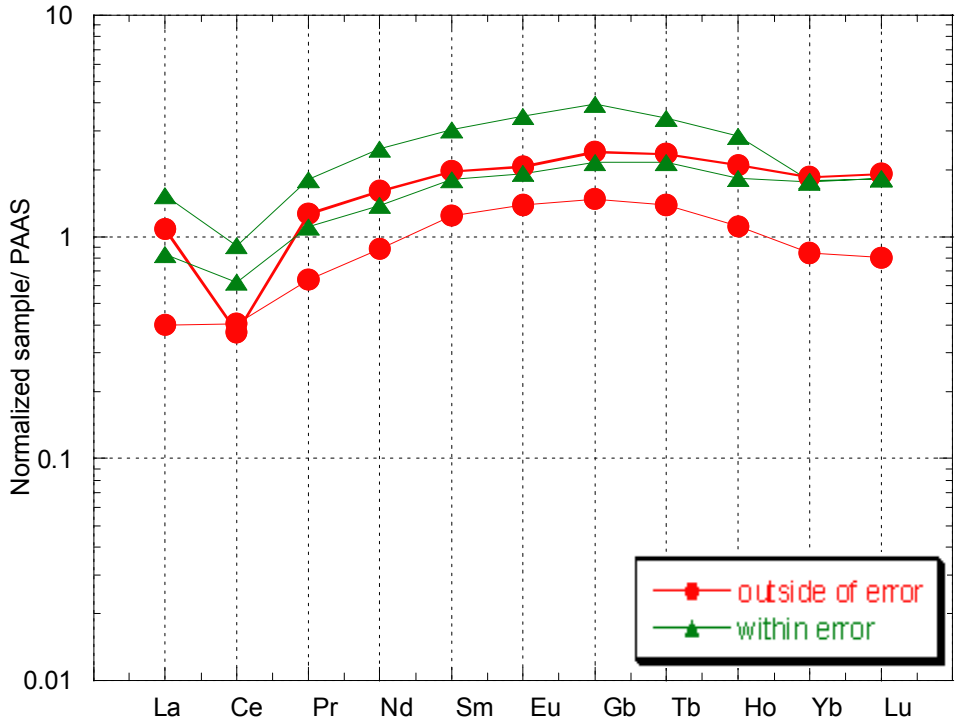

Figure 8-7. REE plot of four samples from ODP Site 690, two of the samples have ε_{Nd} values that fall within error of contemporaneous fossil fish teeth (green triangles) and two do not (red circles). Samples are normalized to the initial sample weight and to PAAS (Taylor and McLellen, 1985).

All of the REE plots from Fe-Mn oxide coatings for this study have a distinctive middle (M-) REE buldge, characterized by enrichment in the MREE and a depletion in the light (L-) REE and heavy (H-) REE. This is consistent with analysis of REE from Fe-Mn oxide coatings from other studies (e.g. Bayon, 2002). To determine if REE patterns are different for extracted samples that fell within error of the fish teeth and those that did not, four samples were plotted from Site 690; two whose ε_{Nd} values fell within error of the teeth and two that did not (figure 8-7). Both sets of samples have similar REE patterns, including MREE enrichment, characteristic of Fe-Mn oxide coatings. There is, however, slight variability in the magnitude of the Ce anomalies.

REE were analyzed from extracted coatings from all locations in this study, including the samples from the Cretaceous (table 8-4). The samples from each Site were averaged to get a REE pattern for each location. These results are plotted on figure 8-8. All the Sites have a MREE bulge and variable negative Ce anomalies. All samples have been normalized to the original sample weight as well as PAAS and, therefore, they do reflect relative concentrations. Samples from Site 690 and 689 in the Southern Ocean have the highest concentration, while the North Atlantic samples have lower concentrations of REE. In particular, concentrations from Site 608 are about an order of magnitude lower than all other sites. The 4 samples analyzed from Cretaceous sediments from Sites 1050 and 1258 have concentrations that fall between the Southern Ocean and North Atlantic.

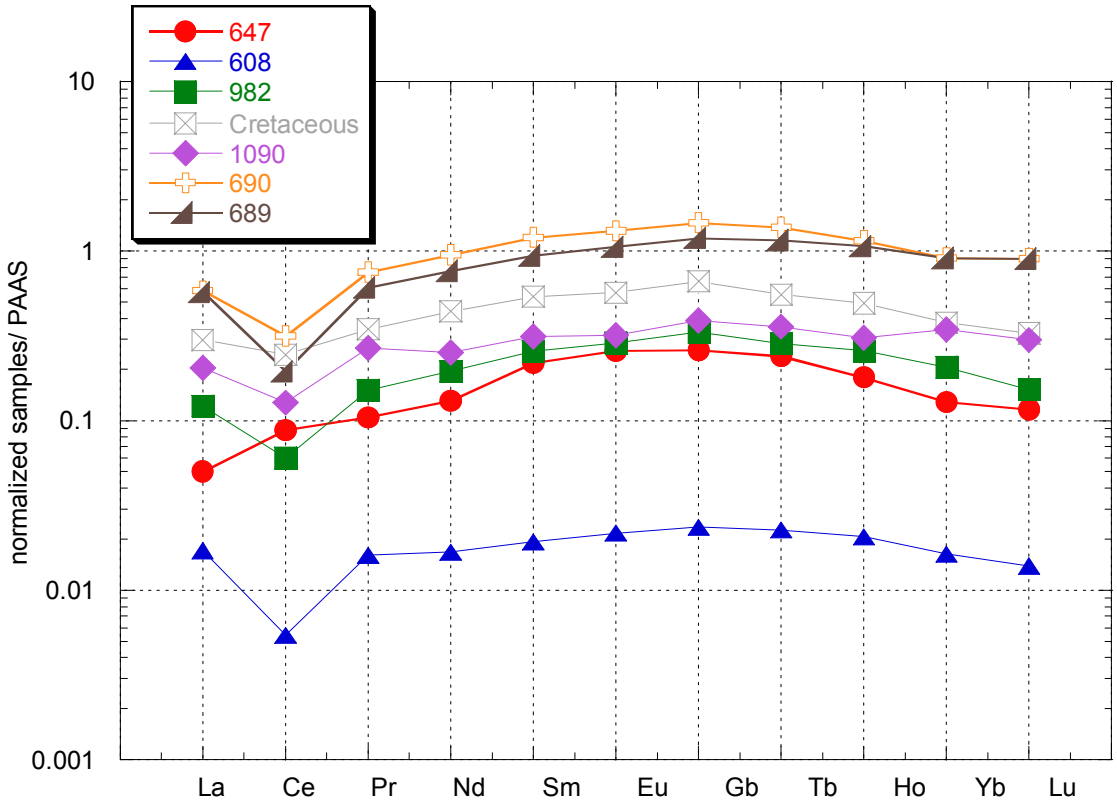

Figure 8-8. REE plot of the average values from extracted coatings from the North Atlantic Sites 608 (triangle), 647 (circle), and 982 (square), the Cretaceous (Sites 1258 and 1050; (box with x), and the Southern Ocean Sites 1090 (diamond), 690 (cross) and 689 (triangle). REE are normalized to PAAS (Taylor and McLellen, 1985) and initial sample weights.

Table 8-4 . REE values from Fe-Mn Oxide Coatings.

Sample	La	Ce	Pr	Nd	Sm	Eu	Gd	Tb	Ho	Yb	Lu
North Atlantic											
608											
608 17-1 102.5	0.017	0.005	0.016	0.017	0.019	0.022	0.024	0.023	0.021	0.016	0.014
647											
647 3-1 104	0.063	0.105	0.129	0.161	0.267	0.317	0.325	0.303	0.226	0.160	0.145
647 13-2,34.5	0.038	0.070	0.080	0.101	0.171	0.200	0.199	0.180	0.132	0.096	0.088
982											
982 34-1 52.5	0.216	0.082	0.250	0.330	0.411	0.471	0.555	0.508	0.446	0.324	0.268
982 36-1 9	0.035	0.020	0.064	0.083	0.131	0.140	0.154	0.120	0.100	0.080	0.028
982 41-5 3-8	0.057	0.030	0.094	0.127	0.195	0.216	0.236	0.192	0.156	0.118	0.078
982 43-3 103.5	0.180	0.078	0.205	0.273	0.354	0.413	0.481	0.435	0.397	0.315	0.270
982 45-2 28	0.053	0.032	0.084	0.111	0.172	0.184	0.204	0.165	0.150	0.134	0.084
982 47-1 162	0.031	0.015	0.048	0.057	0.088	0.099	0.104	0.075	0.078	0.075	0.023
982 51-1 17.5	0.334	0.188	0.401	0.511	0.628	0.703	0.818	0.712	0.622	0.487	0.409
982 52-4 27.5	0.183	0.089	0.190	0.239	0.293	0.322	0.394	0.347	0.348	0.301	0.252
Average NA	0.101	0.060	0.132	0.170	0.231	0.260	0.295	0.256	0.225	0.178	0.135
Southern Ocean											
689											
689 10-3 86.5	1.162	0.478	1.257	1.657	2.059	2.202	2.692	2.557	2.415	2.174	2.345
689 10-5 26	1.125	0.331	1.374	1.853	2.324	2.580	3.022	2.777	2.376	1.673	1.696
689 13-1 127.5	0.466	0.138	0.471	0.487	0.584	0.651	0.652	0.708	0.697	0.713	0.647
689 13-2 104	0.404	0.157	0.493	0.624	0.793	0.886	1.015	0.998	0.910	0.810	0.766
689 13-4 82	0.264	0.073	0.364	0.491	0.648	0.733	0.847	0.774	0.659	0.480	0.455
689 13-6 60	0.438	0.086	0.375	0.374	0.424	0.491	0.446	0.554	0.612	0.661	0.600
689 14-4 85	0.964	0.375	1.074	1.400	1.700	1.953	2.260	2.175	1.979	1.597	1.607
689 15-4 45	0.786	0.320	0.940	1.246	1.553	1.756	2.016	1.905	1.668	1.237	1.240
689 16-3 46	0.352	0.079	0.239	0.216	0.218	0.249	0.228	0.277	0.332	0.413	0.367
689 17-6 61	0.401	0.137	0.283	0.269	0.284	0.334	0.290	0.358	0.451	0.556	0.526
689 17-7 54	0.748	0.285	0.863	1.156	1.415	1.614	1.869	1.730	1.536	1.118	1.117
689 18-2 60	0.253	0.082	0.142	0.120	0.107	0.127	0.105	0.127	0.195	0.289	0.273
Average 689	0.571	0.195	0.613	0.768	0.940	1.056	1.197	1.158	1.072	0.909	0.902
690											
690 8-4 66	0.702	0.217	1.035	1.111	1.450	1.483	1.672	1.640	1.382	1.240	1.091
690 8-5 14	1.088	0.372	1.272	1.604	1.971	2.080	2.422	2.364	2.097	1.857	1.923
690 9-3 148	0.101	0.039	0.147	0.165	0.217	0.230	0.258	0.241	0.209	0.171	0.156
690 9-5 147.5	1.355	0.770	1.721	2.224	2.743	2.984	3.346	3.060	2.538	1.906	1.909
690 10-5 84	0.835	0.625	1.108	1.380	1.814	1.930	2.165	2.173	1.833	1.758	1.834
690 11-5 16.5	1.529	0.908	1.812	2.488	3.038	3.494	3.950	3.426	2.825	1.783	1.825
690 11-7 17	0.021	0.008	0.023	0.026	0.031	0.034	0.041	0.036	0.034	0.025	0.023
690 11-7 17rep	0.235	0.050	0.326	0.365	0.469	0.505	0.497	0.496	0.403	0.268	0.222
690 12-6 94	0.400	0.406	0.643	0.880	1.243	1.394	1.483	1.392	1.112	0.845	0.804
690 12-7 47	0.108	0.066	0.175	0.195	0.272	0.307	0.256	0.262	0.191	0.127	0.099
690 13-3 24	0.029	0.021	0.036	0.040	0.049	0.053	0.062	0.057	0.052	0.035	0.031
Average 690	0.582	0.316	0.754	0.953	1.209	1.318	1.468	1.377	1.153	0.911	0.901
1090											
1090 12-5 112.5	0.205	0.128	0.267	0.251	0.312	0.318	0.388	0.359	0.306	0.346	0.300

Error is ± 5%.

8.5.2 Strontium Isotopes

Strontium has a long residence time in the ocean, thus the Sr isotopic value of the ocean is homogeneous at any one time in earth's history. The assumption is that if the coatings incorporate the ocean water chemistry of the overlying water mass the coating should incorporate the Sr isotopic value as well as the Nd isotopic value of the water mass at that time. Other studies that utilized Fe-Mn oxide coatings as archives for Nd, such as Piotrowski et al. (2004), used Sr isotopes as a tool for evaluating the integrity of the measured ε_{Nd} value.

Sr isotopes were measured on a number of the extracted coatings in this study (table 8-5). These values were compared to $^{87}Sr/^{86}Sr$ values obtained from foraminifera from the same sediment sample, which are assumed to represent the seawater value. Because seawater $^{87}Sr/^{86}Sr$ changes with age, the samples have been plotted on the seawater Sr isotope curve (figure 8-9). They have been divided into two groups; extracted coatings whose ε_{Nd} values fell within error of the ε_{Nd} value of the teeth and those that did not. All of the samples either fell on the Sr curve or were more radiogenic than the curve.

There is some correlation between sample locations and Sr isotopic values. All of the samples from the North Atlantic lie on the curve, while the Southern Ocean samples are mixed. The North Atlantic samples are also younger than the Southern Ocean samples, ~10-13 Ma and younger versus 19.5 Ma and older. There is, however, no correlation between the ages of the Southern Ocean samples that fell on and off the curve. Interestingly a replicate sample (37.0 Ma) yielded two very different Sr isotopic values,

one fell on the Sr curve and one did not even though the Nd isotopic values for the both coatings were valid.

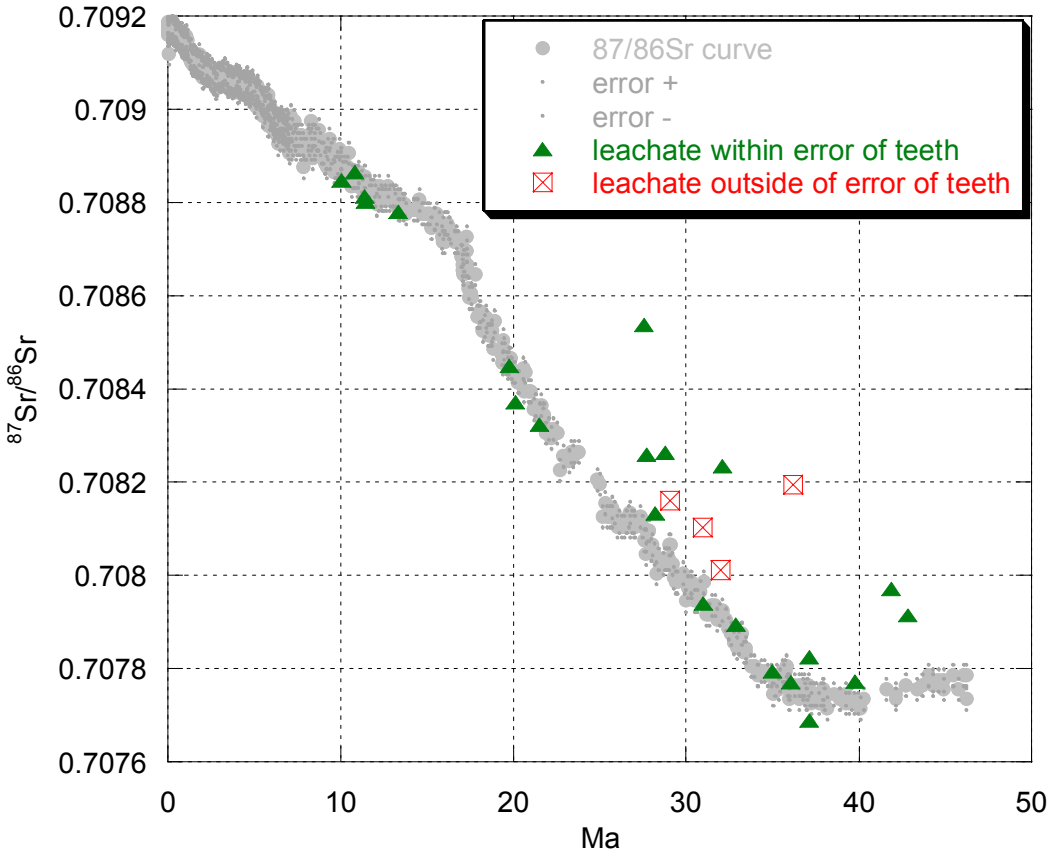

Figure 8-9. Seawater Sr curve over the past 50 Ma (Woodruff and Hodell, 1994; Mead and Hodell, 1995; Farrell et al., 1995; Martin et al., 1999) plotted with $^{87}Sr/^{86}Sr$ values from extracted Fe-Mn oxide coatings. Green triangles are from extracted coatings whose ε_{Nd} value fell within error of the values measured from fossil fish teeth and the red boxes are from extracted coatings whose values fell outside of error of those obtained from the teeth. The $^{87}Sr/^{86}Sr$ error bars are smaller than the symbols.

Table 8-5. $^{87}Sr/^{86}Sr$ values from Extracted Material and Foraminifera from Samples from ODP Sites 689, 690, 982, and 1090

Sample	Age (Ma)	Coatings $^{87/86}Sr$ [2]		Foraminifera $^{87/86}Sr$ [3]	
ε_{Nd} within error of teeth					
689 8-3 129	20.11	0.708371 ±	0.000023	0.708425 ±	0.000023
689 8-3, 4	19.75	0.708450 ±	0.000023	0.708470 ±	0.000023
689 10-5 26	28.20	0.708133 ±	0.000023	0.708045 ±	0.000023
689 13-2 107.5	31.00	0.707940 ±	0.000023	0.707960 ±	0.000023
689 13-4 82	32.89	0.707895 ±	0.000023	0.707855 ±	0.000023
689 14-4 85	35.00	0.707794 ±	0.000023	0.707740 ±	0.000023
689 15-4 45	36.05	0.707772 ±	0.000023	0.707760 ±	0.000023
689 17-7 54	39.79	0.707773 ±	0.000023	0.707725 ±	0.000023
690 8-4, 66.5	27.56	0.708537 ±	0.000023	0.708075 ±	0.000023
690 8-5 17	27.69	0.708259 ±	0.000023	0.708033 ±	0.000023
690 9-3, 148	28.78	0.708263 ±	0.000023	0.708009 ±	0.000023
690 11-1, 17.5	32.12	0.708235 ±	0.000023	0.707886 ±	0.000023
690 11-7, 17	37.11	0.707824 ±	0.000023	0.707735 ±	0.000023
690 11-7, 17 rep	37.11	0.707688 ±	0.000023	0.707735 ±	0.000023
690 12-6 94	41.88	0.707971 ±	0.000023	0.707770 ±	0.000023
690 12-7, 47	42.83	0.707914 ±	0.000023	0.707831 ±	0.000023
982 34-1 52.5	10.80	0.708864 ±	0.000023	0.708855 ±	0.000023
982 36-1 12	10.05	0.708847 ±	0.000023	0.708875 ±	0.000023
982 39-5 22.5	11.38	0.708813 ±	0.000023	0.708840 ±	0.000023
982 41-5 5.5	11.44	0.708802 ±	0.000023	0.708835 ±	0.000023
982 45-2 27.5	13.32	0.708780 ±	0.000023	0.708785 ±	0.000023
1090 12-3, 70	21.51	0.708323 ±	0.000023	0.708354 ±	0.000023
ε_{Nd} outside of error of teeth					
689 13-1, 124.5	32.02	0.708011 ±	0.000023	0.707920 ±	0.000023
690 9-5 147.5	29.06	0.708160 ±	0.000023	0.708005 ±	0.000023
690 10-5 84	30.95	0.708103 ±	0.000023	0.707899 ±	0.000023
690 11-5 16.5	36.22	0.708194 ±	0.000023	0.707724 ±	0.000023

[1.] Ages for 689 from Mead and Hodell, 1995; Spiess, 1990; Shipboard Scientific Party, 1988. Ages for 690 from Shipboard Scientific Party, 1988. Ages for 982 from Shipboard Scientific Party, 1996. Ages for 1090 from Scher, 2006

[2.] Measured $^{87}Sr/^{86}Sr$ of the NBS-987 standard = 0.7120250 ± 0.000023 (2σ). and normalized to $^{86}Sr/^{88}Sr$ = 0.1194.

[3.] Sr values from 689, 690, and 1090 from Scher et al., 2005.

8.5.3 Major Element Ratios

When ε_{Nd} values of the coating do not match with fossil fish teeth values, the assumption is that the fish teeth value is correct and the value obtained from the extracted Fe-Mn oxide coating has been contaminated by detrital Nd. The source of this Nd is most likely clay or terrigenous material that has a non-seawater ε_{Nd} value. To further test

this theory major element ratios were measured on a number of the extracted samples. Al, Na, K, and Ti, some of the common elements in clays, were ratioed against Fe plus Mn, the main elements in coatings. Iron and Mn were added together to account for the high variability seen in the concentrations between the two elements at various locations. The assumption was that for samples with distinct extracted coating and fish teeth ε_{Nd} values the elemental ratios might reflect an increase in the elements contributed from the clays. Elemental ratios were analyzed for 44 samples from Southern Ocean, North Atlantic, and the Cretaceous Sites. For 7 of these samples the ε_{Nd} values of the teeth and coatings did not match (table 8-6). Ti/(Fe+Mn) ratios range from 0.001 to 0.036 and there is no discernable correlation between ratios for extracted coatings whose values fell within error of the teeth and those that did not; in fact the highest values correlate to samples with matching coating and fish teeth values, while samples with distinct coating and fish teeth Nd isotopic values record some of the lowest Ti/(Fe+Mn) values (figure 8-10). This lack of correlation is also seen in the other major element ratios; Mg/(Fe+Mn), Al/(Fe+Mn) and K/(Fe+Mn).

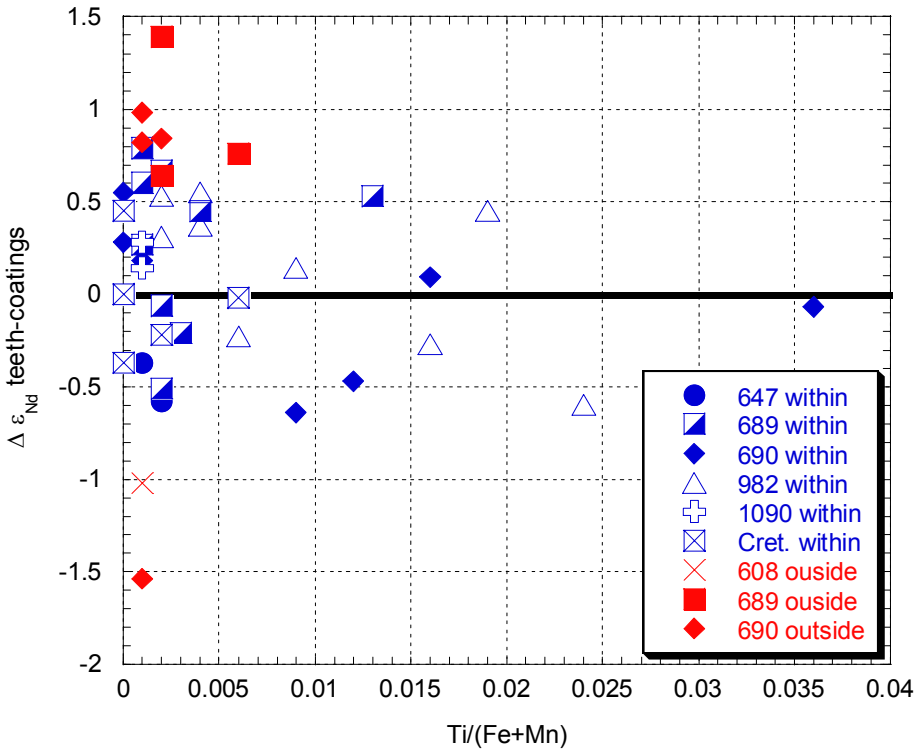

Figure 8-10 Ti/(Fe+Mn) ratios of samples vs. the difference between ε_{Nd} values of the fossil fish teeth and the coatings from Sites 608, 647, 689, 690 , 982, 1090, and the Cretaceous samples from Sites 1050 and 1258. For Sites 608, 647, 689 and 690 the red symbols represent those samples whose ε_{Nd} values for the teeth and the coatings did not match, while blue symbols throughout represent samples whose ε_{Nd} values for the teeth and the coatings did match.

Table 8-6. Major Element Rations from Site 608, 647, 690, 1090, and 1258

Samples	Al/Fe+Mn	Mg/Fe+Mn	Ti/Fe+Mn	Na/Fe+Mn	K/Fe+Mn	ε_{Nd} teeth-ε_{Nd} coating
647 13-1 104	1.167	0.497	0.002	2.376	0.851	-0.58
647 13-2 35	1.154	0.558	0.001	7.158	0.829	-0.37
689 8-1 84	1.117	0.189	0.003	1.765	0.319	-0.21
689 8-3 4	1.345	0.133	0.001	2.883	0.510	0.79
689 8-3 140	0.730	0.270	0.001	4.035	0.197	0.27
689 10-5 26	0.089	0.046	0.002	12.971	0.026	0.67
689 13-2 108	1.858	0.468	0.122	1381.950	1.113	0.15
689 13-4 82	2.443	0.789	0.064	835.928	1.283	0.62
689 13-6 60	0.512	2.884	0.002	5.186	0.310	-0.06
689 14-4 85	10.020	0.694	0.238	3783.426	7.001	0.44
689 15-4 45	6.964	1.578	0.004	1104.572	1.031	0.45
689 16-3 46	0.210	2.634	0.002	3.583	0.095	-0.51
689 17-7 54	1.208	1.120	0.013	678.624	0.573	0.53
689 18-2 60	0.035	2.393	0.001	3.407	0.164	0.60
690 8-4 66	0.063	0.062	0.000	0.142	0.016	0.28
690 8-5 17	0.064	0.057	0.001	15.192	0.021	0.18
690 9-3 148	0.051	0.050	0.000	0.128	0.026	0.55
690 11-7 17	0.178	0.554	0.009	0.684	0.070	-0.64
690 11-7 17 rep	0.067	0.100	0.012	0.774	0.058	-0.47
690 12-7 47	1.556	0.599	0.036	5.113	0.665	-0.07
690 13-3 74	0.534	2.312	0.016	5.614	0.259	0.09
982 34-1 53	0.260	0.128	0.019	14.846	0.121	0.45
982 36-1 12	0.380	0.162	0.004	1.277	0.068	0.55
982 39-5 23	0.918	0.456	0.009	6.711	0.282	0.14
982 43-3 104	0.324	0.063	0.004	2.229	0.113	0.37
982 45-2 28	0.425	0.128	0.002	1.670	0.067	0.53
982 47-1 162	0.525	0.252	0.006	1.730	0.151	-0.23
982 41-5 5.5	0.680	0.155	0.002	2.100	0.136	0.31
982 51-1 17.5	0.252	0.036	0.016	5.079	0.091	-0.27
982 52-4 27.5	0.511	0.163	0.024	31.595	0.519	-0.60
1090 13-1 25	1.419	0.356	0.001	3.120	0.404	0.28
1090 31-4 34	1.206	0.689	0.001	4.233	0.488	0.14
1050 20-1 33	1.601	0.483	0.006	61.866	1.372	-0.02
1050 29-2 102	0.036	0.041	0.000	0.200	0.013	-0.37
1050 31-2 103	0.013	0.013	0.000	0.078	0.023	0.45
1258 38-1 105	0.472	0.365	0.002	7.421	0.162	-0.22
*608 17-1 103	0.089	0.422	0.001	5.467	0.081	-1.02
*689 9-1 26	1.806	0.176	0.002	2.954	0.597	0.64
*689 9-6 63	3.630	0.109	0.002	6.087	0.729	1.39
*689 13-1 128	0.790	3.939	0.006	5.389	0.412	0.76
*690 9-5 148	0.016	0.032	0.001	2.921	0.016	0.98
*690 10-3 87	0.030	0.053	0.002	10.806	0.019	0.84
*690 10-5 84	0.082	0.059	0.001	20.321	0.024	-1.54
*690 11-5 17	0.009	0.045	0.001	2.600	0.009	0.82

* indicates that teeth and coatings values do not fall withing error of one another.

8.5.4 Sequential Extraction Procedure Results

As a final test for the extracted coatings a sequential extraction and dissolution procedure was performed. The method for extraction (Bayon et al., 2002) was slightly different than the extraction method for the single extracted samples. The purpose of this sequential extraction experiment was to determine the Sr and Nd isotopic values, the Nd concentrations, and the REE patterns for the various fractions of a given sample including the carbonate, Fe-Mn oxide coating, and residual fractions.

Using this extraction technique the ε_{Nd} value of the Fe-Mn oxide coatings consistently fell within error of the value for the fossil fish teeth (figure 8-11) even for the samples from Site 608, which previously yielded coatings with values that were too radiogenic. The ε_{Nd} value from the carbonate fraction falls within error of the teeth and coatings for 5 out of the 8 samples, and is not consistently more or less radiogenic for those samples that fall outside of error. The ε_{Nd} value from the residual fraction does not fall within error of the fish teeth for 6 out of the 8 samples, and they are consistently less radiogenic (table 8-7).

Sr isotopes were also measured from the three separate sediment fractions from the sequential extractions (table 8-8). The carbonate fraction values fall within error of the seawater value for six out of the seven samples. For sample 647, 13-4 the carbonate value is less radiogenic than seawater by 0.000455 (figure 8-11B). The Fe-Mn oxide coating values either fall within error or are more radiogenic than the seawater value. The residual fractions for five of six samples are more radiogenic than seawater values. For 982 47-1 all four fractions yield the same $^{87}Sr/^{86}Sr$ value.

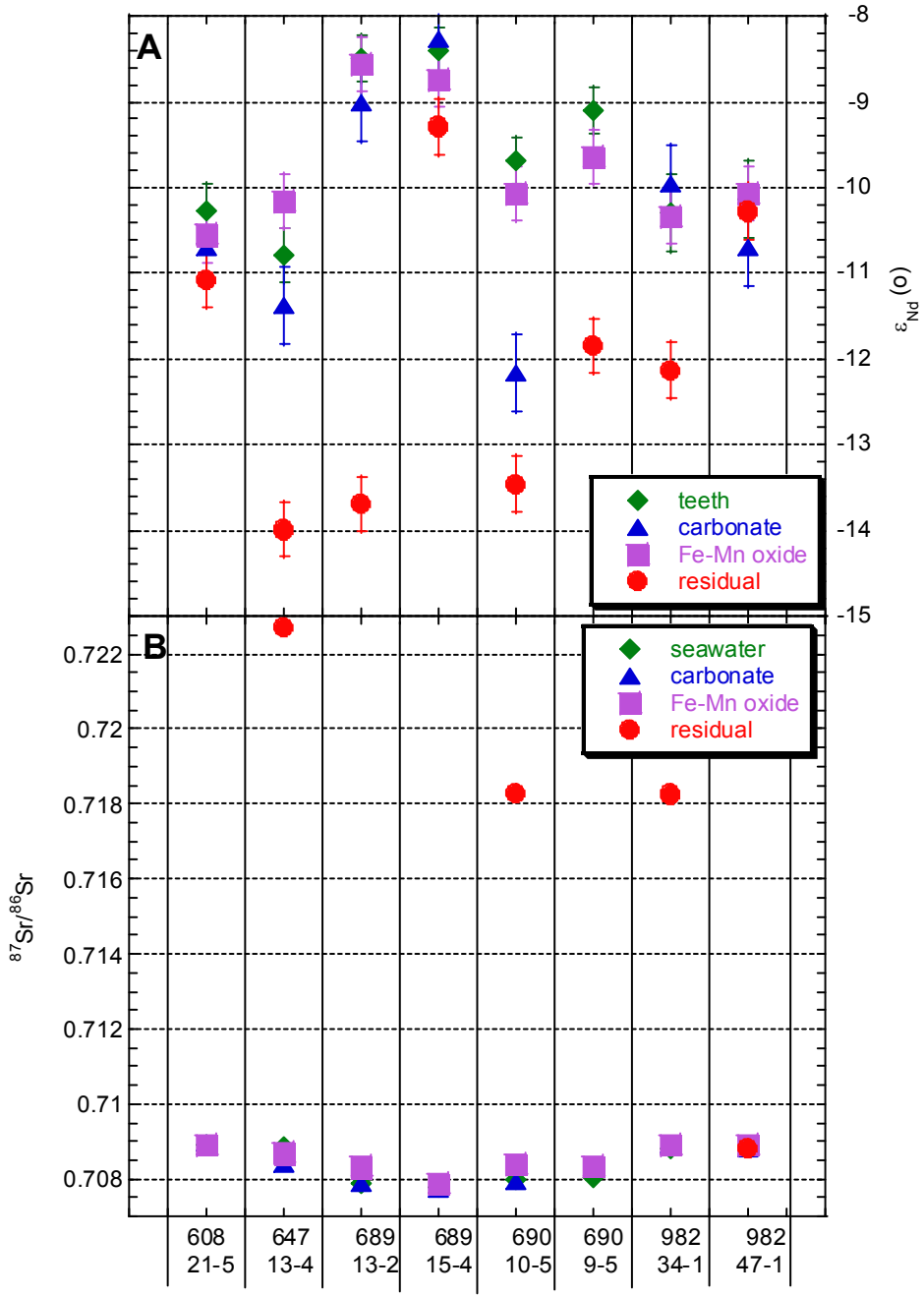

Figure 8-11. $\varepsilon_{Nd(o)}$ and $^{87}Sr/^{86}Sr$ values from 8 sequential extraction samples A) $\varepsilon_{Nd(o)}$ values from 8 sequential extraction samples. Sample 690, 9-5 does not have an $\varepsilon_{Nd(o)}$ value for the carbonate. B) $^{87}Sr/^{86}Sr$ values from 8 sequential extraction samples, errors are smaller than the data points. Each sample represents 4-5 cm from the core sample indicated. Sample 690, 9-5 does not have an $^{87}Sr/^{86}Sr$ value for the carbonate fraction and samples 608, 21-5; 689, 13-2; 689, 154; and 690, 9-5 do not have values for the residual fraction. Seawater values from Hodell and Woodruff, 1994; Farrell et al., 1995; Mead and Hodell, 1995; Martin et al., 1999.

Table 8-7. 143/144Nd values for Fossil Fish Teeth, Carbonate, Fe-Mn Oxide Coatings, and Residual Fractions from the Sequential Extraction Samples

	Teeth[1]		Carbonate		Fe-Mn Oxide		Residual	
	$^{143/144}$Nd	$\varepsilon_{Nd(o)}$[2]	$^{143/144}$Nd	$\varepsilon_{Nd(o)}$	$^{143/144}$Nd	$\varepsilon_{Nd(o)}$	$^{143/144}$Nd	$\varepsilon_{Nd(o)}$
608 21-5	0.512585	-10.28 ± 0.32	0.512090	-10.69 ± 0.45	0.512097	-10.55 ± 0.32	0.512070	-11.08 ± 0.32
647 13-4	0.512583	-10.79 ± 0.32	0.512055	-11.37 ± 0.45	0.512117	-10.16 ± 0.32	0.511921	-13.99 ± 0.32
689 13-2	0.512594	-8.49 ± 0.27	0.512176	-9.01 ± 0.45	0.512199	-8.56 ± 0.32	0.511936	-13.69 ± 0.32
689 15-4	0.512595	-8.40 ± 0.27	0.512214	-8.27 ± 0.45	0.512190	-8.74 ± 0.32	0.512162	-9.29 ± 0.32
690 10-5	0.512588	-9.69 ± 0.27	0.512015	-12.15 ± 0.45	0.512122	-10.07 ± 0.32	0.511948	-13.46 ± 0.32
690 9-5	0.512591	-9.09 ± 0.27			0.512144	-9.64 ± 0.32	0.512031	-11.84 ± 0.32
982 34-1	0.512585	-10.30 ± 0.45	0.512128	-9.95 ± 0.45	0.512108	-10.34 ± 0.32	0.512016	-12.13 ± 0.32
982 47-1	0.512586	-10.14 ± 0.45	0.512090	-10.69 ± 0.45	0.512122	-10.07 ± 0.32	0.512111	-10.28 ± 0.32

1. Measured $^{143}Nd/^{144}Nd$ of the Jndi-1 standard = .512102 ± 0.000014 (2σ).

2. $\varepsilon_{Nd(o)} = [(^{143}Nd/^{144}Nd)_{sample}/(^{143}Nd/^{144}Nd)_{CHUR}-1] \times 10^4$

Table 8-8. 87Sr/86Sr Values for Seawater, Carbonate, Fe-Mn Oxide Coatings, and Residual Fractions from the Sequential Extraction Samples

	Seawater		Carbonate[1]		Fe-Mn Oxide		Residual	
	$^{87}Sr/^{86}Sr$		$^{87}Sr/^{86}Sr$		$^{87}Sr/^{86}Sr$		$^{87}Sr/^{86}Sr$	
608 21-5	0.708920 ±	4.6E-05	0.708954 ±	0.000023	0.708915 ±	0.000023		
647 13-4	0.708855 ±	4.6E-05	0.708400 ±	0.000023	0.708686 ±	0.000023	0.722691 ±	0.000023
689 13-2	0.707905 ±	4.6E-05	0.707874 ±	0.000023	0.708323 ±	0.000023		
689 15-4	0.707760 ±	4.6E-05	0.707737 ±	0.000029	0.707876 ±	0.000023		
690 10-5	0.707970 ±	4.6E-05	0.707938 ±	0.000023	0.708404 ±	0.000023	0.718267 ±	0.000023
690 9-5	0.708035 ±	4.6E-05			0.708360 ±	0.000023		
982 34-1	0.708790 ±	4.6E-05	0.708919 ±	0.000023	0.708922 ±	0.000023	0.718259 ±	0.000023
982 47-1	0.708875 ±	4.6E-05	0.708809 ±	0.000023	0.708906 ±	0.000023	0.708822 ±	0.000023

1. Measured $^{87}Sr/^{86}Sr$ of the NBS-987 standard = 0.7120250 ± 0.000023 (2σ).

REE patterns from the three sediment fractions were also analyzed from each of the extracted samples (table 8-9). Below are the plots for these REE patterns grouped by site (figure 8-12, A-D). In all cases the concentration of the residual fraction is an order of magnitude or more greater than the oxide coating fraction and the carbonate fraction (figures 8-13A-C). The residual fraction from all samples except for 647, 13-4 and 982, 34-1 have patterns similar to those of the coatings, having a MREE bulge. In contrast, sample 647, 13-4 is LREE enriched and sample 982, 34-1 has a very flat pattern similar to that of shale. Interestingly, both 689 samples and 690, 19-6 have a large Eu anomaly. The anomaly is also seen in the carbonate fraction of these samples. The REE patterns for all of the oxide coatings have the distinctive MREE bulge indicative of Fe-Mn oxide coatings and, except for sample 647, 13-4, all of the coating samples exhibit a Ce depletion. The carbonate fraction in all cases has the lowest concentrations (figure 8-13

A-C). The carbonate fraction patterns for samples from 689, 690, and 982 all have patterns that are similar to the seawater REE pattern, while the carbonate patterns from both Sites 608 and 647 have a slight MREE bulge.

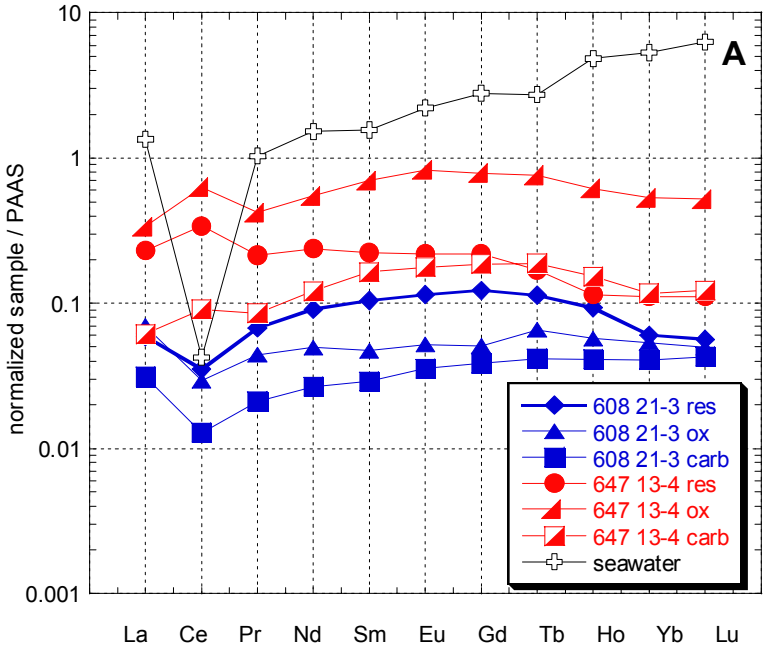

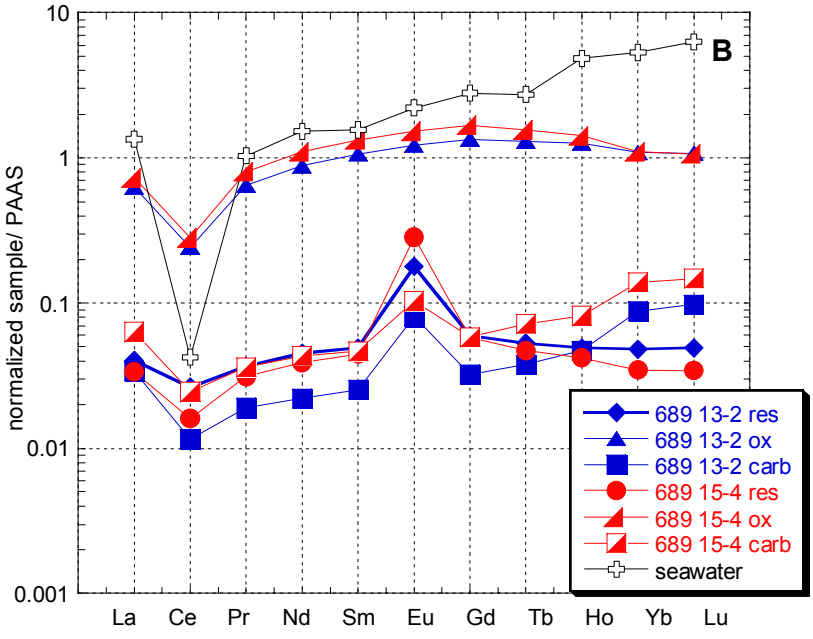

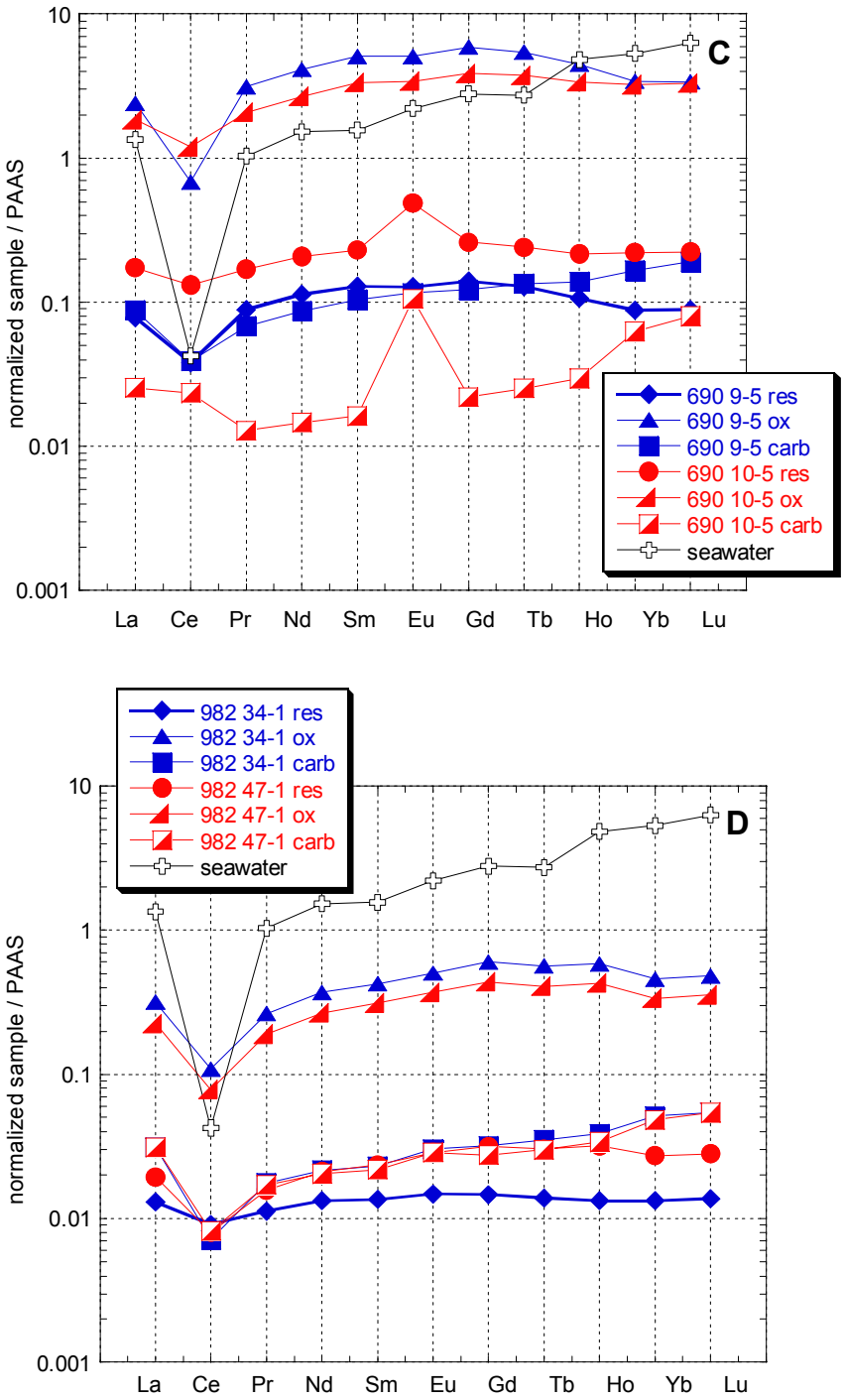

Figure 8-12 REE patterns from 8 sequential extractions. (A) Sites 608 and 647, (B) 689, (C) 690, and (D) 982 for 3 different sediment fractions; the residue (res), the Fe-Mn oxide coating (ox) and the carbonate (carb). Also included is the REE pattern for modern seawater from 3000m (De Baar et al., 1985).

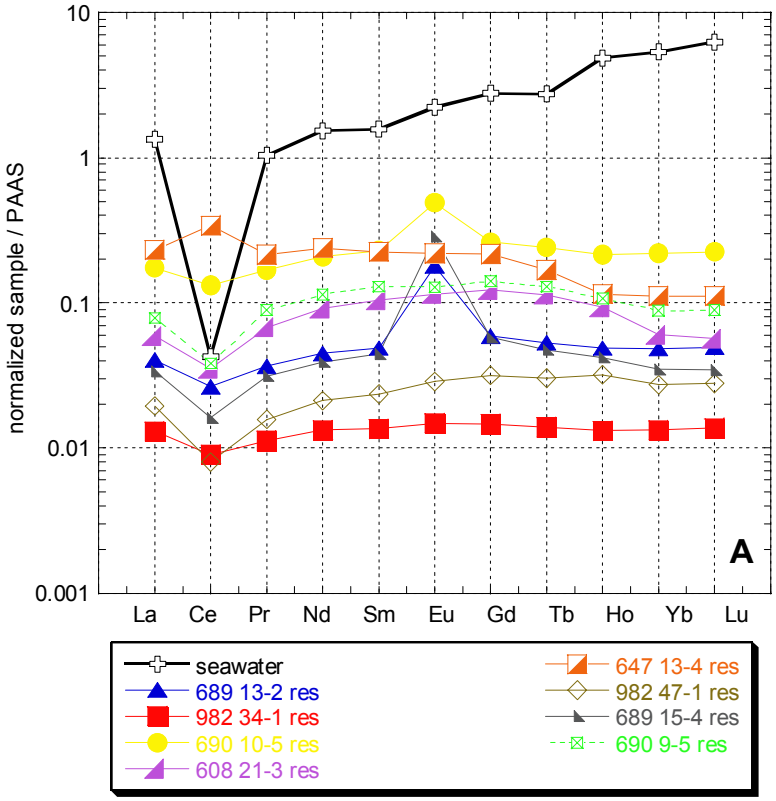
10
1
0.1
0.01
0.001
normalized sample / PAAS
La
Ce
Pr
Nd
Sm
Eu
Gd
Tb
Ho
Yb
Lu
A
seawater
689 13-2 res
982 34-1 res
690 10-5 res
608 21-3 res
647 13-4 res
982 47-1 res
689 15-4 res
690 9-5 res

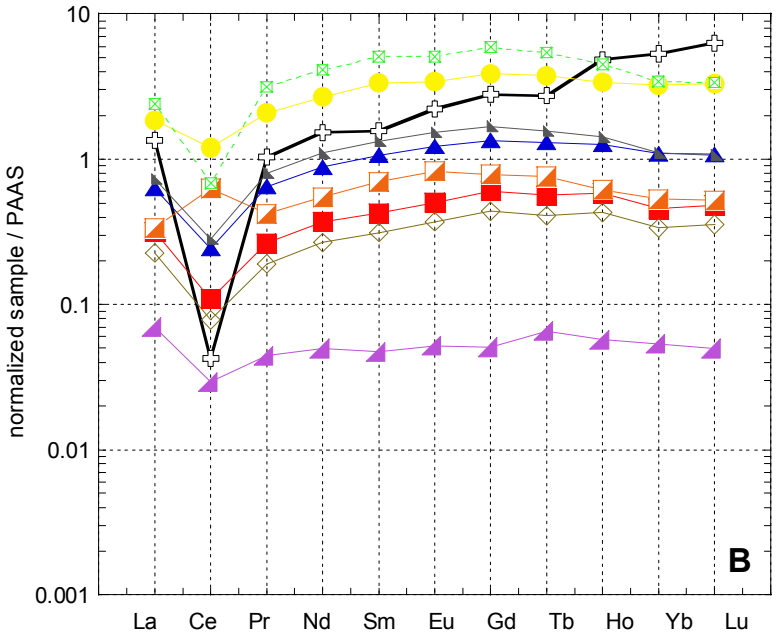
10
1
0.1
0.01
0.001
normalized sample / PAAS
La
Ce
Pr
Nd
Sm
Eu
Gd
Tb
Ho
Yb
Lu
B

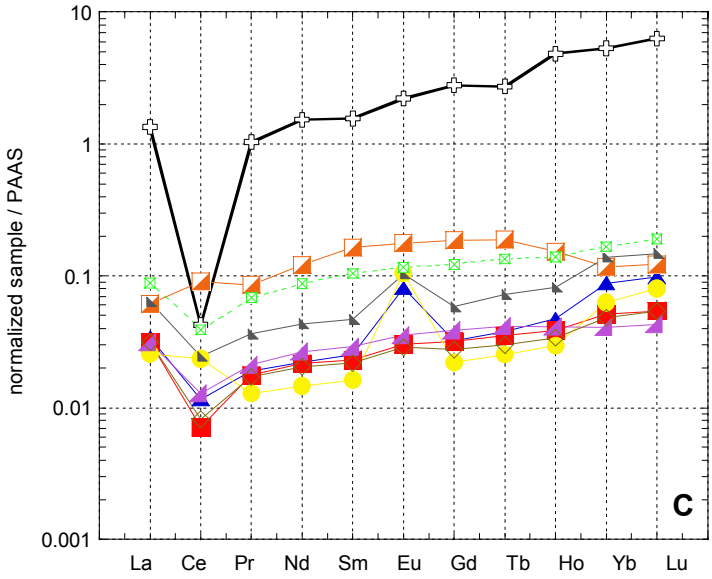

Figures 8-13 REE patterns for 3 sediment fractions for sequential extractions. REE patterns for A) the residual fraction, B) Fe-Mn oxide coating fraction, and C) the carbonate fraction from the sequential extraction samples from sites 608 and 647, 689, 690, and 982 showing the relative concentrations of each fraction group.

Table 8-9. REE Values from Sites 608, 647, 689, 690, and 982 from Three Sediment Fractions

Sample	La	Ce	Pr	Nd	Sm	Eu	Gd	Tb	Ho	Yb	Lu
608 21-3 res[1]	0.059	0.035	0.068	0.091	0.105	0.115	0.122	0.113	0.093	0.060	0.057
647 13-4 res	0.232	0.340	0.214	0.237	0.223	0.219	0.218	0.169	0.115	0.112	0.112
689 13-2 res	0.040	0.026	0.037	0.045	0.049	0.179	0.059	0.053	0.049	0.048	0.049
689 15-4 res	0.034	0.016	0.031	0.039	0.045	0.286	0.058	0.047	0.042	0.035	0.034
690 9-5 res	0.079	0.038	0.089	0.114	0.129	0.128	0.140	0.129	0.106	0.088	0.089
690 10-5 res	0.173	0.132	0.169	0.208	0.229	0.490	0.262	0.242	0.216	0.220	0.223
982 34-1 res	0.013	0.009	0.011	0.013	0.014	0.015	0.015	0.014	0.013	0.013	0.014
982 47-1 res	0.019	0.008	0.016	0.021	0.024	0.029	0.032	0.030	0.032	0.027	0.028
608 21-3 ox[2]	0.070	0.029	0.044	0.050	0.047	0.052	0.051	0.066	0.057	0.054	0.050
647 13-4 ox	0.337	0.630	0.423	0.547	0.701	0.829	0.790	0.765	0.618	0.529	0.520
689 13-2 ox	0.632	0.243	0.651	0.886	1.073	1.223	1.354	1.311	1.264	1.095	1.085
689 15-4 ox	0.728	0.283	0.804	1.100	1.338	1.534	1.674	1.556	1.424	1.099	1.072
690 9-5 ox	2.418	0.688	3.126	4.114	5.130	5.123	5.957	5.430	4.502	3.442	3.406
690 10-5 ox	1.848	1.201	2.091	2.687	3.336	3.436	3.882	3.752	3.396	3.236	3.313
982 34-1 ox	0.317	0.109	0.266	0.371	0.427	0.507	0.603	0.564	0.587	0.459	0.482
982 47-1 ox	0.225	0.078	0.191	0.267	0.312	0.373	0.441	0.409	0.429	0.339	0.355
608 21-3 carb[3]	0.031	0.013	0.021	0.027	0.029	0.035	0.039	0.042	0.041	0.041	0.043
647 13-4 carb	0.062	0.091	0.085	0.120	0.164	0.176	0.187	0.188	0.152	0.117	0.122
689 13-2 carb	0.034	0.012	0.019	0.022	0.025	0.081	0.032	0.038	0.047	0.088	0.098
689 15-4 carb	0.063	0.025	0.036	0.044	0.047	0.103	0.059	0.072	0.082	0.139	0.148
690 9-5 carb	0.088	0.039	0.068	0.087	0.105	0.116	0.122	0.135	0.138	0.165	0.191
690 10-5 carb	0.026	0.023	0.013	0.015	0.016	0.106	0.022	0.025	0.030	0.063	0.080
982 34-1 carb	0.031	0.007	0.018	0.021	0.023	0.030	0.032	0.035	0.039	0.051	0.054
982 47-1 carb	0.031	0.008	0.017	0.020	0.022	0.029	0.027	0.030	0.034	0.048	0.054

[1.] residue fraction [2.] Fe-Mn oxide fraction [3.] carbonate fraction
Error is ± 5%.

CHAPTER 9
DICUSSION OF EXTRACTION RESULTS FROM THE SOUTHERN OCEAN; NORTH ATLANTIC; AND CRETACEOUS AGE SAMPLES

With almost 90% success the extraction procedure applied to the samples in this study effectively removed a deep water ε_{Nd} signal with the Fe-Mn oxide coating fraction of the marine sediments, and recorded . None of the tests of validity, Sr isotopes, REE patterns, nor major element ratios allowed one to distinguish extracted samples that recorded deep water isotopic values correctly from those that did not when compared to ε_{Nd} values obtained from fossil fish teeth. Yet, by experimenting with these variables much more was learned about extraction these coatings and the composition of marine sediments.

9.1 Possible Lithologic Effects on the Extraction Procedure

In the Southern Ocean nearly 90% of all samples analyzed fell within error of the contemporaneous fossil fish teeth (figure 8-3A-C). All but one of the coating values that were not within error of the fish were less radiogenic than the value from the teeth indicating that these samples have been influenced by terrigenous material. This was the primary concern for this extraction project and it appears that in several cases associated sediment contaminated extracted coatings.

Although the lithology at each of the three Southern Ocean sites consists primarily of carbonate sediments, there is some variation in the amount of carbonate, terrigenous material, and opal. Figure 10-1 shows the weight percent of opal, carbonate and terrigenous material for samples from 19 to 25 Ma at Site 1090 (detailed lithological data

is not available for the other sites). They are plotted against the difference between ε_{Nd} values obtained from fossil fish teeth and Fe-Mn oxide coatings. For all of the samples these two values plot within error, even though the lithologies demonstrate a wide range of compositions. This illustrates that the extraction method is effective over a wide range of compositions.

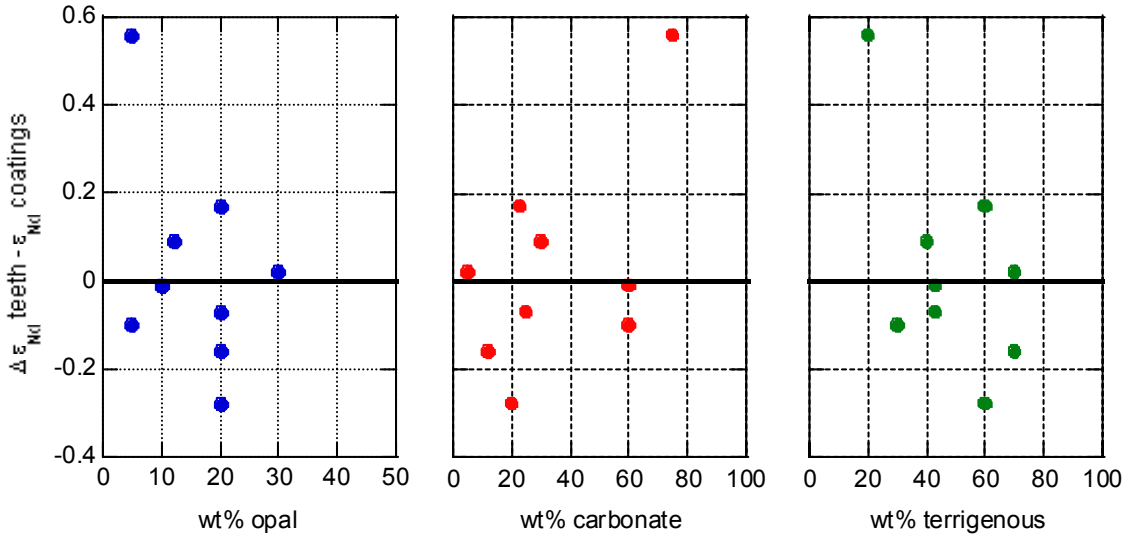

Figure 9-1. Weight percent opal, carbonate, and terrigenous material from Site 1090 from 19.2 to 25.1 Ma plotted against the difference between ε_{Nd} values from fossil fish teeth and Fe-Mn oxide coatings. A plot of 0 indicates the values were the same. Lithologic data from Diekmann, 2004.

In the North Atlantic samples from Sites 647 and 982 produced excellent agreement between fish teeth and oxide coatings (figures 8-4 and 8-5); however, for Site 608 the ε_{Nd} values for all of the coating were more radiogenic than the values obtained from the fish teeth (figure 8-4). This implies a consistent source of contamination that was attacked by the HH solution. A potential radiogenic source of Nd in the North Atlantic could be effects from the mid-ocean ridges (Frank et al, 2006). Of the sampled sites Site 608 is located closest to the ridge system, on the flank of the King's Trough. It

has been shown that Nd in hydrothermal fluids is removed by oxide and sulfide precipitates very close to the ridge (Michard et al., 1983; German et al., 1990). However, even if there were an effect from hydrothermal sources we would expect it to also affect the ε_{Nd} value of the fish teeth, altering them in the same manner as the coatings.

9.2 REE Patterns of Fe-Mn oxide coatings

The purpose of analyzing REE patterns for the extracted coating samples was to determine whether the coatings had been contaminated by 1) a detrital source, which should produce a flatter REE profile because the samples are normalized to PAAS, or 2) a hydrothermal source, which should produce a heavy REE (HREE) enrichment (figure 8-7). There is no difference in the REE patterns for extracted coating samples in which the ε_{Nd} value from the coating agreed with the fish teeth value and those that did not. The patterns for these four samples are very similar, with the distinct MREE bulge common to oxide coatings. This suggests that REE profiles do not provide a mechanism to identify contaminated samples.

There is a slight difference in the Ce anomalies between the two sets of samples in figure 8-7. Although there is much debate on the topic, Ce anomalies are believed to reflect redox conditions at a given location (e.g. Wright et al., 1987; Lécuyer et al., 2004). In most cases there is a very distinct negative Ce anomaly for the samples in this study, suggesting that the sites were influenced by oxidizing conditions. Although the Ce anomalies shown in figure 8-7 are variable, the samples noted as falling outside of error represent the two extremes with the largest and smallest observed Ce anomalies. Assuming that the magnitude of the Ce anomaly reflects the extent of the oxidizing

conditions, this pattern suggests that reducing versus oxidizing conditions do not affect the ε_{Nd} values of the extracted coatings.

Although the REE plots do not distinguish between samples with similar fish tooth and coating Nd isotopic values and those with distinctly different values (figure 8-7), the averages for different locations record slight differences (figure 8-8). The most noticeable difference between the various sites is the relative concentrations. There is very little information known about the mineralogy of the Fe-Mn oxide coatings and one of the major questions about this material is whether it is an open system that can be influenced by the composition of pore waters. If these coatings were an open system with respect to REE, it could be expected that the concentrations of REE in the coatings might increase or decrease as the sediments aged, acquiring or loosing REE into the pore waters. However, the extracted coatings from the Cretaceous (~90Ma) do not have higher or lower concentrations than the younger sediments (figure 8-8). The relative concentrations are not due to the length of burial time, but could be due to the sedimentation rates at the various sites. Table 9-1 shows the average sedimentation rate at the sampled sites along with the approximate Nd concentration from the REE measurements. There is a general correlation between the concentration of Nd and the sedimentation rate; the higher the sedimentation rate the lower the concentration of Nd (figure 9-2). This is reflected in the REE analyzed from the single extracted samples (figure 8-8) and the REE plots from the oxide fraction of the sequential extraction samples (figure 8-13B) also support this conclusion. Using both analytical methods samples from Sites 608, 647, and 982 have the lowest concentrations, while those from Sites 689 and 690 have the highest.

Table 9-1. Site Locations with Average Sedimentation Rate and Average Nd concentration in coatings

Site	average sed.[1] rate (m/m.y.)	average [2] [Nd] ppm
608	34	0.54
647	16	4.19
982	35	6.26
689	5	4.91
690	5.5	30.48
1090	10	8.04
1258	3	14.13

[1] from Initial Reports for each Site
[2] from REE analysis

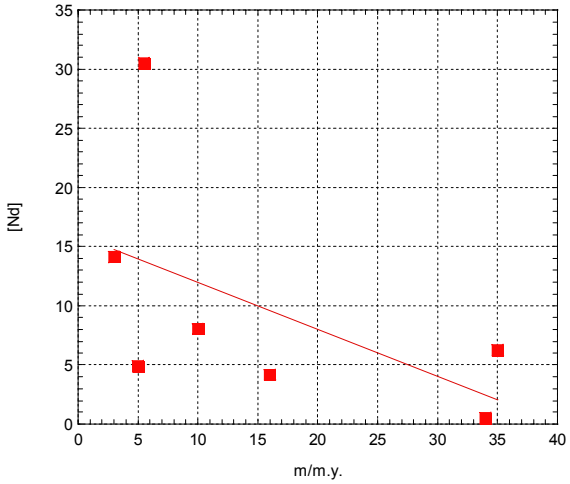

Figure 9.2. Average sedimentation rate versus Nd concentration for Sites 608,647, 982, 689, 690, 1090, and 1258. Line represents the best fit line.

9.3 Sr Isotopes

Sr isotopes were measured from the extracted Fe-Mn oxide coatings and although samples that yielded the same ε_{Nd} value as the contemporaneous fsih teeth fell both on the seawater curve and above it (more radiogenic), the four samples whose ε_{Nd} value did not match the teeth value all were more radiogenic than the Sr seawater curve (figure 8-9). This suggests that these samples have been contaminated by terrigenous material that affected the Sr as well as the Ns isotopic values. Since the Sr isotopic values for most of the residual sediment fraction were more radiogenic than the coatings (as measured from the sequential extraction samples (figure 8-11), implying a continental origin, it is safe to conclude that there is some contamination from the sediments that affects the Sr isotopic values of the extracted coatings.

In a number of samples the Sr isotopic values of the extracted coatings were affected by the associated terrigenous sediment in the sample, but the Nd isotopic values were not. This phenomina is most likely due the particle reaction, as Nd is much less

particle reactive than Sr. The distribution coefficient in Nd is lower and therefore there is less Nd in the pore waters when compared to Sr. Due to pore water mixing Sr is then more variable throughout the sediments.

Martin and Scher (2004) measured Sr isotopic values of fossil fish teeth and determined that these values were commonly less radiogenic than associated foraminifera and the Sr seawater curve. This was interpreted to represent the addition of pore water Sr derived from recrystallization of older carbonates into the apatite of the teeth, indicating that this apatite is not a closed system with respect to Sr. Unlike the teeth, all of the extracted samples either fell on the Sr curve or were more radiogenic, suggesting that the coatings are not influenced by pore water diagenesis or the input from the contaminant overwhelms the diagenetic signal. The radiogenic Sr values in the extracted coatings argue that the source of the contamination is derived from contamination from terrestrial material during sample preparation.

Piotrowski et al. (2004 and 2005) used $^{87}Sr/^{86}Sr$ values to identify extracted Fe-Mn oxide coatings with accurate Nd isotopic values. They measured the Sr isotopic values of all the extracted samples and only accepted the ε_{Nd} values from samples with $^{87}Sr/^{86}Sr$ that fell on the seawater Sr curve for the appropriate age. According to the results of this study, this assessment would be overly conservative. The inaccurate ε_{Nd} values would be rejected by eliminating all samples whose $^{87}Sr/^{86}Sr$ value fell above the seawater curve, but nearly a third of the viable values would also be rejected. The results of this study do not eliminate Sr isotopes as an accurate test of the integrity of the Nd isotopic record, but they indicate that samples with accurate ε_{Nd} values will also be rejected.

9.4 Major Elements

The major element data illustrate high variability within the extracted coatings, but there is very little correlation between the major element ratios and the accuracy of the ε_{Nd} values. It is not clear that the major element data actually reflect the ratios in a pure oxide coating. Brumsack (2005) analyzed major elements in black shales to determine if different suites of elements can give information about the paleoenvironment during the deposition of these shales. In this study he discussed the effectiveness of some of these major elements as tools for identifying source locations for continental input into the oceans. Aluminum is unaffected by biological activity or diagenetic processes and is generally introduced by eolian or fluvial sources. The concentration of Al is generally high in clays, but low in seawater, with a short residence time in the oceans. He identified Al as the most effective element for quantifying terrigenous detrital fractions. Titanium and K are also unaffected by biological activity and predominantly sourced from the continents, thus they are also effective proxies for continental input (e.g. Dellwig et al., 2000; Wehausen and Brumsack, 2002). Sodium is not very effective owing to the high Na concentration in seawater. The variability in the major element ratios is either an effect of the amount of influence from some clay and/or terrigenous material or variability in the amount of Fe and Mn in the coating. Since the extent of continental input varies between each of the locations used in this project, it would be expected that the ratios would also vary with location. There is undoubtedly some input of continental material associated with some of the oxide coatings based on the Sr isotopic results and the large variability in major element ratios (8-10A-B). Yet, this contamination apparently has little to no effect on the Nd isotopic composition of the

coatings as there is no trend among samples that yielded fish teeth ε_{Nd} values and those that did not.

It is fairly difficult to determine what the major elements measured from these coatings indicate. It is clear that Na concentrations are highly affected by the Na from seawater. The Na/(Fe+Mn) ratios vary from nearly 400 to 0.08, suggesting that the samples need to be thoroughly washed in double distilled water prior to extraction. Some of the other elemental ratios indicate concentrations of minor elements Al, Mg, and K that are higher than the concentrations of Mn plus Fe (e.g. Al/(Fe+Mn) ratios up to 10.0, K/(Fe+Mn) ratios up to 7.001, or a Mg/(Fe+Mn ratios of up to 3.939). These high ratios are unlikely to represent pure extractions of Fe-Mn oxide coatings. While the majority of the samples measured have low element to Fe plus Mn values more typical of values reported for Fe-Mn nodule standards (NOD-P and NOD-A), these high values are cause for concern. They suggest that the extraction process is removing material other than what is expected, yet this additional component does not seem be to effecting the Nd isotopic composition.

9.5 Sequential Extraction

The results of the sequential extraction procedure support the conclusion that the ε_{Nd} of Fe-Mn oxide coatings is not altered by the Nd isotopic value of the residual material. To test this conclusion further a mass balance calculation was performed using the Nd concentrations from each fraction of the sequential extraction procedure. Table 9-2 shows the percent Nd contributed to the whole from each of the fractions; carbonate, Fe-Mn oxide coatings, and the residual sediment. The majority of the Nd in almost all the samples was extracted from the Fe-Mn oxide fraction of the sediment. The one case

where it was not was from sample 608, 21-3 where 54.34% of the Nd came from the residual fraction. This discrepancy may account for the incorrect ε_{Nd} values obtained during the single extraction procedure. These mass balance calculations show very decisively that the large of majority of Nd is coming from the coating fraction and if there were some contamination during the extraction procedure from the residual fraction it would have a small impact on the ε_{Nd} value.

Table 9-2. Percent Nd contributed to the bulk sediment from the carbonate, Fe-Mn Oxide, and Residual Fraction Separated during the Sequential Extraction Procedure

Sample	Carbonate[1]	Oxide[1]	Residue[1]
608 21-3	15.92	29.75	54.34
647 13-4	13.29	60.47	26.24
689 13-2	2.31	92.96	4.73
689 15-4	3.68	93.01	3.32
690 9-5	2.02	95.33	2.65
690 10-5	0.50	92.34	7.16
982 34-1	5.29	91.45	3.26
982 47-1	6.65	86.51	6.84

[1]determined using the starting weight of each sample and the weight after each extraction

The fish teeth and Fe-Mn oxide extractions yielded the same ε_{Nd} values for all 8 samples evaluated. These results are a bit different from the single extraction experiment that yielded ~90% agreement between the coatings and the teeth. For the sequential extraction procedure the HH was stronger and the sample was heated while being treated. Although the sequential extraction procedure was chemically more aggressive, the results indicated less influence by potential contaminants. This is evident from both the Nd isotope values (figure 8-11) and the REE patterns (figure 8-12A-D). In most cases the ε_{Nd} values of the oxides and carbonate are much more radiogenic than the residual fractions. In one case (690, 10-5) it looks as if the carbonate fraction might have been affected by the residual fraction, as the ε_{Nd} value fell between the teeth and the residual values. In two cases (608, 21-5 and 982, 47-1) the residual fraction fell within error of

the coating and teeth values. This may indicate that the coatings were not completely removed prior to the digestion of the residue. Although it seems unlikely, the procedure for the sequential extraction isolate the Fe-Mn oxides more effective than the procedure developed for the single extraction, but further tests of this idea are required.

Interestingly the oxide coating fraction from the sequential extraction of sample 608, 21-5 (figure 8-11) yielded accurate ε_{Nd} values when compared to fossil fish teeth and the residue was slightly less radiogenic, but within error. In contrast, the values from two single extraction samples were much more radiogenic than contemporaneous teeth (figure 8-4). One cause of this discrepancy could be related to the REE concentrations inferred from the REE plots of the sequential extraction which show that the sample from Site 608 had the highest concentrations for the residual fraction and the lowest concentrations for the coating (figure 8-13A-B). This is similar to the results of the REE measured from the single extraction samples, which again illustrated that the coating samples from site 608 had the lower concentrations than coatings from other sites (figure 8-8). The low concentration in the coatings at this sitemight allow the residual fraction to have a greater influence on the isotopic signal, thus creating the discrepancy between the teeth and coatings.

Although Site 608 is close to the Mid-Atlantic Ridge, the sequential extraction results do not show any indication of radiogenic Nd from hydrothermal contamination. In fact the residue from the one residue sample tested from Site 608 was slightly less radiogenic than other phases, which is consistent with the terrigenous signature of the other residue samples. Given that it is so difficult to account for the offset observed in the single extraction samples from Site 608 and the agreement observed in the sequential

leach from the site, one potential explanation is that there may have been an analytical problem in the preparation or measurement of the coating samples for the single extractions. There are only two samples from this site and they were analyzed early on in the study before the correction between the TIMS and MC-ICP-MS had been thoroughly characterized; however, these samples were prepared and analyzed along with the single extraction samples from Site 647, and all of the coatings from that site fall within error of the teeth. It is intriguing, however, that the coating values from Site 647 are consistently more radiogenic than the values for the teeth. Additional analyses from both of these sites would help determine whether there really is a component that introduces more radiogenic Nd into the oxide coating extraction.

The $^{87}Sr/^{86}Sr$ data support the idea that Sr isotopes from the coatings are altered in the direction of the radiogenic residual sediment fraction. In a number of samples the residual fraction is more radiogenic than the carbonate and the oxide coatings. The residual sediment seems to have altered the oxide coating values for samples 689, 13-2 and 690, 9-5, as they are offset slightly towards the residual value. Even though the Sr isotopic values were altered for these samples, the ε_{Nd} values appear to be unaffected. This supports the results obtained from the single extraction, which illustrated that Sr isotopic values were altered toward more radiogenic values in a number of samples that showed agreement between fish teeth and oxide coating ε_{Nd} values as well as samples that showed disagreement.

The REE patterns of the sequential extraction samples yield comparable results to the isotopic values. The Fe-Mn oxide REE patterns for all 8 samples have a MREE bulge, representative of oxide coatings (figure 8-12A-D and 8-13A-C). It does not seem

that there was any influence from the residual fraction, which should flatten these patterns. The REE plots for the residual fractions of samples 982, 47-1 and 647, 13-4 seems to be influenced by the coatings with enrichment in the MREEs, indicating that the oxide coatings were not completely removed during the procedure. For most of the samples the carbonate fraction has a pattern similar to that of seawater, however for both 689 samples and 690, 10-5 the carbonate fractions have a large Eu anomaly (figure 8-12B and C). This anomaly mimics the REE pattern of the residual fractions for those samples, suggesting that the carbonate fraction has been contaminated by the residual fraction in that the carbonate may be more of an open system than the Fe-Mn oxide coatings and incorporate some of the residual sediment signature. If this same contamination had affected the oxide coatings a similar anomaly would also be present. Based on the isotopic data as well as the REE patterns, the ε_{Nd} value of the extracted coatings were not influenced by the surrounding sediment when using this procedure.

9.6 An Alternate Explanation

There is one other possible explanation for some of the results obtained in these studies. It may be possible that phosphates present in the sediments are dissolved during the reduction of the Fe-Mn oxide coatings using the HH solution . It is known that these pieces of bone debris and fossil fish scales effectively record deep water Nd isotopic values. In addition, phosphates exhibit a MREE enrichment similar to the pattern characteristic of Fe-Mn oxide coatings. It has also been shown that Sr isotopes from phosphates do not record seawater values, but are altered toward pore waters values (Martin and Scher, 2004), thus explaining the variable Sr isotopic results obtained in this study. This addition of phosphate material may be adding varying amounts of other

major elements, causing the major element ratios measured to yield unexpected results. A very preliminary study was performed measuring P(Fe+Mn) ratios on the carbonate and oxide fractions obtained during the sequential extraction procedure. These values of P(Fe+Mn) for just the oxide fraction ranged from 4.11 to 0.104, while this same ratio for the nodule standards are 0.005 and 0.020 for Nod-P and Nod-A respectively. These results suggest that Phosphorous has been extracted during the HH extracting step of this procedure. The addition of this phosphate material does not seem to be a problem in terms of the extraction of Nd isotopes from Fe-Mn oxide coatings. Since both the oxide coatings and the phosphates are reliable archives for deep water Nd, the addition of the phosphates does nothing more than enhance the desired signal. Further analysis such as phosphorous measurements would be needed to refine this interpretation.

CHAPTER 10
CONCLUSIONS

This study accomplished two distinct goals. First, Nd isotopes preserved in fossil fish teeth were used to study circulation conditions associated with two Late Cretaceous OAEs. Second, Fe-Mn oxide coatings extracted from marine sediments were demonstrated to be effective archives of deep sea Nd isotopes on Cenozoic to Cretaceous timescales. REE plots and Sr isotopes show that the $\varepsilon_{Nd(t)}$ values obtained from Late Cretaceous fossil fish teeth at Demerara Rise (Site 1258), in the equatorial Atlantic have not been altered by diagenesis. Therefore, these fish teeth affectively record deep water Nd isotopic values. Before and after OAE2 and the MCE $\varepsilon_{Nd(t)}$ values at Demerara Rise average –15. This value is distinct from values recorded in the North Atlantic, Pacific and Tethys oceans and suggests the basin surrounding Demerara Rise was relatively isolated and strongly influenced by local weathering inputs off the South American continent. There may have been intermediate to deep water communications, however, between Blake Nose (Site 1050) and the North Pacific (Site 886) which both record relatively radiogenic $\varepsilon_{Nd(t)}$ values of -6 to -4.

During OAE2 $\varepsilon_{Nd(t)}$ values increase by 8 $\varepsilon_{Nd(t)}$ units. This shift is larger than any shift documented throughout the world's oceans and it is tightly correlated to a $6^{o}/_{oo}$ excursion in $\delta^{13}C_{org}$, indicating that changes in deep ocean circulation were involved in the development of OAE2. Previously hypothesized interpretations suggested that deep ocean stagnation could have contributed to enhanced carbon burial; however, the Nd

isotopic results argue for enhanced mixing and ventilation during OAE2 as values approached those of Blake Nose and the Pacific.

Mechanisms that may have affected both $\delta^{13}C_{org}$ and $\varepsilon_{Nd(t)}$ at Demerara Rise include; 1) a change in sea level that may have allowed different water masses to overwhelm sills in the oceans causing increase mixing between water masses, as well as extraction of nutrients from coastal shelves which would have caused increases in primary production, 2) changes to ocean water chemistry caused by the eruption of the Caribbean LIP and increased ocean crust production, which would cause both increased nutrient loading into the oceans and, thus, increased productivity, and the introduction of radiogenic $\varepsilon_{Nd(t)}$ values into the oceans that could have influenced waters at Demerara Rise, and 3) changes to upwelling along the coast of the South American continent that brought nutrients to the surface waters which aided primary production as well as invigorating intermediate to deep ocean circulation. None of these mechanisms resolve all of the problems surrounding OAEs; however, the Nd results clearly illustrate that enhanced deep ocean circulation either played a role in the cause or responded to the anoxic events.

The second half of the study was a systematic evaluation of an extraction procedure to remove Fe-Mn oxide coatings from marine sediments for Nd isotopic analysis. This is the first study to determine the validity of the ε_{Nd} results from the extraction procedure by comparing them to the isotopic ratios obtained from contemporaneous fossil fish teeth. Results are as follows:

1. The extraction procedure is nearly 90% successful at extracting deep water ε_{Nd} signals from oxide coatings from both the Southern Ocean and the North Atlantic on

Cenozoic timescales, as well as from samples from Late Cretaceous sediments from Demerara Rise in the North Atlantic. Although there was excellent agreement between the teeth and coatings at almost every site, the oxide coatings from Site 608 were consistently distinct and more radiogenic than the teeth. All other tests (Sr isotopes, REE patterns, and elemental ratios) suggest that any contamination at this site should be terrigenous and therefore less radiogenic. Additional tests will be required to identify the source of the more radiogenic values, which may be procedural or analytical.

2. Sr isotopes, REE, and major element ratios were all measured on the extracted oxide samples in order to develop a test of validity independent of fossil fish teeth. Neither REE patterns nor major element ratios can be used as stand-alone tests for validity. There was no conclusive trend in either of these tests that would indicate a difference between extracted oxide coating ε_{Nd} values that agreed with teeth and those that did not. REE patterns from all measured samples yielded patterns with MREE enrichment that is typical for Fe-Mn oxide coatings, while the concentrations of the REE appear to be dependent on the sedimentation rate at a given location. Major element ratios varied considerably and there generally was no correlation to whether or not the oxide samples yielded $\varepsilon_{Nd(t)}$ values that agreed with contemporaneous fish teeth values. Sr isotopes are a very conservative method for eliminating $\varepsilon_{Nd(t)}$ values that did not agree with the teeth values. In all cases samples that yielded ε_{Nd} values distinct from the fish tooth values produced $^{87}Sr/^{86}Sr$ values did not fall on the seawater Sr curve; yet many of the samples that yielded agreement between the oxide and teeth ε_{Nd} values also plotted off of the seawater Sr curve. By eliminating all samples that fell off the curve about one third of the viable samples would also be discarded.

3. A sequential extraction procedure performed on 8 samples from sites in both the Southern Ocean and the North Atlantic yielded results that were consistent with results obtained from the single extraction samples. ε_{Nd} values and REE patterns from the oxide coatings were unaffected by the residual sediments, however in a few cases the carbonate fraction was contaminated. Sr isotopes from extracted coatings were susceptible to contamination from the residual sediments, producing Sr isotopic measurements that were altered towards more radiogenic values, as demonstrated by the single extraction samples. Interestingly, the results from the sequential extraction procedure for samples from Site 608 yielded different results than the single extraction. There was no evidence of a source of more radiogenic material, which might suggest that the results obtained from the single extraction analysis could be the result of an analytical problem that needs to be evaluated.

4. Results from this extraction study suggest that this procedure can be used as a method for extracting ε_{Nd} values from Fe-Mn oxide coatings on marine sediments. A few fossil fish teeth samples should be measured from each site, however, to provide a check on the validity of this system at a specific site. Because the coatings yielded such consistent results compared to the fish teeth the extensive cleaning procedure on the teeth prior to analysis may be irrelevant, as it is designed to remove potential contamination due to the oxide coatings.

LIST OF REFERENCES

Abouchami W., Goldstein S. L., Galer S. J. G., Eisenhauer A., Mangini A. (1997) Secular changes of lead and neodymium in central Pacific seawater recorded by a Fe-Mn crust. *Geochimic et Cosmochimica Acta* **61**, 3957-3974.

Albarede F. and Goldstein S. L. (1992) A world map of Nd isotopes in seafloor ferromanganese deposits. *Geology* **20**, 761-763.

Albarede F., Goldstein S. L., Dautel D. (1997) 143Nd/144Nd of Mn nodules from the Southern and Indian oceans, the global oceanic Nd budget, and their bearing on the deep ocean circulation during the Quarternary. *Geochim. Cosmochim. Acta* **61**, 1277-1291.

Arthur M. A., Schlanger S. O., and Jenkyns H. C. (1987) The Cenomanian-Turonian oceanic anoxic event, II. Paleoceanogrpahic controls on organis-matter production and preservation. *Geological Society of London, Special Publication* **26**, 401-420.

Arthur M.A., Dean W.E., Pratt L.M. (1988) Geochemical and climatic effects of increased marine organic carbon burial at the Cenomanian Turonian boundary. *Nature* **335**, 714-717.

Arthur M.A., Jenkyns H.C., Brumsack H., Schlanger S.O. (1990) Stratigraphy, geochemistry, and paleoceanography of organic-carbon-rich Cretaceous sequences, in Ginsburg R.N. and Beaudoin B., Eds. *Cretaceous Resources, Events and Rhythms. NATO ASI Series C* **304** 75-119

Axelsson M.D., Rodushkin I., IngriJ., Öhlander B. (2002) Multielemental analysis of Mn-Fe nodules by ICP-MS: optimization of analytical method. The Analyst, **127**, 76-82.

Barrera E. and Savin S.M. (1999), Evolution of late Campanian-Maastrichtian marine climates and oceans. Barrera, E., and Johnson, C.C., eds., *Evolution of the Cretaceous ocean-climate system,* Volume Special Paper **332**: Boulder, CO, United States, Geological Society of America (GSA) 245-282.

Barron J., Larsen B., and al. e. (1989) Site 738. In *Proc. ODP Init. Rep.*, Vol. **119**, pp. 229-288.

Barron E.J. and Peterson W.H. (1990) Mid-Cretaceous ocean circulation: results from model sensitivity studies. *Paleoceanography* **5**, 319–337.

Barron E.J., Peterson W.H., Thompson S., Pollard D. (1993) Past climate and the role of coean heat transport: Model simulations for the Cretaceous. *Paleoceanography* **8**, 785-798.

Barron E.J., Fawcett P.J., Peterson W.H., Pollard D., Thompson S.L., (1995), A 'simulation' of mid-Cretaceous climate. *Paleoceanography* **10**, 953-962.

Bayon G., German C.R., Boella R.M., Milton J.A., Taylor R.N., Nesbitt R.W. (2002) An improved method for extracting marine sediment fractions and its application to Sr and Nd isotopic analysis. *Chem. Geol.* **187**, 179-199

Belshaw N. S., Freedman P. A., O'Nions R. K., Frank M., Guo Y. (1998) A new variable dispersion double-focusing plasma mass spectrometer with performance illustrated for Pb isotopes. *Int. Jour. Mass Spectrom.* **181**, 51-58.

Bernat M. (1975) Les isotopes de l'uranium et du thorium et les terres rares dans l'environment marine. *Cah. ORSTROM Ser. Geol.* **7**, 65-83.

Bertram C. J. and Elderfield H. (1993) The geochemical balance of the rare earth elements and neodymium isotopes in the oceans. *Geochimica et Cosmochimica Acta* **57**, 1957-1986.

Bice K. L. and Marotzke J. (2001) Numerical evidence against reversed thermohaline circulation in the warm Paleocene/Eocene ocean. *Journal of Geophysical Research* **106**, 11,529-11,542.

Bonatti E., Ligi M., Gasperini L., Peyve A., Raznitsin Y., Chen Y.J. (1994) Transform migration and vertical tectonics at the Romanche fracture zone, equatorial Atlantic. *J. Geophys. Res.* **99**, 21779-21802

Boyle E. A. (1981) Cadmium, Zinc, Copper and Barium in foraminifera tests. *Earth and Planetary Science Letters* **53**, 11-35.

Boyle E. A. and Keigwin L. D. (1985) Comparison of Atlantic and Pacific paleochemical records for the past 215,000 y: Changes in deep ocean circulation and chemical inventories. *Earth and Planetary Science Letters* **76**, 135-150.

Bralower T.J. and Thierstein H.R. (1984) Low productivity and slow deep-water circulation in mid-Cretaceous oceans. *Geology* **12**, 614-618.

Bralower T.J., Arthur, M.A., Leckie M.R., Silter, W.V., Allard D.J., Schlanger, S.O. (1994) Timing and Paleoceanography of Oceanic Dysoxia/Anoxia in the Late Barremian to Early Aptian (Early Cretaceous). *Palaios* **9**, 335-369.

Brass G. W., Southam J. R., Peterson W. H. (1982) Warm saline bottom water in the ancient ocean. *Nature* **296**, 620-623.

Broecker W. S. and Peng T.-H. (1982) *Tracers in the Sea*. Lamont-Doherty Geological Observatory.

Brumsack H.J. (2005) The trace metal content of recent organic carbon-rich sediments: Implications for Cretaceous black shale formation. Paleogeog. Paleoclim. Paleoeco. **232**, 344-361.

Burton K. W., Lee D.-C., Christensen J. N., Halliday A. N., Hein J. R. (1999) Actual timing of neodymium isotopic variations recorded by Fe-Mn crusts in the western North Atlantic. *Earth and Planetary Science Letters* **171**(1), 149-156.

Burton K. W., Ling H.-F., O'Nions R. K. (1997) Closure of the Central American Isthmus and its effect on deep-water formation in the north Atlantic. *Nature* **386**, 382-385.

Bush A.B.G and Philander S.G.H (1997) The late Cretaceous: Simulation with a coupled atmosphere-ocean general circulation model. *Paleoceanography* **12**, 495-516

Calvert S.E., and Pedersen T.F. (1990) Accumulation and preservation of organic carbon in marine sediments; the roles of anoxia vs. production: *AAPG Bulletin* **74**, 454-466.

Charles C.D (1992) Evidence from Southern-Ocean sediments for the effect of North-Atlantic deep water flux on climate. *Nature* **335**, 416-418

Chester R. and Hughes M. J. (1967) A chemical technique for the separation of ferromanganese minerals, carbonate minerals and adsorbed trace elements from pelagic sediments. *Chem. Geol.* **2**, 249-262.

D'Hondt S. and Arthur M.A. (2002) Deep water in the late Maastrichtian ocean: Paleoceanography **17**, 8-1 – 8-11.

de Baar H.J., Bacon M.P., Brewer P.G., Bruland K.W. (1985) Rare earth elements in the Pacific and Atlantic Oceans. *Geochimica et Cosmochimica Acta*, **49**, 1943-1959

de Graciansky P.C., Poag C.W., et al, (1985) *Initial Reports of the Deep Sea Drilling Project*. US Government Printing Agency, Washington, DC, **80.**

Dellwig O., Hinrichs J., Hild, A., Brumsack H.J. (2000) Changing sedimentation in tidal flat sediments of the southern North Sea from the Holocene to the present: A geochemical approach. *J. Sea Res*. **44**, 195-208

De Paolo D.J. and Wasserburg, G.J. (1976) Nd isotopic variations and petrogenetic models, Geophysical Research Letters, 3 743-746

Elderfield H. and Greaves M. J. (1982) The rare earth elements in seawater. *Nature* **296**, 214-219.

Elderfield H. and Sholkovitz E. R. (1987) Rare earth elements in the pore waters of reducing nearshore sediments. *Earth Planet. Sci. Lett.* **82**, 280-288.

Erba E. (1994) Nannofossils and superplumes: the early Aptian "nannoconid crisis." *Paleoceanography* **9**, 483-501.

Erbacher, J., Huber, B.T., Norris, R.D., Markey, M., 2001, Increased thermohaline stratification as a possible cause for an ocean anoxic event in the Cretaceous Period: Nature, v. 409, p. 325-327.

Erbacher, J., Mosher, D.C., Malone, M.J., et al., (2004). *Proc. ODP, Init. Repts.,* 207 [Online]. Available from World Wide Web: http://www-odp.tamu.edu/publications/pubs_ir.htm . [Accessed 2006-04-26]

Erbacher J., Friedrich O., Wilson P.A., Birch H., Mutterlose J. (2005) Stable carbon isotope stratigraphy across Oceanic Anoxic Event 2 of Demerara Rise (Western Tropical Atlantic): *Geochemistry, Geophysics, Geosystems*, **6**.

Flogel S. (2002) On the influence of precessional Milankovitch cycles on the Late Cretaceous climate system: Comparison of GCM results, geochemical, and sedimentary proxies of the western interior seaway of North America, Ph.D. thesis, Univ. Kiel, Germany.

Frakes L.A., Probst J.L., Ludwig W. (1994) Latitudinal distribution of paleotemperature on land and sea from early Cretaceous to middle Miocene. *C.R. Acad. Sci. II* **318**, 1209-1218.

Frank M. (2002) Radiogenic isotopes: tracers of past ocean circulation and erosional input. *Reviews of Geophysics* **40**, 1-1 - 1-38.

Frank M. and O'Nions R. K. (1998) Sources of Pb for the Indian Ocean ferromanganese crusts: a record of Himalayan erosion? *Earth and Planet. Sci. Lett.* **158**, 121-130.

Frank M., Gersonde R., Mangini A. (1999) Sediment redistribution, (super 230) Th (sub ex) ; normalization and implication for the reconstruction of particle flux and export paleoproductivity (ed. G. Fischer and G. Wefer). Springer.

Frank M., Whitely N., Kasten S., Hein J. R., O'Nions K. (2002) North Atlantic Deep Water export to the Southern Ocean over the past 14 Myr: Evidence from Nd and Pb isotopes in ferromanganese crusts. *Paleoceanography* **17**.

Frank M., van de Flierdt T., Halliday A. N., Kubik P. W., Hattendorf B., Gunther D. (2003) Evolution of deepwater mixing and weathering inputs in the central Atlantic Ocean over the past 33 Myr. *Paleocenography* **18**(1091).

Goldstein S. J. and Jacobsen S. B. (1988) Nd and Sr isotope systematics of river water suspended material: Implications for crustal evolution. *Earth Planet. Sci. Lett.* **87**, 249-265.

Goldstein S. L. and Hemming S. H. (2003) Long lived isotopic tracers in oceanography, paleoceanography, and ice sheet dynamics. In *Treatise on Geochemistry*, Vol. Ch. **6.17** (ed. H. Elderfield), 453-489. Elsevier.

Goodney D.E., Margolis S.V., Dudley W.C., Kroopnick P., Williams D.F. (1980) Oxygen and Carbon isotopes of recent calcareous nannofossils as paleoceanographic indicators. *Marine Micropaleontology* **5**, 31-42.

Grandjean P., Cappetta H., Michard A., Albarede F. (1987) The assessment of REE patterns and $^{143}Nd/^{144}Nd$ ratios in fish remains. *Earth and Planetary Science Letters* **84**, 181-196.

Govindaraju K. (1994) Compliation of working values and sample description for 383 Geostandards. *Geostandards Newsletter, Special Issue* **18**, 1-58.

Handoh I.C., Bigg G.R., Jones E.J.W., Iuoue M. (1999) An ocean modeling study of the Cenomanian Atlantic: equatorial paleo-upwelling, organic-rich sediments and the consequences for a connection between the proto-North and South Atlantic. *Geophys. Res. Lett.* **26**, 223-226.

Handoh, I.C., Grant, R.B., Jones, E.J. (2003) Evolution of upwelling in the Atlantic Ocean basin. Paleogeo. Paleoclim. Paleoeco. **202**, 31-58

Haq B.U., Hardenbol J., Vail P.R. (1988) Mesozoic and Cenozoic chronostratigraphy and cycles of sea-level change, in Wilgus C.K., Hastings B.S., Posamentier H., van Wagoner J., Ross C.A., St Kendall C.G. Eds. Sea-level Changes: an Integrated Approach: Society of Economic Paleontologists and Mineralogists Special Publication **42**, 71-108

Haupt BJ and Seidov D (2001) Warm deep-water ocean conveyor during Cretaceous time. *Geology* **29**, 295-298

Hein J.R., Koschinsky, A., Halbach, P., Manheim, FT, Bau, M., Kang, JK, Lubick, N. (1997) Iron and manganese oxide mineralization in the Pacific. *Manganese Mineralization: Geochemistry and Mineralogy of Terrestrial and Maine Deposits, Geological Society of America Special Publication* **119**, 123-138.

Herbin J.P., Montadert L., Muller C., Gomez R., Thurow J., Wiedmann J. (1986) Organic-rich sedimentation at the Cenomanian-Turonian boundary in oceanic and coastal basins in the North Atlanic and Tethys. In Summerhayes C.P., Shackleton N.J. Eds. *North Atlantic palaeoceanography, Geological Society of London Special Publication* **21**, 389-422.

Herrle J.O, Pross J., Friedrich O., Kößler P., Hemleben C. (2003) Forcing mechanisms for mid-Cretaceous black shale formation: evidence from the Upper Aptian and Lower Albian of the Vocontian Basin (SE France) *Palaeogeog., Palaeoclim., Palaeoeco.,* **190**, 399-426

Hess J., Bender M.L., Schilling J.G. (1986) Evolutoin of the ratio of strontium-87 to strontium-86 in seawater from Cretaceous to present. *Science* **231**, 979-984.

Hodell D. A., Mead G. A., Mueller P. A. (1990) Variations in the strontium isotopic composition of seawater (8 Ma to present): Implications for chemical weathering rates and dissolved fluxes. *Chemical Geology* **80**, 291-307.

Hodell D. A. and Woodruff F. (1994) Variations in the strontium isotopic ratio of seawater during the Miocene: Stratigraphic and geochemical implications. *Paleoceanography* **9**, 405-426.

Huber B.T., Norris R.D., MacLeod K.G. (2002) Deep-sea paleotemperature record of extreme warmth during the Cretaceous. *Geology* **30**, 123-126.

Jarvis I., Carson G.A., Cooper M.K.E, Hart M.B., Leary P.N., Tocher B.A., Horne, D., Rosenfeld, A (1988) Microfossil assemblages and the Cenomanian-Turonian (late Cretaceous) oceanic anoxic event. *Cretaceous Res.* **9**, 3-103.

Jeandel C. (1993) Concentration and isotopic compositions of Nd in the South Atlantic Ocean. *Earth and Planet. Sci. Lett.* **117**, 581-591.

Jeandel C., Bishop J. K., Zindler A. (1995) Exchange of neodymium and its isotopes between seawater and small and large particles in the Sargasso Sea. *Geochim. Cosmochim. Acta* **59**, 535-547.

Jeandel C., Thouron D., Fieux M. (1998) Concentrations and isotopic compositions of neodymium in the eastern Indian Ocean and Indonesian straits. *Geochim. Cosmochim. Acta* **62**, 2597-2607.

Jenkyns H.C. (1980) Cretaceous anoxic events: from continents to oceans. *Journal of the Geological Society of London* **137**, 171-188.

Jenkyns H.C. (1991) Impact of Cretaceous Sea Level Rise and Anoxic Events on the Mesozoic Carbonate Platform of Yugoslavia. *The American Association of Petroleum Geologists* **75**, 1007-1017.

Jones E.J.W., Cande S.C., Spathopoulus F. (1995) Evolution of a major oceanographic pathway: the equatorial Atlantic. In: Scutton R.A., Stoker M.S., Shimmield G.B., Tudhope A.W. (Eds), *The Tectonics, Sedimentation and Palaeoceanography of the North Atlantic Region. Spec. Publ*. **90**. Geol. Soc. London, 199-213.

Jones C.E and Jenkyns H.C. (2001) Sea-water strontium isotopes, oceanic anoxia events, and seafloor hydrothermal activity in the Jurassic and Cretaceous. *Amer. Jour. Sci*. **301**, 112-149.

Keto L.S. and Jacobsen S.B. (1987) Nd and Sr isotopic variations of Early Paleozoic oceans. *Earth and Planet. Sci. Lett*. **84**, 27-41

Keto L.S. and Jacobsen S.B. (1988) Nd isotopic variations of Phanerozoic paleoceans. *Earth and Planet. Sci. Lett*. **90**, 395-410

Kennett J. P. (1977) Cenozoic evolution of Antarctic Glaciation, the Circum-Antarctic Ocean and their impact on global paleoceanography. *J. Geophys. Res* **82**, 3843-3860.

Kennett J. P. (1982) *Marine Geology*: Englewood Cliffs, New Jersey, Prentice-Hall.

Kerr A.C. (1998) Oceanic plateau formation: a cause of mass extinction and black shale deposition around the Cenomanian-Turonian boundary? *Journal of the Geological Society of London* **155**, 619-626.

Klemm V., Levasseur S., Frank M., Hein J.R., Halliday A.N. (2005) Osmium isotope stratigraphy of a marine ferromanganese crust *Earth and Planet. Sci. Lett.* **238**, 42-48

Kolonic S., Wagner T., Forster A., Sinninghe Damste J.S,Walsworth- Bell B., Erba E., Turgeon S., Brumsack H.J., Chellai E.I., Tsikos H., Kuhnt W., Kuypers M.M.M. (2005) Black shale deposition on the northwest African Shelf during the Cenomanian/Turonian oceanic anoxic event: Climate coupling and global organic carbon burial. *Paleoceanography* **20**.

Kuhnt W., Thurow J., Wiedmann J., Herbin J.P. (1986) Oceanic anoxic conditions around the Cenomanian/Turonian boundary and the response of the biota. *Mitt. Geol.-Palaontol. Inst. Univ. Hamburg* **60**, 205-246.

Kuypers M.M.M, Pancost R.D., Nijenhuis I.A., Sinninghe Damaste J.S. (2002) Enhanced productivity led to increased organic carbon burial in the euxinic North Atlantic basin during the late Cenomanian oceanic anoxic event. *Paleoceanography* **17**, 1051

Lacan F. and Jeandel C. (2005) Neodymium isotopes as a new tool for quantifying exchange fluxes at the continent-ocean interface. *Eartrh and Planetary Science Letters* **232**, 245-257.

Larson R.L. (1991) Geological consequences of superplumes. *Geology* **19**, 963-966.

Lawver L.A., Polziel, I.M.B, Gahagan C.M., Kygar R.M., Martin K.M., Campbell D. (2003) The PLATES Project. University of Texas Institute for Geophysics. www.ig.utexas.edu/research/projects/plates (Accessed 2006-04-26).

Leckie R. M., Bralower T.J. Cashman R. (2002) Oceanic anoxic events and plankton evolution: Biotic responses to tectonic forcing during the mid-Cretaceous. *Paleoceanography* **17**, 1041.

Lecuyer C., Reynard B., Marineau F. (2004) Stable isotope fractionation between mollusk shells and marine waters from Martinique Island *Chem. Geology* **213**, 293-30

Ling H. F., Burton K. W., O'Nions R. K., Kamber B. S., von Blanckenburg F., Gibb A. J., Hein J. R. (1997) Evolution of Nd and Pb isotopes in Central Pacific seawater from ferromanganese crusts. *Earth and Planet. Sci. Lett.* **146**, 1-12.

MacLeod K.G., and Huber B.T., (1996) Reorganization of ocean structure and deep circulation correlated with Maastrichtian global change: *Nature* **380**, 422-425.

MacLeod K.G., Huber B.T., Isaza Londoño C. (2005) North Atlantic warming during global cooling at the end of the Cretaceous. *Geology* **33**, 437-440.

Martin E. E., Macdougall J. D., Herbert T. D., Paytan A., Kastner M. (1995) Sr and Nd isotopic analyses of marine barite separates. *Geochimica et Cosmochimica Acta* **59**, 1353-1361.

Martin E. E., Shackleton N. J., Zachos J. C., Flower B. P. (1999) Orbitally-tuned Sr isotope chemostratigraphy for the late middle to late Miocene. *Paleoceangraphy* **14**(1), 74-83.

Martin E. E. and Haley B. A. (2000) Fossil fish teeth as proxies for seawater Sr and Nd isotopes. *Geochimica et Cosmochimica Acta* **64**(5), 835-847.

Martin E. E. and Scher H. D. (2004) Preservation of seawater Sr and Nd isotopes in fossil fish teeth: bad news and good news. *Earth and Planetary Science Letters* **220**, 25-39.

Mead G. A. and Hodell D.A. (1995) Controls on the 87Sr/86Sr composition of seawater from the middle Eocene to Oligocene: Hole 689B, Maude Rise, Antarctica, Paleoceanography, **10** 327-346

Michard A., Albareda F., Michard G., Minster J. F., Charlou J. L. (1983) Rare-earth elements and uranium in high-temperature solutions from East Pacific Rise hydrothermal vent field (13N). *Nature* **303**, 795-797.

Ocean Drilling Stratigraphic Network, www.odsn.de. Accessed 2006-3-25.

O'Nions R. K., Frank M., von Blanckenburg F., Ling H. F. (1998) Secular variation of Nd and Pb isotopes in ferromanganese crusts from the Atlantic, Indian and Pacific oceans. *Earth and Planetary Science Letters* **155**, 15-28.

Oppo D. W. and Fairbanks R. G. (1987) Variabilty in the deep and intermediate water circulation of the Atlantic Ocean. *Earth and Planetary Science Letters* **86**, 1-15.

Orth C.J., Attrep M.J., Quintana L.R., Elder W.P., Kauffman E.G., Diner R., Villamil T. (1993) Elemental abundance anomalies in the late Cenomanian extinction interval: A search for the source(s). Earth Planet. Sci. Lett. **117**, 189-204.

Palmer M. R. (1985) Rare earth elements in foraminifera tests. *Earth and Planetary Science Letters* **73**, 285-298.

Palmer M. R. and Elderfield H. (1985) Variations in the Nd isotopic composition of foraminifera from Atlantic Ocean sediments. *Earth and Planetary Science Letters* **73**, 299-305.

Palmer M.R. and Edmond J.M. (1989) The strontium isotope compostion of river water. *Geochim. et Cosmo. Acta* **56**, 2099-2111.

Pederson T.F. and Calvert S.E. (1990) Anoxia vs. productivity: what controls the formation of orgnic-carbon-rich sediments and sedimentary rocks? *American Association of Petroleum Geologists Bulletin* **74**, 454-466.

Piepgras D. J., Wasserburg G. J., Dasch E. J. (1979) The isotopic composition of Nd in different ocean masses. *Earth and Planetary Science Letters* **45**, 223-236.

Piepgras, D.J. and Wasserburg, G.J. (1980) Neodymium isotopic variation in seawater. *Earth and Planetary Science Letters* **50**, 128-138.

Piepgras D. J. and Wasserburg G. J. (1982) Isotopic composition of neodymium in waters from the Drake Passage. *Science* **217**, 207-214

Piepgras D. J. and Wasserburg G. J. (1985) Strontium and neodymium isotopes in hot springs on the East Pacific Rise and Guaymas Basin. *Earth and Planetary Science Letters* **72**, 341-356.

Piepgras D. J. and Wasserburg G. J. (1987) Rare earth element transport in the western North Atlantic inferred from Nd isotopic observations. *Geochimica et Cosmochimica Acta* **51**, 1257-1271.

Piepgras D. J. and Jacobsen S. B. (1988) The isotopic composition of neodymium in the North Pacific. *Geochim. Cosmochim. Acta* **52**, 1373-1381.

Pin C. and Bassin C. (1992) Evaluation of a Sr-specific extraction chromatographic method for isotopic analysis in geologic materials. *Anal. Chim. Acta* **269**, 249-255.

Piotrowski A. M., Goldstein S. L., Hemming S. H., Fairbanks R. G. (2004) Intensification and variability of ocean thermohaline circulation through the last deglaciation. *Earth and Planetary Science Letters* **225**, 205-220.

Piotrowski A. M., Goldstein S. L., Hemming S. H., Fairbanks R. G. (2005) Temporal relationships of carbon cycling and ocean circulation at glacial boundaries. *Science* **307**, 1933-1938.

Pomies C. (2000) Neodymium isotopes in modern foraminifera from Indian Ocean: Assessment of the use of Nd isotope composition of foraminifera as a tracer for palaeo-oceanic circulation changes, Goldschmidt 2000 Journal of Conference Abstracts, 5 (2).

Poulsen C.J., Barron, E.J., Johnson C.C., Fawcett, P. (1999) Links between major climatic factors and regional oceanic circulation in the mid-Cretaceous. Evolution of the Cretaceous Climate System, ed. Barrera E and Johnson, C. The Geological Soceity of America, Special Papers.

Poulsen C.J., Barron E.J., Arthur M.A., Peterson W.H. (2001) Response of the mid-Cretaceous global oceanic circulation to tectonic and CO_2 forcings. *Paleoceanography* **16**, 576-592.

Poulsen C.J., Gendaszek A.S., Jacob R.L. (2003) Did the rifting of the Atlantic Ocean cause the Cretaceous thermal maximum. *Geology* **31**, 115-118.

Puceat E., Lécuyer C., Reisberg L. (2005) Neodymium isotope evolution of NW Tethyan upper ocean waters throughout the Cretaceous *Earth and Planet. Scie. Lett.* **236**, 705-720.

Puteanus D. and Halbach P. (1988) Correlation of Co concentration and growth rate — A method for age determination of ferromanganese crusts . *Chem. Geology* **69**, 73-85

Reynard B., Lecuyer C., Grandjean P. (1999) Crystal-chemical controls on rare-earth element concentrations in fossil biogenic apatites and implications for paleoenvironmental reconstructions. *Chemical Geology* **155**, 233-241.

Ruddiman, W. F., Kidd, R. B., Thomas, E., et al., (1987) *Init. Repts. DSDP* **94**: Washington (U.S. Govt. Printing Office).

Rutberg R. L., Hemming S. H., Goldstein S. L. (2000) Reduced North Atlantic Deep Water flux to the glacial Southern Ocean inferred from neodymium isotope ratios. *Nature* **405**, 935-938.

Sageman, B.B., Meyers, S. (2002) Production and Preservation in the Cretaceous Western Interior Sea: Workshop on Cretaceous Climate and Ocean Dynamics National Science Foundation and JOI/USSSP, July 14-17, 2002, Florissant, CO.

Sageman, B.B, Meyers, S.R., Arthur, M.A. (2006) Orbital time scale and new C-isotope record for Cenomanian-Turonian boundary stratotype. *Geology* **34** 125-128.

Savin S.M (1977) History of Earth's Surface-Temperature during past 100-Million years. *Annual Review of Earth and Planetary Sciences* **5**, 319-355.

Scher H. D. and Martin E. E. (2004) Circulation in the Southern Ocean during the Paleogene inferred from Nd isotopes. *Earth and Planetary Science Letters* **228**, 391-405.

Scher H.D. and Martin E.E. (2006) Timing and Climatic Consequences of the Opening of Drake Passage. Science 312, 428-430.

Schlanger S. O. and Jenkyns H. C. (1976) Cretaceous oceanic anoxic events- causes and consequences. *Geologische Mijnbouw`*, 55179-55184.

Segl M., Mangini A., Bonani G., Hoffmann H.J., Moenzoni E., Ness M., Suter M., Wolfli W. (1984) 10Be dating of the inner structure of Mn-encrustations applying the Zurich tendem accelerator, Nuclear Instrum. Methods Phys. Res., B, 5 359-364

Shaw H. F. and Wasserburg G. J. (1985) Sm-Nd in marine carbonates and phosphates: Implications for Nd in seawater and crustal ages. *Geochimica et Cosmochimica Acta* **54**, 2433-2438.

Shimizu H., Tachikawa K., Masuda A., Nozaki Y. (1994) Cerium and neodymium isotope ratios and REE patterns in seawater from the North Pacific Ocean. *Geochim. Cosmochim. Acta* **58**, 323-333.

Shipboard Scientific Party, 1987. Site 647. *In* Srivastava, S.P., Arthur, M., Clement, B., et al., *Proc., Init. Repts*. (Pt. A), ODP, **104**, 675-905.

Shipboard Scientific Party, 1988. Sites 689 and 690. *In* Barker, P.F., Kennet, J.P., et al., Proc. *ODP, Init. Repts*., 113: College Station, TX (Ocean Drilling Program), 89-292.

Shipboard Scientific Party, 1993. Site 886. *In* Rea, D.K., Basov, I.A., Janecek, T.R., Palmer-Julson, A., et al., 1993. *Proc. ODP, Init. Repts*., 145: College Station, TX (Ocean Drilling Program), 303-334.

Shipboard Scientific Party, 1996. Sites 982. *In* Jansen, E., Raymo, M.E., Blum, P., e tal., Proc. *ODP, Init. Repts*., 162: College Station, TX (Ocean Drilling Program), 91-138.

Shipboard Scientific Party, 1998. Site 1050. In Norris, R.D., Kroon, D., Klaus, A., et al., Proc. ODP, Init. Repts., 171B, 47–91 [Online]. Available from World Wide Web: http://www-odp.tamu.edu/publications/171B_IR/CHAP_03.PDF.[Accessed 2006-04-26]

Shipboard Scientific Party, 1999. Site 1090. *In* Gersonde, R., Hodell, D.A., Blum, P., et al., *Proc. ODP, Init. Repts.,* 177 [Online]. Available from World Wide Web: <http://www-odp.tamu.edu/publications/177_IR/CHAP_01/Output/chap_01.htm>. [Accessed 2006-04-26]

Sinton C.W. and Duncan R.A. (1997) Potential links between ocean plateau volcanism and global ocean anoxia at the Cenomanian-Turonian boundary. *Economic Geology* **92**, 234-246.

Snow L.J., Duncan R.A., Bralower T.J. (2005) Trace element abundances in the Rock Canyon Anticline, Pueblo, Colorado, marine sedimentary section and their relationship to Caribbean plateau construction and oxygen anoxic event 2. *Paleoceanography* **20**

Spiess V. (1990) Cenozoic magnetostratigraphy of Leg 113 drill sites, Maud Rise, Weddell Sea, Antarctica, Proceedings of the Ocean Drilling Program, Scientific Results **113**, 261-315.

Staudigel H., Doyle P., Zindler A. (1985) Sr and Nd isotope systematics in fish teeth. *Earth and Planetary Science Letters* **76**, 45-56.

Stille P. and Fischer H. (1990) Secular variation in the isotopic composition of Nd in Tethys seawater. *Geochim. Cosmochim. Acta* **54**, 3139-3145.

Tachikawa K., Jeandel C., Roy-Barman M. (1999) A new approach to the Nd residence time in the ocean. *Earth and Planetary Science Letters* **170**, 433-446.

Tachikawa K., Athias V., Jeandel C. (2003) Neodymium budget in the modern ocean and paleo-oceanographic implications. *Jour. Geophys. Res.* **108**, 3254, doi:10.1029/1999JC000285.

Taylor S.R., and McLellen S.M. (1985) The Continental Crust: Its Composition and Evolution. Blackwell, Oxford**. 312**.

Thomas D. J., Brawlower T. J., Jones C. E. (2003) Neodymium isotopic reconstructions of the late Paleocene-early Eocene therrmohaline circulation. *Earth and Planetary Science Letters* **209**, 309-322.

Thomas, D.J., Evidence of deep water production in the North Pacific Ocean during the early Cenozoic warm interval, Nature 430 65-68

van de Flierdt T., Frank M., Halliday A. N., Hein J. R., Hattendorf B., Gunther D., Kubik P. W. (2004) Deep and bottom water export from the Southern Ocean to the Pacific over the past 38 million years. *Paleoceanography* **19(1)**.

Vance D. and Burton K. W. (1999) Neodymium isotopes in planktonic foraminifera: A record of the response of continental weathering and ocean circulation rates to climate change. *Earth Planet. Sci. Lett.* **173**, 365-379.

Vogt P.R. (1989) Volcanogenic upwelling of anoxic, nutrient-rich water: A possible factoring Carbonate-bank/reef demise and benthic faunal extinctions. *Geol. Soc. Am. Bull*. **101**, 1225-1245.

Von Blanckenburg, F., O'Nions, R.K. (1999) Response of beryllium and radiogenic isotope ratios in northern Atlantic Deep Water to the onset of northern hemisphere glaciation. *Earth Planet. Sci. Lett.* **167**, 175-182.

Wehausen R. and Brumsack H. (2002) Astronomical forcing of the East Asian monsoon mirrored by the composition of Pliocene South China Sea sediments. *Earth and Planet. Sci. Lett.* **201**, 621-636

Weissert H (1989) C-Isotope stratigraphy, A monitor of paleoenvironmental change- A case study from the Early Cretaceous. *Surveys in Geophysics* **10**, 1-61

White, W.M. and Dupre, B. (1985) Isotope and Trace element geochemistry of sediments from the Barbados Ridge-Demerara Plain Region, Atlantic Ocean. *Geochim. Cosmochim. Acta,* **49**, 1875-1886.

Wilson P.A.and Norris R.D. (2001) Warm tropical ocean surface and global anoxia during the mid-Cretaceous period. *Nature* **412**, 425-429.

Winter, B., Johnson, C.M., Clark, D.L., (1997) Strontium, neodymium and lead isotope variations of authigenic silicate sediment components from the late Cenozoic Arctic Ocean. Implications for sediment provenance and the source of trace metals in sea water. *Geochim. Cosmochim. Acta* **60** 4957-4963.

Wonders A.A.H. (1980) Middle and Late Cretaceous planktonic foraminifera of the Western Mediterranean area. *Utrecht Micropaleontol. Bull.* **24**, 1-157.

Wright J., Seymour R. S., Shaw H. F. (1984) REE and Nd isotopes in conodont apatite: Variations with geological age and depositional environment. *Geological Society of America Special Paper* **196**, 325-340.

Wright J., Schrader H., Holser W. T. (1987) Paleoredox variations in ancient oceans recorded by rare earth elements in fossil apatite. *Geochimica et Cosmochimica Acta* **51**, 631-644.

BIOGRAPHICAL SKETCH

Susanna Whitman Blair was named after her mother's favorite poet, Walt Whitman. Her primary education, elementary through high-school, was completed in Baltimore, Maryland, a place that still feels like home to her. During a summer camp, she attended in high-school, she first became interested in geology and knew that when it was time to go to college she at the very least wanted a school that had a good geology department. She found this at Colgate University in Hamilton, NY, and began her studies there in the fall of 1999. During this time she did research on the volcanic history of the Galapagos Islands and was fortunate enough to travel there to do some field work. This exposure to scientific research was the experience she needed to know that graduate studies were what she wanted to do next. She completed her degree in the spring of 2003 with a Bachelor of Arts with a focus in geology, knowing that she would be attending the University of Florida in the fall to begin work on her master's degree. At UF her research focused on Nd isotopes as a proxy for ocean circulation. Susanna plans on graduating in the summer of 2006 and shortly will be working for an environmental consulting firm in Jacksonville.